Unitarity violation in mixed-action lattice QCD

DIPLOMARBEIT

zur Erlangung des akademischen Grades
Diplom-Physiker
(Dipl.-Phys.)
im Fach Physik

eingereicht an der
Mathematisch-Naturwissenschaftlichen Fakultät I
Humboldt-Universität zu Berlin

von
Andreas Furchner
geboren am 12.05.1983 in Königs Wusterhausen

Präsident der Humboldt-Universität zu Berlin:
Prof. Dr. Dr. h. c. Christoph Markschies

Dekan der Mathematisch-Naturwissenschaftlichen Fakultät I:
Prof. Dr. Lutz-Helmut Schön

Gutachter:

1. Prof. Dr. Ulli Wolff, HU Berlin
2. Priv.-Doz. Dr. Karl Jansen, DESY Zeuthen

eingereicht am: 23. Februar 2010
Tag der mündlichen Prüfung: 26. März 2010

Contents

Introduction

In the standard model of particle physics, quantum chromodynamics (QCD) is the established theory of strong interactions. Depending on the energy scale, its building blocks, the quarks and gluons, show a quite distinct behavior, which is not fully understood yet: On the one hand, they seem to be the relevant degrees of freedom at high energies since the coupling between them is small, and the quarks are found to be nearly non-interacting. This property of QCD is known as asymptotic freedom and allows for perturbation theory and precise quantitative statements, which are in good agreement with the experiment.

On the other hand, the growing of the coupling at low energies, i. e., at large distances, and the associated confinement of quarks into hadrons demand different strategies for exploring the dynamics of QCD.

One way of handling the theory is lattice QCD, a non-perturbative approach making possible investigations in both the high- and the low-energy regime of QCD. This is achieved by discretizing the action using a Euclidean space-time lattice. The non-zero lattice spacing and the finite volume of the system provide an ultraviolet and an infrared regulator, which renders the previously ill-defined path integral finite and opens the door for numerical evaluations using Monte-Carlo methods.

At first glance, lattice QCD simulations seem like a very promising approach as they allow for the determination of physical quantities from first principles. One does, however, encounter a serious problem: The computational costs grow with decreasing lattice spacing, increasing volume, and decreasing quark masses. Despite sophisticated algorithms and continuously growing computer power, it is not yet possible to perform simulations at the quark masses realized in nature. As a consequence, extrapolations to the physical point must be performed. Furthermore, the continuum limit as well as the infinite volume limit have to be taken, since no physical observable may depend on the regulators. A connection between lattice results and physical quantities is therefore only possible if the systematic errors associated with the quark masses, the lattice spacing, and the finite volume are under control.

This is the point where effective theories prove to be powerful tools, since they allow to systematically study these effects. Chiral perturbation theory (ChPT) [1, 2] is such an effective field theory. Compared to the lattice, it represents a completely different approach to low-energy QCD: It treats the light pseudoscalar mesons – namely the pions, the kaons, and the eta meson – as Nambu–Goldstone bosons of the spontaneously broken chiral symmetry, and yields an expansion in powers of momenta and quark masses about the chiral limit. ChPT also allows to account for non-zero lattice spacings and for finite volume effects. The former is achieved by matching the Symanzik's effective theory [3, 4] for the used lattice action to an effective chiral Lagrangian [5, 6], whereas the finite volume dependence is incorporated by restricting the theory to a confined system with appropriate boundary conditions [7–9].

In view of lattice QCD, chiral perturbation theory can now fulfill the important purpose of providing fitting formulae for the observables in question. These formulae can guide extrapolations to the physical quark masses as well as to the continuum and the infinite volume. Besides that, ChPT is valuable for another reason:

In lattice simulations, one is free to use different sea and valence quark masses, or, even more drastically, different discretizations in the two sectors—both, though, on the sacrifice of the theory's unitarity [10–12]. The reasons for performing these *partially quenched* and *mixed-action* simulations are related to the computational costs. Most of the computational effort is spent in the sea sector where statistically independent gauge configurations are generated [11]. A usually small overhead goes into the computation of the propagators, a process which involves the valence quark masses.

Full unquenched simulations with Ginsparg–Wilson (GW) fermions [13–16]—that is, with discretizations satisfying the Ginsparg–Wilson relation [17] and thus preserving chiral symmetry on the lattice [18]—are not yet feasible for large volumes and quark masses near the physical point [19]. It therefore seems like a good compromise to choose GW fermions in the valence sector while using a relatively cheap discretization in the sea sector, such as Wilson [20], twisted mass [21], or staggered [22] fermions.

The advantage of this mixed-action approach is the saving of computing time plus the fact that at least the valence sector of the theory benefits from the properties of GW fermions. One can expect corresponding observables to show a reduced lattice spacing dependence [23]. Furthermore, the problem of operator mixing, which is a severe obstacle for example in the computation of weak matrix elements, is suppressed [12, 24]. Due to the exact chiral symmetry of GW fermions even at non-zero lattice spacing (in the massless limit), it is also possible to simulate with much lighter quark masses compared to, e.g., simulations with Wilson fermions.

The question is, how one can extract physical information from these unphysical partially quenched (PQ) and mixed-action (MA) lattice simulations. Chiral perturbation theory in its extension to PQChPT [25–27, 11, 12] and MAChPT [23, 28–31] provides the framework to systematically quantify the associated unitarity-violating effects and therefore allows to restore unitarity by taking the continuum limit and recovering the physical point where sea and valence quark masses are equal. The unphysical effects manifest themself in double poles and negative signs in the propagators of the chiral effective theory. Moreover, for mixed actions, new operators coming with new unknown low-energy constants arise due to the lack of symmetry between the sea and the valence sector.

A quantity which is extremely sensitive to unitarity-violating effects and therefore perfectly fit to study the size of unitarity violating occurring in mixed-action simulations, is the scalar two-point function. It was first investigated in the quenched approximation and found to have unphysical negative values at large time separations [32, 33]. Later, a ChPT expression for partially quenched two-flavor QCD was derived [34], which was then generalized to the use of staggered quarks [35, 36]. A mixed-action formula for degenerate Wilson and/or Ginsparg–Wilson quarks was given in Ref. [37]. Further extensive studies with staggered sea and Ginsparg–Wilson valence quarks were performed in Refs. [35, 38].

In this diploma thesis, the isospin-one scalar two-point function for Wilson sea and Ginsparg–Wilsons valence quarks is studied, focusing on two- and three-flavor QCD with (and without) isospin symmetry. The calculation is inspired by the partially quenched and staggered-sea/GW-valence results in Refs. [34, 35]. The authors give finite volume expressions for the correlator as well as an asymptotic formula for large time separations. The exact formulae, however, involve lengthy expressions with multiple sums over lattice momenta and are therefore rather inconvenient to use in a fitting process. Moreover, it is not clear how the infinite volume limit is being approached.

For these reasons, the calculations in the present work are organized in a different way: The correlator is at first computed in the infinite volume in partially quenched ChPT. This already makes the unphysical effects associated with unequal sea and valence masses visible. Afterwards, the results are extended to mixed actions, which modifies the shape of the correlator and especially affects the double pole contribution. The main task is to account for the finite volume and to deal with the occurring sums.

The final aim is to derive two fitting formulae, which are applicable for either small or large lattice volumes. Provided that mixed-action ChPT describes all effects of unitarity violation observed in lattice data [38, 39], a fit of the scalar correlator would then allow to extract the size of the two unitarity-violating effects—*partial quenching* and its generalization *mixed actions*. This will be useful knowledge for future computations of physical observables like meson masses and decay constants obtained from mixed-action simulations.

The present work is relevant for example for Bernardoni et. al. [40].

The outline of this thesis is as follows:

In Chapter 1, an introduction to chiral perturbation theory is given. The extension to partially quenched and mixed-action ChPT is explained in Chapter 2. The third chapter is devoted to the scalar two-point function in the infinite volume. Finally, in the last chapter, the impact of a finite volume on the correlator is studied, which in the end yields the desired fitting formulae.

1. Chiral perturbation theory

In the first chapter, a short introduction to quantum chromodynamics and its symmetries is given [41–44, 24], focusing especially on chiral symmetry. This will be the cornerstone for the development of chiral perturbation theory, which is presented afterwards. Throughout this chapter, the theory is considered in Minkowski space. Later, when making the connection to lattice QCD, the notation is switched to Euclidean space.

1.1. Continuum QCD and chiral symmetry

Quantum chromodynamics, the theory of strong interactions, is the $SU(3)$ Yang–Mills theory of color-charged fermions – the quarks. The gauge bosons that mediate the strong force between them are called gluons. In contrast to quantum electrodynamics where the gauge bosons, the photons, are not electrically charged, the gluons do also carry color charge, which results in self interactions and makes the theory difficult to solve. The QCD Lagrangian is given by

$$
\begin{aligned}
\mathcal{L}_{\mathrm{QCD}} &= \mathcal{L}_{\mathrm{quark}} + \mathcal{L}_{\mathrm{gauge}} \\
&= \sum_{i=1}^{N_f} \bar{q}_i(i\slashed{D} - m_i)q_i - \sum_{a=1}^{8} \frac{1}{4} G_{\mu\nu}^a G^{a,\mu\nu} \, .
\end{aligned}
\tag{1.1}
$$

The quark fields q_i are color triplets and come in $N_f = 6$ different flavors (u, d, s, c, b, t) with masses m_i. For simplicity, spinor and color indices have been suppressed. The gauge fields A_μ^a that enter the theory through the gauge principle appear in the covariant derivative (Einstein summation convention implied from now on),

$$
\slashed{D} = \gamma^\mu \left(\partial_\mu - ig A_\mu^a T^a \right) \, ,
\tag{1.2}
$$

and in the field-strength tensor $G_{\mu\nu}^a$,

$$
G_{\mu\nu}^a = \partial_\mu A_\nu^a - \partial_\nu A_\mu^a - g f^{abc} A_\mu^b A_\nu^c \, ,
\tag{1.3}
$$

in which the last term gives rise to gluonic three- and four-point self interaction vertices. g is the strong coupling constant, and f^{abc} are the $SU(3)$ structure constants obeying

$$
\left[T^a, T^b \right] = i f^{abc} T^c \, ,
\tag{1.4}
$$

where T^a are the $N_f^2 - 1 = 8$ generators of $SU(3)$, namely the Gell-Mann matrices. For short-hand notation, the fermionic part of $\mathcal{L}_{\mathrm{QCD}}$ will be abbreviated by

$$
\mathcal{L}_{\mathrm{quark}} = \bar{q}(i\slashed{D} - m)q \, ,
\tag{1.5}
$$

where the N_f quark fields are collected in the vector

$$q^T = (u, d, s, \ldots)^T \tag{1.6}$$

and the quark masses are put into the diagonal mass matrix

$$m = \mathrm{diag}(m_u, m_d, m_s, \ldots) \,. \tag{1.7}$$

By construction, $\mathcal{L}_{\mathrm{QCD}}$ is invariant under $SU(3)_c$ color transformations where the quark fields transform according to the fundamental representation, and the gauge fields according to the adjoint representation of $SU(3)_c$.

Next to the $SU(3)_c$ color symmetry, the QCD Lagrangian possesses additional symmetries: It is invariant under separate parity (P) and charge conjugation (C) transformations due to the absence of axial vector coupling constants and due to the real-valued nature of the couplings m_i and g_s. In principle, one can construct another gauge invariant term out of the gauge fields itself – the so-called theta term – which would be responsible for explicit P and CP violation. This term, however, is dropped since strong CP violation is not observed in nature.

Furthermore, there are several (approximate) flavor symmetries: For degenerate quark masses, $\mathcal{L}_{\mathrm{QCD}}$ is flavor-blind and invariant under global $U(N_f)$ transformations. In the massless case, there is an even larger symmetry group, which comes in view when the quark fields are separated into their chiral components q_L and q_R using the projectors

$$P_L = \frac{\mathbb{1} - \gamma_5}{2} \,, \qquad P_R = \frac{\mathbb{1} + \gamma_5}{2} \,, \tag{1.8}$$

that satisfy

$$P_L + P_R = \mathbb{1} \,, \quad P_{L,R}^2 = P_{L,R} \,, \quad \text{and} \quad P_L P_R = P_R P_L = 0 \,. \tag{1.9}$$

The traceless, hermitian matrix γ_5, acting in spinor space, fulfills $\gamma_5^2 = \mathbb{1}$ and anticommutes with all gamma matrices and hence also with the Dirac operator,

$$\{\gamma_5, \gamma_\mu\} = 0 \,, \qquad \{\gamma_5, \slashed{D}\} = 0 \,. \tag{1.10}$$

With

$$q_{L,R} = P_{L,R} \cdot q \,, \qquad \bar{q}_{L,R} = \bar{q} \cdot P_{R,L} \,, \tag{1.11}$$

the fermionic part of $\mathcal{L}_{\mathrm{QCD}}$ takes the form

$$\mathcal{L}_{\mathrm{quark}} = \bar{q}_L i \slashed{D} q_L + \bar{q}_R i \slashed{D} q_R - \bar{q}_L m q_R - \bar{q}_R m q_L \,. \tag{1.12}$$

Now, it is obvious that the left- and right-handed field components decouple in the massless limit (which is therefore often called the *chiral limit*), and $\mathcal{L}_{\mathrm{QCD}}$ becomes invariant under independent *global* $U(N_f)$ transformations L and R,

$$\left. \begin{array}{c} q_L \to L q_L \\ q_R \to R q_R \end{array} \right\} \quad \Rightarrow \quad q \to L q_L + R q_R \,. \tag{1.13}$$

On the classical level, these symmetries lead to $2(N_f)^2$ conserved left- and right-handed Noether currents

$$J_\mu^{L,a} = \bar{q}_L \gamma_\mu T^a q_L \,, \qquad J_\mu^{R,a} = \bar{q}_R \gamma_\mu T^a q_R \,, \tag{1.14a}$$

$$\mathcal{J}_\mu^L = \bar{q}_L \gamma_\mu q_L \,, \qquad\quad \mathcal{J}_\mu^R = \bar{q}_R \gamma_\mu q_R \,, \tag{1.14b}$$

and correspondingly to $2(N_f)^2$ conserved Noether charges. Here, T^a denote the $N_f^2 - 1$ generators of $SU(N_f)$.

This global chiral $U(N_f)_L \otimes U(N_f)_R$ symmetry of the massless QCD Lagrangian is often equivalently expressed as the vector and axial vector symmetry $U(N_f)_V \otimes U(N_f)_A$. The vector transformations, where the left- and right-handed fields transform with the same phase, $R = L = U_V$, lead to the conserved vector Noether currents

$$V_\mu^a = \bar{q} \gamma_\mu T^a q = J_\mu^{R,a} + J_\mu^{L,a} \,, \tag{1.15a}$$

$$\mathcal{V}_\mu = \bar{q} \gamma_\mu q \quad = \mathcal{J}_\mu^R + \mathcal{J}_\mu^L \,. \tag{1.15b}$$

The associated conserved Noether charges correspond to isospin conservation generalized to N_f flavors, and baryon number conservation, respectively.

The transformations of q_R and q_L with opposite phase, $R = L^\dagger = U_A$, are called axial vector transformations or *chiral* transformations. They mix the left- and right-handed quark components and result in the conserved axial vector Noether currents

$$A_\mu^a = \bar{q} \gamma_\mu \gamma_5 T^a q = J_\mu^{R,a} - J_\mu^{L,a} \,, \tag{1.16a}$$

$$\mathcal{A}_\mu = \bar{q} \gamma_\mu \gamma_5 q \quad = \mathcal{J}_\mu^R - \mathcal{J}_\mu^L \,. \tag{1.16b}$$

If the quark masses are turned on, the transformation of the mass matrix m in (1.12) under $U(N_f)_V \otimes U(N_f)_A$ yields the following modifications of the vector and axial vector divergences:

$$\partial^\mu V_\mu^a = i\bar{q}(mT^a - T^a m)q \tag{1.17a}$$

$$\partial^\mu A_\mu^a = i\bar{q}(mT^a + T^a m)\gamma_5 q \tag{1.17b}$$

$$\partial^\mu \mathcal{V}_\mu = 0 \tag{1.17c}$$

$$\partial^\mu \mathcal{A}_\mu = 2i\bar{q}m\gamma_5 q \tag{1.17d}$$

Apparently, isospin symmetry extends also to degenerate quark masses, Eq. (1.17a), which is the flavor-blindness of $\mathcal{L}_{\text{QCD}}$ that was mentioned before. In this case, one would expect hadrons to be classifiable as irreducible representations of $SU(3)_V$, that is, they fall into multiplets of degenerate states. Baryon number conservation (1.17c) of course holds even for unequal masses. The axial symmetries, however, are explicitly broken by the quark masses.

To conclude, the QCD Lagrangian exhibits an exact chiral symmetry,

$$SU(N_f)_L \otimes SU(N_f)_R \otimes U(1)_V \otimes U(1)_A \,, \tag{1.18}$$

if all quarks are massless, and if the Dirac operator is diagonal in flavor space *and* anticommutes with γ_5. The $SU(N_f)_L \otimes SU(N_f)_R$ part is often referred to as the chiral group.

How are these symmetries realized in nature? Compared to the QCD scale Λ_{QCD}, the up and down quarks are very light and nearly degenerate to find the isospin symmetry $SU(2)_V$ being a good approximation. Examples are the proton-neutron doublet (p, n), the pion triplet (π^+, π^0, π^-), and the kaons doublets (K^+, K^0) and $(K^-, \bar{K}^0)$. Taking into account the strange quark, the corresponding hadrons can be classified as multiplets of $SU(3)_V$. The mass splittings within these multiplets, however, are rather large which reflects the size of the quark mass difference between the up/down and the strange quark. Baryon number conservation is found to be true for the strong interaction. But what about the axial vector symmetries? Exact chiral symmetry implied for each observed hadron a partner particle of opposite parity and same mass. In the real hadron spectrum, then, one would expect the masses of these partners to differ only slightly according to the size of the symmetry breaking quark masses. The fact that this (approximate) axial symmetry is not observed leads to the conclusion that chiral symmetry is spontaneously broken down to its vector subgroup,

$$SU(3)_L \otimes SU(3)_R \to SU(3)_V . \tag{1.19}$$

This, in turn, requires eight massless spin-zero Nambu–Goldstone bosons – one for each broken generator of $SU(3)_A$. At energies below the mass of the rho meson, $M_\rho = 775\,\text{MeV}$, the rich hadronic particle spectrum reduces to an octet of nearly massless pseudoscalar mesons, namely the pions, kaons, and the eta meson,

$$\Phi = \frac{1}{\sqrt{2}} \begin{pmatrix} \frac{1}{\sqrt{2}}\pi^0 + \frac{1}{\sqrt{6}}\eta & \pi^+ & K^+ \\ \pi^- & -\frac{1}{\sqrt{2}}\pi^0 + \frac{1}{\sqrt{6}}\eta & K^0 \\ K^- & \bar{K}^0 & -\sqrt{\frac{2}{3}}\eta \end{pmatrix} . \tag{1.20}$$

These are now identified as the pseudo-Goldstone bosons of the spontaneously broken axial vector symmetry (The prefix "pseudo" refers to their small non-zero mass, which is explained by the explicit chiral symmetry breaking due to the quark masses.). Chiral perturbation theory is based on this observation. It incorporates the light mesons (1.20) as the only dynamical degrees of freedom into an effective field theory and allows to compute correlation functions, hadron masses, etc. in the low-energy regime of QCD $(E \ll M_\rho)$ [1, 2].

Lastly, when quantizing the classical QCD Lagrangian, the $U(1)_A$ axial symmetry cannot be preserved due to quantum corrections. In order to keep the theory gauge invariant, one is forced to regularize and renormalize the divergence (1.17d) such that it receives an additional non-vanishing contribution, even in the chiral limit. The symmetry of massless QCD, thus, reduces to

$$SU(N_f)_L \otimes SU(N_f)_R \otimes U(1)_V . \tag{1.21}$$

This so-called *axial* or *chiral anomaly* explains the absence of a ninth Goldstone boson associated with the spontaneous breakdown of $U(3)_L \otimes U(3)_R$, and why instead the flavor-singlet eta prime meson is found to be considerably heavier than the pions, kaons, and the eta meson, $M_{\eta'} \sim 1\,\text{GeV}$.

1.2. Chiral perturbation theory in the continuum

In order to construct an effective field theory, one at first has to identify the relevant degrees of freedom, which in the case of QCD are the pions, kaons, and the eta meson. The masses of these pseudo-Goldstone bosons are characteristically smaller than any typical hadron mass, for example the mass of the rho meson or the proton, $M_{\mathrm{GB}} \ll \Lambda_{\mathrm{had}} \sim 1$ GeV, Secondly, all symmetries of the underlying theory as well as the pattern of symmetry breaking must be known. With these ingredients, it is then possible to construct the most general effective Lagrangian, valid below the energy scale Λ_{had}, that contains only the light mesons as dynamical degrees of freedom [45]. All heavier states disappear from the theory and enter only in so-called low-energy constants (LECs), which describe the lack of knowledge about the short-distance properties of the underlying theory. The effective Lagrangian cannot be derived directly from the QCD Lagrangian. Its construction is entirely based on symmetry arguments.

At first, one needs to parameterize the Nambu–Goldstone bosons that are associated with the spontaneous breakdown of chiral symmetry,

$$\underbrace{SU(3)_L \otimes SU(3)_R}_{\equiv G} \longrightarrow \underbrace{SU(3)_V}_{\equiv H} . \tag{1.22}$$

An order parameter for this breaking is the quark condensate

$$\langle 0|\bar{q}^i q^j|0\rangle = \langle 0| \left(\bar{q}_R^i q_L^j + \bar{q}_L^i q_R^j \right) |0\rangle = \lambda \delta_{ij} , \tag{1.23}$$

where i and j denote flavor indices, and the vacuum expectation value λ is proportional to the QCD scale, $\lambda \propto \Lambda_{\mathrm{QCD}}^3$. The condensate transforms like a mass term under the chiral group G,

$$\langle 0|\bar{q}^i q^j|0\rangle \xrightarrow{G} \lambda(LR^\dagger + RL^\dagger)^{ij} , \tag{1.24}$$

and apparently, a non-zero condensate is equivalent to spontaneous breaking of chiral symmetry, for then $\langle \bar{q}q \rangle$ is invariant only under the vector subgroup H, that is, if $L = R$. Of course, there exists a manifold of equivalent vacua that can be rotated into another, but one can choose

$$\Sigma^{ij} = (LR^\dagger)^{ij} \quad \text{with } L = R , \tag{1.25}$$

such that the matrix $\Sigma^{ij} = \delta^{ij}$ corresponds to the vacuum in Eq. (1.23). The fluctuations around that vacuum correspond to the light mesons that are associated with the spontaneous symmetry breaking. The most common and very convenient way to collect the Goldstone fields is the exponential parameterization [2],

$$\Sigma(x) = \exp\left(\frac{2i}{f}\Phi(x)\right) , \tag{1.26}$$

where $\Phi(x)$ denotes the meson octet of Eq. (1.20), and it is given by linear combinations of the broken generators T^a of $SU(3)$,

$$\Phi(x) = \sum_{a=1}^{8} \pi^a(x) T^a . \tag{1.27}$$

For dimensional reasons, the parameter f was introduced. Note that for chiral $SU(2)$, a runs from 1 to 3, and the corresponding meson triplet is that of the pions in the upper-left 2×2 block of Eq. (1.20) without the η.

With the parameterization of the meson fields at hand, one can now approach the construction of an effective Lagrangian. It proves to be useful to keep track of the symmetry breaking mass term by promoting the diagonal mass matrix $m = \text{diag}(m_u, m_d, m_s)$ to a complex *spurion* field that obeys the same transformation behavior under the chiral group G as the meson matrix Σ,

$$\Sigma \xrightarrow{G} L\,\Sigma\,R^\dagger\,, \qquad m \xrightarrow{G} L\,m\,R^\dagger\,, \tag{1.28}$$
$$\Sigma^\dagger \xrightarrow{G} R\,\Sigma^\dagger L^\dagger\,, \qquad m^\dagger \xrightarrow{G} R\,m^\dagger L^\dagger\,.$$

In the effective Lagrangian, then, one sets the masses to their physical values and thus explicitly breaks chiral symmetry in the same manner as in QCD.

Following Weinberg [45], the properties of S-matrix elements of the underlying quantum field theory (QCD), which are unitarity, causality, crossing symmetry, cluster decomposition, and Lorentz invariance, can be preserved in the effective theory if one constructs the most general local, Lorentz invariant Lagrangian that satisfies the internal symmetries. The building blocks are the meson matrix Σ, its derivative $\partial_\mu \Sigma$, the spurion m, and the hermitian conjugate counterparts $\Sigma^\dagger$, $\partial_\mu \Sigma^\dagger$, and $m^\dagger$. One can now construct scalar terms that are invariant under $SU(3)_L \otimes SU(3)_R$, parity, and charge conjugation by taking the trace or combinations of traces over products of these building blocks. Because of Lorentz invariance, only even powers of derivatives can appear. Furthermore, terms including solely the sigma fields collapse to a constant ($\Sigma\Sigma^\dagger = \mathbb{1}$) and thus do not contribute to the equations of motion. This in turn means that, for massless quarks, all interactions become weak and finally vanish at small momenta. It is therefore possible to organize the effective field theory as an expansion in terms of derivatives (momenta p). The non-zero quark masses are treated as small perturbation to the chirally invariant Lagrangian,

$$\mathcal{L}_{\text{eff}} = \sum_{ij} \mathcal{L}_{ij}\,, \qquad \mathcal{L}_{ij} = \mathcal{O}(p^i m^j)\,. \tag{1.29}$$

The number d of derivative and spurion insertions, ∂_μ and m, determines the order of the term in question, where here, the power counting $\partial^2 \sim m$ is assumed, that is, $d = i + 2j$ as will be justified later. The effective Lagrangian, then, is of the form

$$\mathcal{L}_{\text{eff}} = \sum_d \mathcal{L}_d = \mathcal{L}_2 + \mathcal{L}_4 + \mathcal{L}_6 + \dots\,. \tag{1.30}$$

At leading order (LO), the chiral Lagrangian consists only of the two simplest non-trivial terms,

$$\mathcal{L}_2 = \frac{f^2}{4}\text{tr}(\partial_\mu \Sigma\, \partial^\mu \Sigma^\dagger) + \frac{f^2 B_0}{2}\text{tr}(m\Sigma^\dagger + \Sigma m^\dagger)\,, \tag{1.31}$$

and is, due to the cyclicity of the traces, indeed invariant under chiral transformations (1.28). The low-energy constant f equals the pion decay constant f_π in the chiral limit [1].

It gives the Lagrangian the dimension four. While other normalizations including factors of $\sqrt{2}$ are common, f is chosen such that $f_\pi = 92.4$ MeV. The mass term comes with a new LEC B_0, which is related to the quark condensate [1]. All other prefactors are conventional.

With the quark masses set to their physical values, one can expand Σ in the meson fields Eq. (1.20),

$$\mathcal{L}_2 = \frac{1}{2}\partial_\mu\pi^0\,\partial^\mu\pi^0 - B_0(m_u + m_d)\pi^0\pi^0 + \partial_\mu\pi^+\,\partial^\mu\pi^- - 2B_0(m_u + m_d)\pi^+\pi^-$$
$$+ \text{ kaons, eta, } \pi^0\text{-}\eta \text{ mixterm} + \mathcal{O}(\Phi^4)\,, \tag{1.32}$$

and read off the tree-level meson masses. In the limit of isospin symmetry, $m_u = m_d \equiv \hat{m}$, the π^0 and the η do not mix, and one gets

$$M_\pi^2 = 2B_0\hat{m}\,, \quad M_K^2 = B_0(\hat{m} + m_s)\,, \quad M_\eta^2 = \frac{2}{3}B_0(\hat{m} + 2m_s)\,. \tag{1.33}$$

The finding that the squared meson masses are linear in the quark masses justifies, in retrospect, the power counting $\partial^2 \sim m$.

Before proceeding, one should pause for a moment and remember that one wishes to compute correlation functions in the effective theory as one does in QCD itself. These might involve for instance the vector and axial vector currents Eqs. (1.15) and (1.16). Of course, one could apply the Noether theorem and carry out the ChPT calculation. Instead, a more elegant way was shown by Gasser and Leutwyler [1, 2]. They start from the massless QCD action and couple the fields to additional external left- and right-handed sources l_μ and r_μ, as well as to the scalar densities s and p:

$$\mathcal{L}_{\text{QCD}} = \bar{q}_L(i\slashed{D} + \gamma_\mu l^\mu)q_L + \bar{q}_R(i\slashed{D} + \gamma_\mu r^\mu)q_R - \bar{q}_L(s + ip)q_R - \bar{q}_R(s - ip)q_L$$
$$- G^a_{\mu\nu}G^{a,\mu\nu} \tag{1.34}$$

The space-time dependent sources are hermitian 3×3 matrices acting in flavor space, and they are given by

$$l_\mu = l^0_\mu + l^a_\mu T^a\,, \quad r_\mu = r^0_\mu + r^a_\mu T^a\,, \quad s = s^0 + s^a T^a\,, \quad p = p^0 + p^a T^a\,. \tag{1.35}$$

Setting

$$l_\mu = r_\mu = p = 0 \quad \text{and} \quad s = m\,, \tag{1.36}$$

reproduces the standard QCD Lagrangian. The method of external sources gives comfortable access to the chiral Noether currents Eq. (1.14), and the vector and axial vector currents Eqs. (1.15), (1.16). They are simply computed by differentiating $\mathcal{L}_{\text{QCD}}$ with respect to l_μ and r_μ. For example,

$$A^a_\mu(x) = J^{R,a}_\mu(x) - J^{L,a}_\mu(x) = \frac{\partial\mathcal{L}_{\text{QCD}}}{\partial r^\mu_a(x)} - \frac{\partial\mathcal{L}_{\text{QCD}}}{\partial l^\mu_a(x)} = \bar{q}(x)\gamma_\mu\gamma_5 T^a q(x)\,. \tag{1.37}$$

The generalized Lagrangian (1.34) allows for the definition of a generating functional,

$$Z_{\text{QCD}} = \int \mathcal{D}A\,\mathcal{D}\bar{q}\,\mathcal{D}q\,\mathrm{e}^{i\int \mathrm{d}^4 x\,\mathcal{L}_{\text{QCD}}(l_\mu, r_\mu, s, p)}\,, \tag{1.38}$$

10

from which correlation functions can be obtained by taking the appropriate functional derivatives with respect to the sources. For instance, the isospin-one scalar two-point function, the main object of interest in the present work, is computed by

$$\langle 0|\bar{d}(x)u(x)\,\bar{u}(0)d(0)|0\rangle = \frac{-1}{Z_{\mathrm{QCD}}[0]}\frac{\delta^2 Z_{\mathrm{QCD}}}{\delta s^0_{ud}(0)\,\delta s^0_{du}(x)}\bigg|_{\substack{s=m\\l_\mu=r_\mu=p=0}}, \tag{1.39}$$

where the normalizing $Z_{\mathrm{QCD}}[0]$ denotes the generating functional with sources set to Eq. (1.36).

In order for the correlation functions to obey the Ward identities of QCD, these sources have to transform like gauge fields [46],

$$l_\mu \xrightarrow{G} L\,l_\mu\,L^\dagger + i\partial_\mu LL^\dagger\,, \qquad\qquad s+ip \xrightarrow{G} L(s+ip)R^\dagger\,, \tag{1.40}$$
$$r_\mu \xrightarrow{G} Rr_\mu R^\dagger + i\partial_\mu RR^\dagger\,, \qquad\qquad s-ip \xrightarrow{G} R(s-ip)L^\dagger\,,$$

under *local* chiral transformations $(L(x), R(x)) \in G = SU(3)_L \otimes SU(3)_R$.

The aim now is to construct a generating functional for the effective theory,

$$Z_{\mathrm{ChPT}} = \int \mathcal{D}\Sigma\,\mathrm{e}^{i\int \mathrm{d}^4x\,\mathcal{L}_{\mathrm{eff}}(l_\mu,r_\mu,s,p)}\,, \tag{1.41}$$

which matches Z_{QCD} order by order in the chiral expansion, that is,

$$Z_{\mathrm{ChPT}}(l_\mu,r_\mu,s,p) = Z_{\mathrm{QCD}}(l_\mu,r_\mu,s,p)\,, \tag{1.42}$$

up to truncation errors. Then, correlation functions will be calculable by using the same functional derivatives with respect to the sources as in QCD. In order to do this matching and to reproduce the Ward identities of QCD in the effective theory, one therefore demands the chiral Lagrangian to be invariant under *local* chiral transformations. This lets the sources enter in two ways – once through covariant derivatives,

$$\partial_\mu\Sigma \to D_\mu\Sigma = \partial_\mu\Sigma + il_\mu\Sigma - i\Sigma r_\mu\,, \tag{1.43}$$

which transform under G as
$$D_\mu\Sigma \xrightarrow{G} L\,D_\mu\Sigma\,R^\dagger\,, \tag{1.44}$$

and additionally through the two field-strength tensors

$$L_{\mu\nu} = \partial_\mu l_\nu - \partial_\nu l_\mu + i[l_\mu, l_\nu] \xrightarrow{G} L\,L_{\mu\nu}\,L^\dagger\,,$$
$$R_{\mu\nu} = \partial_\mu r_\nu - \partial_\nu r_\mu + i[r_\mu, r_\nu] \xrightarrow{G} R\,R_{\mu\nu}\,R^\dagger\,. \tag{1.45}$$

Lastly, with the scalar densities s and p combined into the matrix χ,

$$\chi \equiv 2B_0(s+ip) \xrightarrow{G} L\chi R^\dagger\,, \qquad \chi^\dagger = 2B_0(s-ip) \xrightarrow{G} R\chi L^\dagger\,, \tag{1.46}$$

one has all the building blocks that are needed to construct the most general chiral Lagrangian—namely Σ, $\Sigma^\dagger$, $D_\mu\Sigma$, $D_\mu\Sigma^\dagger$, χ, $\chi^\dagger$, $L_{\mu\nu}$, and $R_{\mu\nu}$.

The $\mathcal{O}(p^2)$ chiral Lagrangian of Eq. (1.31) generalizes to

$$\mathcal{L}_2 = \frac{f^2}{4}\mathrm{tr}(D_\mu\Sigma\, D^\mu\Sigma^\dagger) + \frac{f^2}{4}\mathrm{tr}(\chi\Sigma^\dagger + \Sigma\chi^\dagger)\,. \tag{1.47}$$

With this leading order chiral Lagrangian at hand, it is possible to compute the scalar two-point function Eq. (1.39) for non-zero space-time separations x to lowest order in chiral perturbation theory. This is the topic of Chapter 3.

It is now time to write down the most general $\mathcal{O}(p^4)$ chiral Lagrangian[1],

$$\begin{aligned}
\mathcal{L}_4 = &+ L_1[\mathrm{tr}(D_\mu\Sigma\, D^\mu\Sigma^\dagger)]^2 + L_2\,\mathrm{tr}(D_\mu\Sigma\, D_\nu\Sigma^\dagger)\,\mathrm{tr}(D^\mu\Sigma\, D^\nu\Sigma^\dagger) \\
&+ L_3\,\mathrm{tr}(D_\mu\Sigma\, D^\mu\Sigma^\dagger\, D_\nu\Sigma\, D^\nu\Sigma^\dagger) \\
&+ L_4\,\mathrm{tr}(D_\mu\Sigma\, D^\mu\Sigma^\dagger)\mathrm{tr}(\chi\Sigma^\dagger + \Sigma\chi^\dagger) + L_5\,\mathrm{tr}(D_\mu\Sigma\, D^\mu\Sigma^\dagger[\chi\Sigma^\dagger + \Sigma\chi^\dagger]) \\
&+ L_6[\mathrm{tr}(\chi\Sigma^\dagger + \Sigma\chi^\dagger)]^2 + L_7[\mathrm{tr}(\chi\Sigma^\dagger - \Sigma\chi^\dagger)]^2 \\
&+ L_8\,\mathrm{tr}(\chi\Sigma^\dagger\chi\Sigma^\dagger + \Sigma\chi^\dagger\Sigma\chi^\dagger) \\
&+ iL_9\mathrm{tr}(L_{\mu\nu}D^\mu\Sigma\, D^\nu\Sigma^\dagger + R_{\mu\nu}D^\mu\Sigma^\dagger\, D^\nu\Sigma) + L_{10}\,\mathrm{tr}(L_{\mu\nu}\Sigma\, R^{\mu\nu}\Sigma^\dagger) \\
&+ H_1\,\mathrm{tr}(L_{\mu\nu}L^{\mu\nu} + R_{\mu\nu}R^{\mu\nu}) + H_2\,\mathrm{tr}(\chi\chi^\dagger) + \mathcal{L}_{\mathrm{WZW}}\,. \tag{1.48}
\end{aligned}$$

It consists of ten terms that are associated with new low-energy constants $L_1 - L_{10}$. Like all LECs, they encode the lack of knowledge about the short-distance properties of QCD dynamics. Furthermore, two terms involving so-called high-energy constants (HECs) appear. They do not involve Σ and have thus no physical relevance. They do, however, contribute as contact terms to correlation functions and are needed in the process of renormalization. In contrast to the LECs, the HECs do depend on the regulator that is used to handle the occurring divergencies; hence the name. The second term $H_2\mathrm{tr}(\chi\chi^\dagger)$ has yet another meaning: It contributes to the mass dependence of the quark condensate, which is a quantity that cannot be measured experimentally but is computable on the lattice. All twelve coupling constants are, in principle, calculable functions of the remaining parameters of QCD, which are the heavy-quark masses and the QCD scale Λ_{QCD}. De facto, they are determined by phenomenological input and by fitting lattice data to extrapolation formulae obtained by ChPT calculations.

In order to perform an actual computation, the chiral Lagrangian Eq. (1.30) is expanded in terms of the meson fields to read off Feynman rules and calculate Feynman diagrams. Dimensional counting according to Weinberg [45] shows that a connected diagram with N_d vertices of $\mathcal{O}(p^d)$, $d = 2, 4, \ldots$, and N_L loops is of order

$$D = 2N_L + 2 + \sum_d N_d(d - 2)\,, \tag{1.49}$$

that is, every loop contributes two additional powers of momenta to the diagram in question. In a NLO computation ($D = 4$), for example, one therefore needs only the

---

[1] The gauging process of $U(3)_L \otimes U(3)_R$ indeed reproduces the axial anomaly in ChPT and leads to the Wess-Zumino-Witten term $\mathcal{L}_{\mathrm{WZW}}$. It does not play a rôle in this thesis and is therefore left unspecified. Note also that not all operators are linearly independent in the $SU(2)$ case, and $\mathcal{L}_4$ could be simplified using Cayley–Hamilton trace relations [11].

tree-level diagrams of $\mathcal{L}_2$ and $\mathcal{L}_4$, and the one-loop diagrams of $\mathcal{L}_2$. The general pattern for this extended power counting scheme is (Note that $\mathcal{L}_6$ contains over 90 terms and calculations become extremely cumbersome.):

$$
\begin{aligned}
\text{LO:} \quad & \mathcal{L}_2^{\text{tree}} \\
\text{NLO:} \quad & \mathcal{L}_2^{1-\text{loop}},\ \mathcal{L}_4^{\text{tree}} \\
\text{NNLO:} \quad & \mathcal{L}_2^{2-\text{loop}},\ \mathcal{L}_4^{1-\text{loop}},\ \mathcal{L}_6^{\text{tree}} \\
& \quad \vdots \qquad\qquad \vdots
\end{aligned}
\tag{1.50}
$$

In the follwing chapter, the construction of ChPT is generalized to partially quenched ChPT, the effective theory for QCD with unequal sea and valence quark masses. Afterwards, it is shown how the effects of the lattice spacing can be accounted for. Lastly, ChPT is considered for different discretizations in the sea and the valence sector of the theory.

2. Chiral perturbation theory and the lattice

Starting point for lattice QCD is the Euclidean path integral formulation,

$$ Z = \int \mathcal{D}A\, \mathcal{D}\bar{q}\, \mathcal{D}q \, \mathrm{e}^{-S_G[A] - \int \mathrm{d}^4 x\, \bar{q}(\slashed{D} + m)q} \,, \tag{2.1} $$

where $S_G[A] = \int \mathrm{d}^4 x\, \mathcal{L}_{\mathrm{gauge}}$ denotes the gauge part of the QCD action. One discretizes the action using a Euclidean space-time lattice [20]. While the quark fields reside on the lattice points, the gauge fields are represented by $SU(3)$ matrices connecting two neighboring points. The lattice naturally regularizes the ill-defined path integral with an ultraviolet momentum cutoff inversely proportional to the lattice spacing a. Furthermore, by restricting the lattice to a finite extent L (with fixed boundary conditions), the theory becomes also infrared-regularized. Now, the path integral is finite, and it is possible to perform numerical computations using Monte-Carlo methods.

Correlation functions, hadron masses, and other quantities that are obtained from such simulations will in general depend on the regulators. Moreover, since the computational costs of lattice QCD simulations turn out not only to scale with positive powers of the volume and the inverse lattice spacing, but also to grow with decreasing quark masses, these simulations must still be performed at quark masses larger than those realized in nature. All in all, a connection to physical observables demands good control over the systematic errors stemming from the discretization, the finite volume, and the used quark masses.

A method to systematically study the lattice spacing effects is known as Symanzik's effective theory (SET), [3]. Symanzik showed that close to the continuum limit, lattice QCD can be described by an effective continuum theory with effective operators multiplying appropriate powers of the lattice spacing. SET is a systematic expansion in powers of the lattice spacing. Chiral perturbation theory on the other hand is an expansion in small momenta and in the light quark masses, and it seems therefore perfectly suitable to guide extrapolations to the physical point – given, one is in the mass regime of ChPT's validity. Using now the same spurion technique as for the construction of continuum chiral perturbation theory, one can match SET to ChPT and thus make the dependence on the lattice spacing explicit, order to order in the chiral expansion [5, 6, 10]. The finite lattice extent can also be taken into account by regarding ChPT in a finite volume [7–9]. In an actual lattice simulation, as will be shown below, one has the freedom of choosing different sea and valence quark masses. *Valence* quarks mean those quarks that compose hadrons, whereas *sea* quarks are the dynamical quarks appearing in quantum loop fluctuations. One might even go one step further and use a completely different discretization for the Dirac operator in the sea and in the valence sector.

The standard example to motivate these two approaches, is the pion two-point correlation function. A pion, being a pseudoscalar, can be represented by the interpolating

field

$$\pi^+(x) \equiv \bar{d}(x)\gamma_5 u(x) \, . \tag{2.2}$$

The correlator, then, is given by

$$
\begin{aligned}
\langle 0|\pi^-(x)\,\pi^+(0)|0\rangle &= \langle 0|\bar{u}(x)\gamma_5 d(x)\ \bar{d}(0)\gamma_5 u(0)|0\rangle \\
&= \frac{1}{Z}\int \mathcal{D}A\,\mathcal{D}\bar{q}\,\mathcal{D}q\,\left[\bar{u}(x)\gamma_5 d(x)\right]\left[\bar{d}(0)\gamma_5 u(0)\right]\,\mathrm{e}^{-S_G[A]-\int \bar{q}(\slashed{D}+m)q} \\
&= -\frac{1}{Z}\int \mathcal{D}A\,\mathrm{tr}\!\left[\gamma_5 G_d(x,0)\gamma_5 G_u(0,x)\right]\mathrm{e}^{-S_G[A]}\prod_q \det(\slashed{D}_{\mathrm{sea}}+m_{\mathrm{sea},q}) \\
&= -\left\langle \mathrm{tr}\!\left[\gamma_5 G_d(x,0)\gamma_5 G_u(0,x)\right]\right\rangle_{\mathrm{gauge}} \, .
\end{aligned}
\tag{2.3}
$$

From the second to the third line, the integration over the Grassmann-valued quark fields $\bar{q}$ and q yields the quark determinant. The quark propagators

$$G_q(x,y) = \left(\frac{1}{\slashed{D}_{\mathrm{val}}+m_{\mathrm{val},q}}\right)_{xy} \tag{2.4}$$

and the trace over spinor and color indices result from Wick-contracting the quarks within the interpolating fields. The last term indicates an averaging over the gauge configurations weighted with the quark determinant. As indicated with the subscripts *sea* and *val*, the quark masses and the Dirac operator enter in two different ways: once through the quark determinant and once through the quark propagators.

Generating statistically independent gauge configurations, which involves the sea masses, is the most time-consuming step in a lattice simulation. It is, however, independent of computing correlation functions, the step in which the valence masses enter. There is thus no reason on the lattice for not choosing $m_{\mathrm{sea}} \neq m_{\mathrm{val}}$, or even more drastically, $\slashed{D}_{\mathrm{sea}} \neq \slashed{D}_{\mathrm{val}}$.

The first scenario with $m_{\mathrm{sea}} \neq m_{\mathrm{val}}$ is referred to as *partial quenching*[2] [25–27, 11, 12]. Clearly, it violates the unitarity of the theory, but having in mind the mentioned computational costs, it makes sense to perform simulations at different valence quark masses while keeping the sea masses fixed, in contrast to varying both quark masses at the same time. Partially quenched simulations open the door to a wider range of feasible quark masses; the benefit, however, is that the corresponding effective theory, *partially quenched chiral perturbation theory* (PQChPT), involves the same low-energy constants as standard ChPT and yields also the same results in the unitarity-restoring limit of equal valence and sea quark masses. It is therefore possible to gain more information about the ChPT couplings, which again is necessary to perform a reliable extrapolation to the physical point.

An introduction to partially quenched QCD and its effective theory PQChPT will be given in the next Section 2.1. The aim is to parameterize the unphysical effects stemming from partial quenching. Since one recovers QCD by setting $m_{\mathrm{sea}} = m_{\mathrm{val}}$, one expects these effects to come with the difference of sea and valence quark masses.

---

[2] The term has its origin in the quenched approximation of QCD where the quark determinant cancels by giving the sea quarks an infinitely heavy mass.

The second scenario, in which computations are performed with different Dirac operators, $\slashed{D}_{\mathrm{sea}} \neq \slashed{D}_{\mathrm{val}}$, is called *mixed-action* (MA) or *hybrid-action* simulations. The motivation for doing so is, similarly to the partially quenched case, related to the computational effort. When discretizing the action, one inevitably has to give up some of the symmetries of continuum QCD. The most obvious one is rotational $O(4)$ invariance, which on the lattice reduces to a discrete subgroup. But also chiral symmetry can often not be preserved. The computationally cheap Wilson action [20], for instance, explicitly breaks this important symmetry through an additional term, the Wilson-term, which is introduced to prevent the so-called fermion doubling problem. On the other hand, Dirac operators of Ginsparg–Wilson type [13–16], for example, preserve chiral symmetry but are computationally very expensive [19]. An important aspect which favors the use of symmetry-preserving discretizations is the fact that the more symmetry one loses in the process of discretization, the stronger the operator mixing becomes on the lattice [12]. This, especially, is a crucial disadvantage for the computation of weak matrix elements [24]. Note that the operator mixing mainly depends on the symmetries of operators constructed from valence quarks. Further, the symmetry properties of correlation functions like Eq. (2.3) are entirely determined by the symmetry properties of the valence Dirac operator. In view of computing time, it therefore seems like a good compromise to choose a cheap discretization, like the Wilson action [20], in the sea sector, and more symmetry-preserving discretization in the valence sector [40, 47–49].

In mixed-action simulations, unitarity can – due to different lattice artifacts in the two sectors – *not* be restored by setting $m_{\mathrm{sea}} = m_{\mathrm{val}}$ [10, 31]. This stands in contrast to partially quenched simulations where the bare quark masses can always be tuned to yield the same renormalized quark mass. Near the continuum limit, however, it should be possible to construct an effective theory à la Symanzik and match it to an effective mixed-action chiral Lagrangian [23, 28, 29]. In this way, the unitarity-violating effects will become explicit in form of the lattice spacing attached to operators that depend either solely on the sea or the valence sector, or on those which mix both. The method of matching SET to ChPT, and how mixed-action ChPT is constructed are the topics of Section 2.2. Finally, in Chapter 3, the impact of the two unphysical effects, partial quenching and mixed actions, on physical observables will be studied using the example of the isospin-one scalar correlator. The calculation is extended in Chapter 4 to account for the finite volume, which will show to enhance the unphysical effects.

2.1. Partially quenched chiral perturbation theory

2.1.1. Constructing the effective theory

The construction of chiral perturbation theory was based on the symmetries of the underlying QCD Lagrangian. As a first step, it is thus imperative to formulate partially quenched QCD (PQQCD) – that is, to explicitly distinguish between sea and valence quarks – and to understand its symmetries. An elegant way was proposed by Morel [50]. Next to N_S sea and N_V valence quarks, he introduces N_V bosonic spin-$\frac{1}{2}$ *ghost* quarks
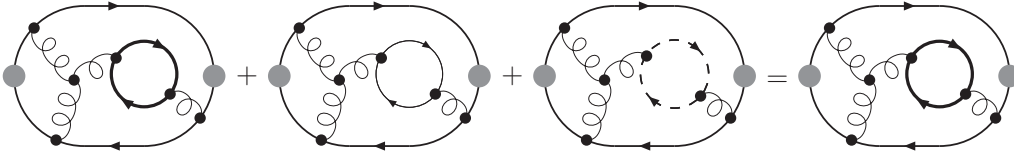
Figure 2.1.: A typical PQQCD diagram with sea, valence, and ghost quark loop contributions (illustrated with thick, thin, and dashed lines, respectively). Valence and ghost loops cancel leaving only sea quark loops.

(labeled in the following with $\tilde{q}$), which have the same mass as their valence counterparts. The fermionic part of the PQQCD Lagrangian then reads [11, 12]

$$\mathcal{L}_{\text{PQQCD}}^{\text{quark}} = \sum_{i=1}^{N_S} \bar{q}_{\text{sea}_i}(\slashed{D}_{\text{sea}} + m_{\text{sea}_i})q_{\text{sea}_i} + \sum_{j=1}^{N_V} \left[\bar{q}_{\text{val}_j}(\slashed{D}_{\text{val}} + m_{\text{val}_j})q_{\text{val}_j} + \tilde{q}_j^\dagger(\slashed{D}_{\text{val}} + m_{\text{val}_j})\tilde{q}_j \right]$$

$$\equiv \bar{q}(\slashed{D} + m)q\,, \tag{2.5}$$

where the quarks and their masses are collected as usual,

$$q^T = (q_{\text{sea}}, q_{\text{val}}, \tilde{q})\,, \quad \bar{q} = (\bar{q}_{\text{sea}}, \bar{q}_{\text{val}}, \tilde{q}^\dagger)\,, \quad m = \text{diag}\,(m_{\text{sea}}, m_{\text{val}}, m_{\text{val}})\,. \tag{2.6}$$

The two Dirac operators $\slashed{D}_{\text{sea}}$ and $\slashed{D}_{\text{val}}$ indicate the different discretizations one uses in mixed-action QCD. For PQQCD, however, they are the same.
Due to the bosonic nature of the ghost fields,

$$\int \mathcal{D}\tilde{q}^\dagger \mathcal{D}\tilde{q}\, e^{-\int \tilde{q}_{\text{val}}^\dagger(\slashed{D}_{\text{val}} + m_{\text{val}})\tilde{q}_{\text{val}}} = \frac{1}{\det(\slashed{D}_{\text{val}} + m_{\text{val}})}\,, \tag{2.7}$$

the valence and ghost quark determinants cancel exactly,

$$Z_{\text{PQQCD}} = \int \mathcal{D}A\, \mathcal{D}\bar{q}\, \mathcal{D}q\, e^{-S_G[A] - \int d^4 x\, \bar{q}(\slashed{D} + m)q} = \int \mathcal{D}A\, e^{-S_G[A]} \det(\slashed{D}_{\text{sea}} + m_{\text{sea}})\,. \tag{2.8}$$

In the language of diagrams, valence and ghost loops cancel, since they come with a relative minus sign, leaving only the sea quark loops. This is illustrated in Fig. 2.1.
The partially quenched theory is sick. It is not possible to rotate back to Minkowski space without violating the spin-statistics theorem [11, 12]. Nevertheless, since lattice QCD works in Euclidean space, one can use the corresponding effective theory, PQChPT, as a tool for obtaining fitting formulae for these simulations. In this way – as in standard ChPT – one can fix the low-energy constants and then extrapolate to the point of equal sea and valence masses.
Having the Lagrangian at hand, one can now analyze its symmetries. Besides a $U(1)_V$ and an anomalous $U(1)_A$ symmetry, the massless PQQCD Lagrangian exhibits the *graded* symmetry[3] [27, 12]

$$G \equiv SU(N_S + N_V | N_V)_L \otimes SU(N_S + N_V | N_V)_R\,, \tag{2.9}$$

---

[3] The exact symmetry is actually not that of Eq. (2.9). This is due to the fact that the ghost fields $\tilde{q}$ and $\tilde{q}^\dagger$ are not independent, that is, their chiral components do not transform independently as it is the case with fermionic quarks. This is necessary for the convergence of the ghost functional integral. However, the results of PQChPT based on this apparent symmetry are identical to those received by using the true symmetry group [27].

which will be the starting point for the construction of partially quenched chiral perturbation theory. Since in QCD, chiral symmetry is spontaneously broken, and QCD is contained in PQQCD, one assumes the symmetry G to be spontaneously broken down to the graded vector symmetry subgroup,

$$G \longrightarrow H = SU(N_S + N_V | N_V)_V \,. \tag{2.10}$$

Before parameterizing the associated $(N_S + 2N_V)^2 - 1$ Goldstone fields and building invariant scalars using the trace technique introduced in Chapter 1, it is useful to get familiar with some properties of graded groups [51, 11]. Consider for example the matrix $U \in SU(N_S + N_V | N_V)$,

$$U = \begin{pmatrix} A & B \\ C & D \end{pmatrix} \,, \tag{2.11}$$

with the following matrix dimensions:

$$
\begin{aligned}
&A \colon\ (N_S + N_V) \times (N_S + N_V) \,, & &B \colon\ (N_S + N_V) \times N_V \\
&C \colon\ N_V \times (N_S + N_V) \,, & &D \colon\ N_V \times N_V
\end{aligned}
$$

The term *graded* refers to the fact that A and D contain commuting, and B and C contain anticommuting variables. U is a unitary matrix if complex conjugation is defined as $(U_{ab} U_{cd})^* = U_{cd}^* U_{ab}^*$; and thus $(U_1 U_2)^\dagger = U_2^\dagger U_1^\dagger$. For graded matrices, the trace generalizes to a "supertrace",

$$\mathrm{str}\, U = \mathrm{tr}\, A - \mathrm{tr}\, D \,, \tag{2.12}$$

to maintain cyclicity, e. g., $\mathrm{str}\,(U_1 U_2 U_3) = \mathrm{str}\,(U_2 U_3 U_1)$. One conveniently introduces a grading factor ϵ_a to write

$$\mathrm{str}\, U = \sum_{a=1}^{N_S + 2N_V} \epsilon_a U_{aa} \,, \tag{2.13}$$

that is, $\epsilon_a = +1$ for $a \in \{1, \ldots, N_S + N_V\}$, and $\epsilon_a = -1$ for $a \in \{N_S + N_V + 1, \ldots, N_S + 2N_V\}$. Similar to the trace, the determinant is generalized to a "superdeterminant",

$$\mathrm{sdet}\, U = \exp\left(\mathrm{str}\,\ln U\right) = \frac{\det(A - BD^{-1}C)}{\det D} \,, \tag{2.14}$$

which satisfies $\mathrm{sdet}\,(U_1 U_2) = \mathrm{sdet}\, U_1 \cdot \mathrm{sdet}\, U_2$.

Now back to the construction of PQChPT. The original argument of Weinberg for constructing a local effective field theory (EFT) is based on the unitarity of the underlying theory [45]. Since PQQCD is not unitary, one has to assume that there exists a local EFT which satisfies the symmetries of PQQCD and contains the corresponding Goldstone fields as the relevant degrees of freedom [11]. One therefore parameterizes these Goldstone fields as in Chapter 1 by a unitary matrix

$$\Sigma(x) = \exp\left(\frac{2i}{f}\Phi(x)\right) \,, \tag{2.15}$$

with

$$\Phi(x) = \sum_a \Phi^a(x) T^a = \begin{pmatrix} \varphi(x) & \eta(x) \\ \bar{\eta}(x) & \tilde{\varphi}(x) \end{pmatrix} . \qquad (2.16)$$

The matrix Σ transforms under the graded symmetry group G as

$$\Sigma \xrightarrow{G} L \Sigma R^\dagger, \qquad \Sigma^\dagger \xrightarrow{G} R \Sigma^\dagger L^\dagger, \qquad (L, R) \in G. \qquad (2.17)$$

Note that the constraint $\mathrm{sdet}\,\Sigma = 1$ implies $\mathrm{str}\,\Phi = \mathrm{tr}\,\varphi - \mathrm{tr}\,\tilde{\varphi} = 0$. The Nambu–Goldstone "bosons" $\Phi(x)$ are either bosonic or fermionic, depending on the quark content. Nevertheless, they will be referred to as mesons. The quark-antiquark Nambu–Goldstone bosons (NGBs) are contained in φ, while $\tilde{\varphi}$ consists of ghost-antighost NGBs. η and $\tilde{\eta}$ contain the quark-antighost and ghost-antiquark fermionic NGBs, respectively. The T^a are the $N_S + 2N_V$ supertraceless generators of H. In practice, working in this basis is rather inconvenient. Instead, one usually proceeds as follows. First, the constraint $\mathrm{sdet}\,\Sigma = 1$ is removed, and hence $\Sigma \in U(N_S + N_V | N_V)$. This is the equivalent to keeping the heavy η' meson in unquenched ChPT. Further, one parameterizes the diagonal of Φ in terms of the single-flavor fields instead of the physical fields[4]:

$$(\Phi_{ab}) = \frac{1}{\sqrt{2}} (\pi_{ab}) = \frac{1}{\sqrt{2}} \begin{pmatrix} U & \pi^+ & K^+ & Q_{ux} & Q_{uy} & T_{u\tilde{x}} & T_{u\tilde{y}} \\ \pi^- & D & K^0 & Q_{dx} & Q_{dy} & T_{d\tilde{x}} & T_{d\tilde{y}} \\ K^- & \bar{K}^0 & S & Q_{sx} & Q_{sy} & T_{s\tilde{x}} & T_{s\tilde{y}} \\ Q_{ux}^\dagger & Q_{dx}^\dagger & Q_{sx}^\dagger & X & P^+ & R_{x\tilde{x}} & R_{x\tilde{y}} \\ Q_{uy}^\dagger & Q_{dy}^\dagger & Q_{sy}^\dagger & P^- & Y & R_{y\tilde{x}} & R_{y\tilde{y}} \\ T_{u\tilde{x}}^\dagger & T_{d\tilde{x}}^\dagger & T_{s\tilde{x}}^\dagger & R_{x\tilde{x}}^\dagger & R_{y\tilde{x}}^\dagger & \tilde{X} & \tilde{P}^+ \\ T_{u\tilde{y}}^\dagger & T_{d\tilde{y}}^\dagger & T_{s\tilde{y}}^\dagger & R_{x\tilde{y}}^\dagger & R_{y\tilde{y}}^\dagger & \tilde{P}^- & \tilde{Y} \end{pmatrix} \qquad (2.18)$$

Here, the indices u, d, and s refer to up, down, and strange sea quarks. x and y denote valence quarks, and $\tilde{x}$ and $\tilde{y}$ label the corresponding ghost quarks. The diagonal elements of $\Phi(x)$, namely U, D, S, X, Y, $\tilde{X}$, and $\tilde{Y}$, are the single-flavor states $u\bar{u}$, $d\bar{d}$ and so forth. X, P^+, P^-, and Y stand for the valence-valence bound states $x\bar{x}$, $x\bar{y}$, $y\bar{x}$, and $y\bar{y}$. Similarly, $\tilde{X}$, $\tilde{P}^+$, $\tilde{P}^-$, and $\tilde{Y}$ are the ghost-ghost states $\tilde{x}\tilde{x}^\dagger$, $\tilde{x}\tilde{y}^\dagger$, $\tilde{y}\tilde{x}^\dagger$, and $\tilde{y}\tilde{y}^\dagger$. Q, R, and T denote the sea-valence, valence-ghost, and sea-ghost bound states, respectively.
Another notation for π_{ab} that will be employed later in Chapter 3 is the use of corresponding quark labels instead of the numbering from 1 to 7. For example, $K^+ = \pi_{us}$, $X = \pi_{xx}$, $P^- = \pi_{yx}$, $Y = \pi_{yy}$, and so forth.
The super-singlet field Φ_0 can now be defined as the supertrace of Φ,

$$\Phi_0 = \frac{1}{\sqrt{N_S}} \mathrm{str}\,\Phi. \qquad (2.19)$$

Due to the axial anomaly, the super-singlet is a heavy meson. This is accounted for in the effective Lagrangian by giving it a large mass $m_0 \sim \Lambda_{\mathrm{had}}$,

$$\mathcal{L}_{\mathrm{PQChPT}} \to \mathcal{L}_{\mathrm{PQChPT}} + \frac{m_0^2}{N_S} (\mathrm{str}\,\Phi)^2 . \qquad (2.20)$$

---

[4] The number of valence quarks is not fixed, since they do not contribute to the dynamics. $\Phi(x)$, however, is given for $N_V = 2$, which is sufficient for the present calculations.

At the end of a calculation, one projects out the singlet by sending $m_0 \to \infty$, [27].

The chiral symmetry of the PQQCD Lagrangian was found to be $G = SU(N_S + N_V|N_V)_L \otimes SU(N_S + N_V|N_V)_R$. The task is now to construct the most general local, Euclidean-invariant, and G-invariant Lagrangian. In order to do that, the mass matrix m of Eq. (2.6) is promoted to a spurion $\chi = 2B_0(s + ip)$, which transforms under G as $\chi \longrightarrow L\chi R^\dagger$. In the end, χ will be set to its constant value, $\chi = 2B_0 m$. As before, the building blocks are Σ, $D_\mu\Sigma$, χ, their hermitian conjugate counterparts, and $L_{\mu\nu}$ and $R_{\mu\nu}$. The covariant derivative D_μ and the field-strength tensors $L_{\mu\nu}$ and $R_{\mu\nu}$ involving the sources l_μ and r_μ are just graded generalizations of the corresponding terms in ChPT. It turns out that the PQ chiral Lagrangian, $\mathcal{L}_{\text{PQChPT}} \equiv \mathcal{L}_2 + \mathcal{L}_4 + \ldots$, is almost identical to the standard ChPT version, with slight modifications [11]:

$$\mathcal{L}_2 = \frac{f^2}{4}\text{str}(D_\mu\Sigma\, D_\mu\Sigma^\dagger) - \frac{f^2}{4}\text{str}(\chi\Sigma^\dagger + \Sigma\chi^\dagger) + m_0^2\Phi_0^2 \tag{2.21}$$

$$\begin{aligned}
\mathcal{L}_4 = &-L_1[\text{str}(D_\mu\Sigma\, D_\mu\Sigma^\dagger)]^2 - L_2\,\text{str}(D_\mu\Sigma\, D_\nu\Sigma^\dagger)\,\text{str}(D_\mu\Sigma\, D_\nu\Sigma^\dagger) \\
&+ L_3\,\text{str}(D_\mu\Sigma\, D_\mu\Sigma^\dagger\, D_\nu\Sigma\, D_\nu\Sigma^\dagger) \\
&+ L_4\,\text{str}(D_\mu\Sigma\, D_\mu\Sigma^\dagger)\,\text{str}(\chi\Sigma^\dagger + \Sigma\chi^\dagger) + L_5\,\text{str}(D_\mu\Sigma\, D_\mu\Sigma^\dagger[\chi\Sigma^\dagger + \Sigma\chi^\dagger]) \\
&- L_6[\text{str}(\chi\Sigma^\dagger + \Sigma\chi^\dagger)]^2 - L_7[\text{str}(\chi\Sigma^\dagger - \Sigma\chi^\dagger)]^2 \\
&- L_8\,\text{str}(\chi\Sigma^\dagger\chi\Sigma^\dagger + \Sigma\chi^\dagger\Sigma\chi^\dagger) \\
&+ iL_9\text{str}(L_{\mu\nu}D_\mu\Sigma\, D_\nu\Sigma^\dagger + R_{\mu\nu}D_\mu\Sigma^\dagger\, D_\nu\Sigma) + L_{10}\,\text{str}(L_{\mu\nu}\Sigma\, R_{\mu\nu}\Sigma^\dagger) \\
&+ H_1\,\text{str}(L_{\mu\nu}L_{\mu\nu} + R_{\mu\nu}R_{\mu\nu}) - H_2\,\text{str}(\chi\chi^\dagger) + \mathcal{L}_{\text{WZW,PQ}} \\
&+ L_{\text{PQ}}\mathcal{O}_{\text{PQ}}
\end{aligned} \tag{2.22}$$

Obviously, traces are replaced by supertraces. At $\mathcal{O}(p^4)$, one finds a new term $L_{\text{PQ}}\mathcal{O}_{\text{PQ}}$ containing four derivatives. In unquenched ChPT for $N_S \le 3$, that term was not independent from the other terms in the Lagrangian, which could be seen using Cayley–Hamilton trace relations [11]. These, however, do not hold for graded matrices. Additionally to the mass term $m_0^2\Phi_0^2$ of the super-singlet, one should also write down a kinetic term. In fact, since besides parity, Φ_0 is not constrained by symmetry, one should multiply every term in Eq. (2.21) by an arbitrary even function of Φ_0 coming with new free parameters [26]. This, however, is unnecessary because the dependence on these parameters vanishes if the super-singlet is decoupled by sending $m_0 \to \infty$, [27].

Lastly, it is very important mentioning that the low- and high-energy constants L_i and H_i are the same as in unquenched ChPT. The reason is simply because QCD is contained in PQQCD, and any correlation function with valence masses set equal to the sea masses is identical to the corresponding QCD correlation function. PQChPT will thus prove to be a powerful, though unphysical tool, to determine the free parameters of ChPT by varying either the sea or the valence masses. Later, this will become clearer in the example of the valence-valence pion mass given to NLO.

2.1.2. Tree-level meson masses and propagators

In the following computations, the sources l_μ, r_μ, and the scalar density p are not needed. The covariant derivatives D_μ in $\mathcal{L}_{\text{PQChPT}}$ are therefore substituted for the normal partial derivatives ∂_μ, and the notation is changed to $\chi \equiv 2B_0 m$, with the diagonal mass matrix m of Eq. (2.6). When reading off the meson masses, the notation $\chi \equiv M^2$ is used. The tree-level meson masses and propagators are obtained from $\mathcal{L}_2$ by expanding it up to quadratic order in the meson fields $\Phi(x) = \frac{1}{\sqrt{2}}\pi(x)$,

$$\mathcal{L}_2^{\text{LO}} = \frac{1}{2}\text{str}(\partial_\mu \pi \, \partial_\mu \pi) + \frac{1}{2}\text{str}(\chi \pi^2) + \frac{m_0^2}{2N_S}(\text{str}\,\pi)^2 \,. \tag{2.23}$$

For the flavor-off-diagonal states, the charged mesons, one finds the tree-level squared meson masses[5]

$$M_{ab}^2 \equiv \frac{M_a^2 + M_b^2}{2} = B_0(m_a + m_b)\,, \qquad a \neq b\,, \tag{2.24}$$

and the propagators

$$G_{ab}^{\text{con}}(p^2) \equiv \int \mathrm{d}^4 x \, e^{-ipx} \, \langle \pi_{ab}(x)\pi_{ba}(0)\rangle^{\text{con}} = \frac{\epsilon_b}{p^2 + M_{ab}^2}\,, \qquad a \neq b\,, \tag{2.25}$$

where ϵ_b takes into account that the ghosts come with an extra minus sign from the supertrace Eq. (2.13),

$$\epsilon_b = \begin{cases} +1, & \text{if } b \text{ is a sea or a valence index}\,, \\ -1, & \text{if } b \text{ is a ghost index}\,. \end{cases} \tag{2.26}$$

This is the first sign of sickness of the partially quenched theory. While the bosonic propagators involving only sea and valence quarks have the normal "physical" sign and thus the usual Klein–Gordon form, the ghost-ghost propagators have an unphysical sign. In particular, the fermionic propagators can have either sign:

$$\frac{1}{p^2 + M_{ab}^2} = \begin{cases} G_{ab}^{\text{con}} = G_{ba}^{\text{con}}\,, & ab = SS,\, SV,\, VV \\ -G_{ab}^{\text{con}} = -G_{ba}^{\text{con}}\,, & ab = GG \\ -G_{ab}^{\text{con}} = G_{ba}^{\text{con}}\,, & ab = SG,\, VG \end{cases} \tag{2.27}$$

However, it is these unphysical minus signs that will lead to cancelations between closed valence and closed ghost loop contributions. The propagators Eq. (2.27) are referred to as connected propagators in terms of quark-flow:

$$G_{ab}^{\text{con}}(p^2) = \overset{a}{\underset{b}{\rule{3cm}{0pt}}} \tag{2.28}$$

---

[5] In what follows, the sea masses M_1, M_2, and M_3 are denoted by M_u, M_d, M_s). Similarly, the valence/ghost ones $M_4 = M_6$ and $M_5 = M_7$ read M_x and, respectively, M_y.

The propagators of the flavor-diagonal states, the neutral mesons, are not that easily calculable due to the super-singlet that mixes the neutral single-flavor states U, D, and S. The corresponding part of the Lagrangian reads

$$\mathcal{L}_2^{N,\text{LO}} = \sum_a \frac{\epsilon_a}{2} \left(\partial_\mu \pi_{aa}\, \partial_\mu \pi_{aa} + \chi_a \pi_{aa}^2 \right) + \frac{m_0^2}{2N_S} \left(\sum_a \epsilon_a \pi_{aa} \right)^2 , \tag{2.29}$$

where a runs from 1 to $N_S + 2N_V$. The full neutral propagator is deduced from

$$G_N^{-1} = G_0^{-1} + H , \tag{2.30}$$

where G_0^{-1} is the free propagator,

$$(G_0^{-1})_{ab} = (p^2 + M_a^2)\epsilon_a \delta_{ab} , \tag{2.31}$$

which stems from the first sum in Eq. (2.29). It equals the propagator Eq. (2.25) for charged mesons. The second sum leads to a non-diagonal contribution

$$H_{ab} = \frac{m_0^2}{N_S} \epsilon_a \epsilon_b . \tag{2.32}$$

This term can be treated as a two-point vertex, which leads to a geometric sum. The result for the inverse of G_N^{-1} is [26, 52]

$$G_N = G_0 - \frac{G_0 H G_0}{1 + \text{tr}\,(G_0 H)} . \tag{2.33}$$

In the denominator, valence and ghost contributions to the trace cancel due to the opposite sign of ϵ_a in Eq. (2.31). The full neutral propagator thus becomes

$$G_{ab}^N(p^2) \equiv \int \mathrm{d}^4x\, \mathrm{e}^{-ipx} \langle \pi_{aa}(x)\pi_{bb}(0) \rangle \tag{2.34}$$

$$= \frac{\epsilon_a \delta_{ab}}{p^2 + M_a^2} - \frac{m_0^2}{N_S} \frac{1}{(p^2 + M_a^2)(p^2 + M_b^2)} \frac{1}{1 + \frac{m_0^2}{N_S} \sum_{i=1}^{N_S} \frac{1}{p^2 + M_i^2}} .$$

Diagrammatically, it can be represented by the free propagator (connected contribution) plus a sum of so-called hairpin diagrams containing m_0^2 insertions (disconnected contributions) with sea quarks running in the loops:

$$\tag{2.35}$$

The diagonal elements G_{aa}^N seem to contain double poles, which is unphysical when restricting to the sea quark sector $a = \text{sea}$. Thus, there must be hidden cancelations coming from the denominator of the last fraction [11]. This denominator, involving the sum over the sea sector, is a third-order polynomial in p^2. It has poles at the physical masses for the π^0, η, and η' mesons. One can rewrite Eq. (2.34) and finally find a nice form for the neutral propagator [52],

$$
G_{ab}^N(p^2) \equiv \int \mathrm{d}^4 x\, \mathrm{e}^{-ipx} \left\langle \pi_{aa}(x)\pi_{bb}(0) \right\rangle = \delta_{ab} G_{ab}^{\mathrm{con}}(p^2) + G_{ab}^{\mathrm{disc}}(p^2)
$$

$$
= \frac{\epsilon_a \delta_{ab}}{p^2 + M_a^2} - \frac{m_0^2}{N_S} \frac{1}{(p^2 + M_a^2)(p^2 + M_b^2)} \frac{(p^2 + M_u^2)(p^2 + M_d^2)(p^2 + M_s^2)}{(p^2 + M_{\pi_0}^2)(p^2 + M_\eta^2)(p^2 + M_{\eta'}^2)}.
$$
(2.36)

For clarity, the number of sea flavors, N_S, is not written out explicitly. Note that the propagator for $N_S = 2$ sea flavors can be obtained simply by dropping the factors $(p^2 + \chi_s)$ and the $(p^2 + \chi_\eta)$.

For $N_S = 3$, the physical sea meson tree-level masses read (up to corrections of order M^4/m_0^2)

$$
M_{\pi_0}^2 = \frac{M_u^2 + M_d^2 + M_s^2}{3} - \frac{1}{3}\sqrt{M_u^4 + M_d^4 + M_s^4 - M_u^2 M_d^2 - M_u^2 M_s^2 - M_d^2 M_s^2},
$$

$$
M_\eta^2 = \frac{M_u^2 + M_d^2 + M_s^2}{3} + \frac{1}{3}\sqrt{M_u^4 + M_d^4 + M_s^4 - M_u^2 M_d^2 - M_u^2 M_s^2 - M_d^2 M_s^2}, \quad (2.37)
$$

$$
M_{\eta'}^2 = m_0^2 + \frac{1}{3}\left(M_u^2 + M_d^2 + M_s^2\right).
$$

Now, it is convenient to integrate out the super-singlet. In the limit $m_0 \to \infty$, the neutral propagator reduces to [52]

$$
G_{ab}^N(p^2) = \frac{\epsilon_a \delta_{ab}}{p^2 + M_a^2} - \frac{1}{N_S} \frac{(p^2 + M_u^2)(p^2 + M_d^2)(p^2 + M_s^2)}{(p^2 + M_a^2)(p^2 + M_b^2) \cdot (p^2 + M_{\pi_0}^2)(p^2 + M_\eta^2)}, \quad (2.38)
$$

and the mentioned cancelations become obvious. When a and b denote sea flavors (u, d, or s), they cancel the corresponding terms in the numerator, and the propagator can be written as a sum of single pole propagators using partial fraction decomposition. This cancelation makes sense, since the sea sector should not know anything about the valence and the ghost sector of the theory. On the contrary, if $a = b$ denote a valence or a ghost quark, there is a double pole. This is a clear manifestation that partially quenched QCD is sick. Problems that arise with this unphysical pole will be discussed in a moment, but first the commonly used limit of isospin symmetry in the sea sector ($M_u = M_d$) will be shown. The tree-level pion and the eta mass simplify to

$$
M_{\pi_0} = M_u, \qquad M_\eta^2 = \frac{M_u^2 + 2M_s^2}{3}, \quad (2.39)
$$

and hence, the neutral propagator reduces to

$$
G_{ab}^N(p^2) = \frac{\epsilon_a \delta_{ab}}{p^2 + M_a^2} - \frac{1}{N_S} \frac{(p^2 + M_u^2)(p^2 + M_s^2)}{(p^2 + M_a^2)(p^2 + M_b^2) \cdot (p^2 + M_\eta^2)}. \quad (2.40)
$$

A further simplification would be the total degeneracy $M_u = M_d = M_s$, for which the pion and the eta meson are degenerate with all single-flavor states U, D, and S, and thus the factors $(p^2 + M_s^2)$ and $(p^2 + M_\eta^2)$ cancel each other.

It is useful in an actual computation to rewrite the disconnected part of the propagator with the help of partial fraction decomposition. The residues one finds are denoted as [53]

$$
R_v\!\left(\begin{smallmatrix} u,d,s \\ a,b,\pi_0,\eta \end{smallmatrix}\right) \equiv \frac{\prod\limits_{i=u,d,s}(M_i^2 - M_v^2)}{\prod\limits_{\substack{j=a,b,\pi_0,\eta \\ j\neq v}}(M_j^2 - M_v^2)} \quad \text{and} \quad D_v^w\!\left(\begin{smallmatrix} u,d,s \\ a,b,\pi_0,\eta \end{smallmatrix}\right) \equiv -\frac{\partial}{\partial M_w^2} R_v\!\left(\begin{smallmatrix} u,d,s \\ a,b,\pi_0,\eta \end{smallmatrix}\right). \quad (2.41)
$$

The upper and lower neutral meson states in the parenthesis of R_v correspond to the product indices i and j, respectively, where the factor with $j = v$ is excluded from the product in the denominator.

For flavors $a \neq b$, Eq. (2.38) contains only single poles and can be expressed as

$$
G_{ab}^{\mathrm{disc}}(p^2) = -\frac{1}{N_S} \sum_{v=a,b,\pi_0,\eta} \frac{R_v\!\left(\begin{smallmatrix} u,d,s \\ a,b,\pi_0,\eta \end{smallmatrix}\right)}{p^2 + M_v^2} . \quad (2.42)
$$

On the other hand, if $a = b$, the double pole leads to a different decomposition,

$$
G_{aa}^{\mathrm{disc}}(p^2) = -\frac{1}{N_S} \frac{R_a\!\left(\begin{smallmatrix} u,d,s \\ \pi_0,\eta \end{smallmatrix}\right)}{(p^2 + M_a^2)^2} - \frac{1}{N_S} \sum_{v=a,\pi_0,\eta} \frac{D_v^a\!\left(\begin{smallmatrix} u,d,s \\ a,\pi_0,\eta \end{smallmatrix}\right)}{p^2 + M_v^2} . \quad (2.43)
$$

Clearly, the first term vanishes when a denotes a sea meson. For $a \neq$ sea, however, the unphysical double pole comes with factors of $M_{\mathrm{sea}}^2 - M_{val}^2 = 2B_0(m_{\mathrm{sea}} - m_{\mathrm{val}}) \equiv \Delta_{\mathrm{PQ}}^2$, as anticipated, and thus vanishes only in the limit of equal valence and sea quark masses. Δ_{PQ} can therefore be regarded as a characteristic parameter for the effects of partial quenching. Intuitively, it seems plausible to keep this difference small to avoid large unphysical effects, and indeed, one quickly realizes that the double pole affects many observables. As an example, the valence-valence pion mass to one-loop order for degenerate sea ($M_u = M_d = \ldots \equiv M_{\mathrm{sea}}$) and degenerate valence quark masses ($M_x = M_y \equiv M_{\mathrm{val}}$) is given [54]:

$$
\begin{aligned}
\frac{M_x^{2,\,\mathrm{NLO}}}{M_x^{2,\,\mathrm{tree}}} = 1 &+ \frac{1}{16\pi^2 f^2 N_S}\left[(2M_{\mathrm{val}}^2 - M_{\mathrm{sea}}^2)\ln\!\left(\frac{M_{\mathrm{val}}^2}{\mu^2}\right) + (M_{\mathrm{val}}^2 - M_{\mathrm{sea}}^2) \right] \\
&+ \frac{8N_S}{f^2}\left[2L_6^r - L_4^r\right] M_{\mathrm{sea}}^2 + \frac{8}{f^2}\left[2L_8^r - L_5^r\right] M_{\mathrm{val}}^2
\end{aligned} \quad (2.44)
$$

Here, the effect of the double pole is an infrared divergence of the so-called chiral logarithm when sending the valence mass to zero at fixed sea mass. The chiral limit can therefore only be approached if the ratio of valence and sea mass is held constant.

There are many observables which are strongly affected by the double pole, for instance the nucleon-nucleon potential [55] and the isospin-one scalar two-point function [34, 35, 38]. The present work focuses on this scalar correlator. The impact of partial quenching

as well as the use of mixed actions (the topic of the next section) is studied in Chapters 3 and 4.

Two last remarks are due. First, by setting the valence mass equal to the sea mass in Eq. (2.44), one obtains the known expression from standard ChPT containing no infrared-divergent logarithm [2].

The second remark concerns the determination of the low-energy constants L_i. When using fitting formulae for lattice simulations that are obtained from partially quenched ChPT, one has more different masses at hand and thus more knobs to turn compared to standard unquenched ChPT. In the example given above, one can vary either the sea or the valence mass to determine $2L_6^r - L_4^r$ or $2L_8^r - L_5^r$, whereas with $M_{\text{sea}} = M_{\text{val}}$, one has only access to the combination $N_S [2L_6^r - L_4^r] + [2L_8^r - L_5^r]$.

2.2. Mixed-action chiral perturbation theory

The aim of this section is to incorporate the lattice spacing into standard and partially quenched ChPT, and to generalize the considerations to the scenario of Wilson quarks in the sea and Ginsparg-Wilson quarks in the valence sector. The resulting mixed-action chiral perturbation theory then allows to make the unitarity-violating effects of partial quenching and the use of different discretizations explicit. An analysis of the scalar correlator, a quantity that is strongly afflicted by these effects, follows in Chapters 3 and 4.

2.2.1. Matching Symanzik's effective theory

The idea of how to take the lattice spacing into account in chiral perturbation theory is very similar to the construction of ChPT itself [5, 6]. There, the quark masses were treated as a perturbation to the chirally invariant Lagrangian. Promoting the quark mass matrix to a spurion had then allowed for the construction of an effective Lagrangian made of chirally invariant terms and to reproduce the correct pattern of symmetry breaking of the QCD Lagrangian when setting the masses to their physical values. Now, concerning the lattice spacing, one faces a two-step matching process. At first, one writes down the Symanzik's effective theory (SET), which is a systematic expansion in the lattice spacing for the used lattice action. Then, one applies a spurion analysis, as it is done for the quark masses, to every term in the Symanzik expansion in order to map the symmetries and the pattern of symmetry breaking from the SET to an effective chiral Lagrangian. Finally, the spurions are assigned to their constant values, and thus the lattice spacing dependence is made explicit. Note that symmetry breaking in this context does not only refer to chiral symmetry but also to rotational $O(4)$ invariance and to other symmetries like flavor symmetry which may not be respected by the lattice action.

It is now time to describe the outlined procedure in more detail. Symanzik showed that at momenta much smaller than the lattice cutoff, $p \ll \frac{\pi}{a}$, the lattice theory can be described by an effective continuum theory [3]. The resulting effective action,

$$S_{\text{Sym}} = S_0 + a S_1 + a^2 S_2 + \dots ,\qquad(2.45)$$

consists, by construction, of the continuum dimension-zero QCD action S_0 and of higher dimensional effective operators contained in $S_1, S_2, \ldots$ which multiply appropriate powers of the lattice spacing a. The leading term in the expansion is S_0, which is why, for sufficiently small a (and quark masses m), the lattice theory exhibits the same spontaneous symmetry breaking pattern as the continuum theory [5, 6], and the low-energy dynamics are therefore still dominated by the usual pseudo-Goldstone bosons (the light mesons) stemming from the continuum term S_0. They now receive their small masses from the explicit chiral symmetry breaking quark masses *and* from discretization effects. The Symanzik action consists of all possible operators compatible with the symmetries of the underlying lattice theory, that is, the SET will inevitably contain those operators which respect the symmetries of the corresponding continuum action and those which break them. In order to match the SET to an effective chiral Lagrangian [5, 6], one makes use of the familiar spurion analysis. Promoting the constant prefactors in symmetry breaking terms to spurion fields with appropriate behavior under chiral transformations renders these terms chirally invariant. The chiral Lagrangian can then be constructed from the Goldstone fields and these spurions.

Take for example the Wilson action for unquenched QCD and consider the leading correction to the continuum term appearing in S_1 [4],

$$ac_1 \int \mathrm{d}^4x\, \bar{q}(x) i\sigma_{\mu\nu} G_{\mu\nu}(x) q(x) \,, \tag{2.46}$$

which is nothing but a Pauli term containing the field-strength tensor $G_{\mu\nu}$ and an unknown coefficient c_1. This term can be made invariant under chiral transformations by promoting ac_1 to a complex spurion field A,

$$ac_1\, \bar{q} i\sigma_{\mu\nu} G_{\mu\nu} q \rightarrow \bar{q}_L i\sigma_{\mu\nu} G_{\mu\nu} A q_R + \bar{q}_R i\sigma_{\mu\nu} G_{\mu\nu} A^\dagger q_L \,, \tag{2.47}$$

and letting it transform as

$$A \xrightarrow{G} L\, A\, R^\dagger \,, \qquad A^\dagger \xrightarrow{G} R\, A^\dagger L^\dagger \,. \tag{2.48}$$

This is exactly the same transformation behavior that was imposed on the mass matrix m in order to make the continuum Lagrangian chirally invariant. Consequently, (2.48) results in analogous terms in the chiral Lagrangian, for instance at leading order in ChPT,

$$-\frac{f^2 W_0}{2} \mathrm{tr}(A\Sigma^\dagger + \Sigma A^\dagger) \,, \tag{2.49}$$

where W_0 denotes a new low-energy constant similar to B_0. The spurion A is now set to its constant value, $A \rightarrow ac_1 \mathbb{1}_{N_S \times N_S}$, and c_1 is absorbed into W_0. Comparing the resulting term to the mass term,

$$-\hat{a}\frac{f^2}{4} \mathrm{tr}(\Sigma^\dagger + \Sigma) \,, \qquad \hat{a} \equiv 2W_0 a \,, \tag{2.50}$$

$$-\frac{f^2}{4} \mathrm{tr}(\chi\Sigma^\dagger + \Sigma\chi) \,, \qquad \chi \equiv 2B_0 m \,, \tag{2.51}$$

shows, that this order-a effect can be absorbed into the quark mass matrix according to

$$m \to m' = m + \frac{W_0}{B_0} a \mathbb{1}_{N_S \times N_S} \,. \tag{2.52}$$

Note that the Wilson action contains the so-called Wilson term, which explicitly breaks chiral symmetry. In the SET, this corresponds to a dimension-three operator $c\,\bar{q}q$ multiplying the inverse lattice spacing, where c is an unknown constant. The bare lattice quark masses m_0 which occur in the action therefore receive an additive mass renormalization c/a. Commonly, one uses a vanishing pion mass for the definiton of the lattice renormalized quark masses

$$M_\pi^2 = 2B_0 m' \qquad \Leftrightarrow \qquad m' = Z_m\left(m_0 - \frac{c}{a}\right) = 0\,. \tag{2.53}$$

In this way, the critical mass $m_c = \frac{c}{a}$ automatically accounts for the order-a shifts in Eq. (2.52).

The mentioned remaining $\mathcal{O}(a)$ terms in the effective Lagrangian can be simply written down by copying every mass term in Eq. (1.48), replacing one power of χ with the lattice spacing $\hat{a}$, and renaming the associated low-energy constant L_i to W_i. The result is Wilson chiral perturbation theory (WChPT) [56] including lattice spacing effects up to order-a.

Now, how does the transition from WChPT to partially quenched WChPT happen? It turns out [28] that the operators in the Symanzik expansion have exactly the same form, and one only has to substitute the quark vectors q and $\bar{q}$ for the partially quenched ones Eq. (2.6), which comprise the sea, valence, and ghost quarks. As a consequence, the terms appearing in the effective Lagrangian are also the same, except for the replacement $\mathrm{tr} \to \mathrm{str}$ and the fact that the meson matrix $\Sigma = \exp(\frac{2i}{f}\Phi)$ describes the $(N_S + 2N_V)^2 - 1$ Goldstone fields of partially quenched QCD. The resulting effective Lagrangian, containing lattice spacing effects up to and including $\mathcal{O}(a^2)$, consists of the continuum partially quenched Lagrangian[6]

$$\mathcal{L}_{\mathrm{PQChPT}} = \mathcal{L}_2 + \mathcal{L}_4 + \ldots \tag{2.54}$$

$$\mathcal{L}_2 = \frac{f^2}{4}\mathrm{str}(\partial_\mu \Sigma \, \partial_\mu \Sigma^\dagger) - \frac{f^2}{4}\mathrm{str}(\chi\Sigma^\dagger + \Sigma\chi) + m_0^2 \Phi_0^2$$

$$\begin{aligned}
\mathcal{L}_4 = &-L_1[\mathrm{str}(\partial_\mu \Sigma \, \partial_\mu \Sigma^\dagger)]^2 - L_2\,\mathrm{str}(\partial_\mu \Sigma \, \partial_\nu \Sigma^\dagger)\,\mathrm{str}(\partial_\mu \Sigma \, \partial_\nu \Sigma^\dagger)\\
&+ L_3\,\mathrm{str}(\partial_\mu \Sigma \, \partial_\mu \Sigma^\dagger \, \partial_\nu \Sigma \, \partial_\nu \Sigma^\dagger) + L_4\,\mathrm{str}(\partial_\mu \Sigma \, \partial_\mu \Sigma^\dagger)\,\mathrm{str}(\chi\Sigma^\dagger + \Sigma\chi)\\
&+ L_5\,\mathrm{str}(\partial_\mu \Sigma \, \partial_\mu \Sigma^\dagger[\chi\Sigma^\dagger + \Sigma\chi]) - L_6[\mathrm{str}(\chi\Sigma^\dagger + \Sigma\chi)]^2\\
&- L_7[\mathrm{str}(\chi\Sigma^\dagger - \Sigma\chi)]^2 - L_8\,\mathrm{str}(\chi\Sigma^\dagger\chi\Sigma^\dagger + \Sigma\chi\Sigma\chi)\\
&- H_2\,\mathrm{str}(\chi\chi) \tag{2.55}
\end{aligned}$$

---

[6] Remember that the sources l_μ and r_μ as well as the scalar density p were set to zero.

and of the following a-dependent terms[7]:

$$\mathcal{L}[a] = -\hat{a}\,\frac{f^2}{4}\,\mathrm{str}(\Sigma^\dagger + \Sigma) \tag{2.56}$$
$$+ \hat{a}W_4\,\mathrm{str}(\partial_\mu\Sigma\,\partial_\mu\Sigma^\dagger)\,\mathrm{str}(\Sigma^\dagger + \Sigma)$$
$$+ \hat{a}W_5\,\mathrm{str}(\partial_\mu\Sigma\,\partial_\mu\Sigma^\dagger[\Sigma^\dagger + \Sigma])$$
$$- \hat{a}W_6\,\mathrm{str}(\chi\Sigma^\dagger + \Sigma\chi)\,\mathrm{str}(\Sigma^\dagger + \Sigma)$$
$$- \hat{a}W_7\,\mathrm{str}(\chi\Sigma^\dagger - \Sigma\chi)\,\mathrm{str}(\Sigma^\dagger - \Sigma)$$
$$- \hat{a}W_8\,\mathrm{str}(\chi\Sigma^\dagger\Sigma^\dagger + \Sigma\Sigma\chi)$$

$$\mathcal{L}[a^2] = -\hat{a}^2 W_6'\,[\mathrm{str}(\Sigma^\dagger + \Sigma)]^2 - \hat{a}^2 W_7'\,[\mathrm{str}(\Sigma^\dagger - \Sigma)]^2 \tag{2.57}$$
$$- \hat{a}^2 W_8'\,\mathrm{str}(\Sigma^\dagger\Sigma^\dagger + \Sigma\Sigma)$$

The given Lagrangian is valid in the so-called GSM regime (the regime of *generic small quark masses*) [57, 58], in which the lattice spacing a counts as one power of m, or equivalently as two powers of p. The leading order Lagrangian therefore contains terms of $\mathcal{O}(p^2, m, a)$, whereas the NLO Lagrangian comprises terms of $\mathcal{O}(p^4, p^2 m, p^2 a, m^2, ma, a^2)$. The next and most relevant step for the present work is the extension of the described matching process to mixed-action ChPT with Wilson quarks in the sea and Ginsparg–Wilson quarks in the valence sector.

Dirac operators of GW-type satisfy the Ginsparg–Wilson relation [17],

$$\{\gamma_5, D\} = aD\gamma_5 D\,, \tag{2.58}$$

which in the continuum limit reproduces the continuum condition for chiral symmetry. The consequence of this relation is an exact chiral symmetry of the fermion action [18]. One can thus conclude that the continuum chiral Lagrangian will be nearly unchanged when matching the SET for Ginsparg–Wilson fermions. In the GW action, rotational $O(4)$ invariance is the only explicitly broken symmetry. This manifests itself in operators of $\mathcal{O}(a^2)$ or higher in the Symanzik expansion [28]. Corresponding terms in the effective Lagrangian must carry at least four partial derivatives ∂_μ. Multiplying these with two or more powers of the lattice spacing makes these terms negligible to the order that is considered in the present work.[8]

Now, with Wilson quarks in the sea and GW quarks in the valence sector, the symmetry of the lattice action is no longer $G_{\mathrm{PQ}} = SU(N_S + N_V|N_V)_L \otimes SU(N_S + N_V|N_V)_R$, but rather [28]

$$G_{\mathrm{MA}} = \underbrace{SU(N_S)_L \otimes SU(N_S)_R}_{G_{\mathrm{sea}}} \otimes \underbrace{SU(N_V|N_V)_L \otimes SU(N_V|N_V)_R}_{G_{\mathrm{val}}}\,. \tag{2.59}$$

---

[7] Effects of order a^2 originate from dimension-six operators contained in S_2 in the Symanzik expansion. The corresponding spurion analysis was done in Ref. [28].

[8] Of course, rotational $O(4)$ invariance is also broken by the Wilson action, but with the same reasoning one finds the effects on the chiral Lagrangian to be of too high an order.

In the limit of vanishing quark masses, G_{val} becomes an exact symmetry; G_{sea}, however, is explicitly broken down to $SU(N_S)_V$ by the Wilson term.

The leading term, S_0, in the Symanzik expansion is the continuum action of partially quenched QCD, which is invariant under G_{PQ} for massless quarks. Now, the argument is as before: For small enough lattice spacings a and quark masses m, the continuum term S_0 determines the pattern of spontaneous symmetry breaking in the effective theory [23, 28]. This means that the low-energy dynamics of mixed-action QCD can be described by the same $(N_S + 2N_V)^2 - 1$ Goldstone bosons of PQQCD. The effective chiral Lagrangian is then constructed from the SET by introducing spurions that make the Symanzik action invariant under G_{PQ}. In the end, as usual, the spurions are assigned to their constant values.

The complete derivation can be found in Ref. [28]. The result is quite similar to the case discussed before where the same Wilson action was used in both the sea and the valence sector. The mixed-action effective Lagrangian,

$$\mathcal{L}_{\text{MA}} = \mathcal{L}_{\text{PQChPT}} + \mathcal{L}[a] + \mathcal{L}[a^2] + \dots, \tag{2.60}$$

is made up of the continuum partially quenched Lagrangian, Eq. (2.54), and of the following lattice spacing dependent parts:

$$
\begin{aligned}
\mathcal{L}[a] = &- \hat{a}\, \frac{f^2}{4}\, \text{str}(P_S\Sigma^\dagger + \Sigma P_S) \\
&+ \hat{a}W_4\, \text{str}(\partial_\mu\Sigma\,\partial_\mu\Sigma^\dagger)\, \text{str}(P_S\Sigma^\dagger + \Sigma P_S) \\
&+ \hat{a}W_5\, \text{str}(\partial_\mu\Sigma\,\partial_\mu\Sigma^\dagger[P_S\Sigma^\dagger + \Sigma P_S]) \\
&- \hat{a}W_6\, \text{str}(\chi\Sigma^\dagger + \Sigma\chi)\, \text{str}(P_S\Sigma^\dagger + \Sigma P_S) \\
&- \hat{a}W_7\, \text{str}(\chi\Sigma^\dagger - \Sigma\chi)\, \text{str}(P_S\Sigma^\dagger - \Sigma P_S) \\
&- \hat{a}W_8\, \text{str}(\chi\Sigma^\dagger P_S\Sigma^\dagger + \Sigma P_S\Sigma\chi)
\end{aligned} \tag{2.61}
$$

$$
\begin{aligned}
\mathcal{L}[a^2] = &- \hat{a}^2 W_6'\, [\text{str}(P_S\Sigma^\dagger + \Sigma P_S)]^2 - \hat{a}^2 W_7'\, [\text{str}(P_S\Sigma^\dagger - \Sigma P_S)]^2 \\
&- \hat{a}^2 W_8'\, \text{str}(P_S\Sigma^\dagger P_S\Sigma^\dagger + \Sigma P_S\Sigma P_S) - \hat{a}^2 W_M\, \text{str}(P_S\Sigma P_S\Sigma^\dagger)
\end{aligned} \tag{2.62}
$$

Except for the W_M-term in the order-a^2 Lagrangian, $\mathcal{L}[a]$ and $\mathcal{L}[a^2]$ are carbon copies of Eqs. (2.56) and (2.57) with insertions of P_S at appropriate places. $P_S = \text{diag}(\mathbb{1}_{N_S \times N_S}, 0)$ is nothing but a projector on the sea sector, which guarantees that there are no $\mathcal{O}(a)$ and $\mathcal{O}(a^2)$ effects in the pure valence sector of the theory. This is expected due to the exact chiral symmetry of GW quarks.

As before, the order-a shift of Eq. (2.52) can be applied, this time, however, only to the sea masses. Whenever such a mass shows up in the following considerations, this shift is implied,

$$
\begin{aligned}
M_i^2 &= 2B_0 m_i + 2W_0 a\,, &\qquad i &= u, d, s\,, &\tag{2.63} \\
M_v^2 &= 2B_0 m_v\,, &\qquad v &= x, y\,. &\tag{2.64}
\end{aligned}
$$

Note that for $\mathcal{O}(a)$-improved Wilson fermions, this shift as well as all $\mathcal{O}(a)$ terms in the effective Lagrangian vanish.

Where does the new term $-\hat{a}^2 W_M \operatorname{str}(P_S \Sigma P_S \Sigma^\dagger)$, in the following referred to as mix-term, come from? Due to the different discretizations, there is no transformation that can rotate sea quarks into valence quarks and vice versa. This reduced symmetry allows for new operators in the Symanzik expansion and consequently leads to this new term coming with a new low-energy constant W_M.[9] In fact, the nature of this term is universal for all mixed-action theories [30].

2.2.2. Changes in the tree-level masses and propagators

With the effective Lagrangian at hand, it is now possible to tackle calculations. At first, the tree-level squared meson masses for charged mesons, now afflicted by lattice spacing effects, will be computed. In the GSM regime, nothing really changes, since only the sea quark masses receive an additional shift proportional to a. Expanding the Lagrangian in the meson fields $\Phi(x) = \frac{1}{\sqrt{2}}\pi(x)$ therefore simply yields

$$M_{ab}^2 \equiv \frac{M_a^2 + M_b^2}{2} \,. \tag{2.65}$$

When decreasing the quark masses at fixed lattice spacing in a lattice simulation, one will eventually reach the point where the LO quark mass term and the NLO a^2-terms are of comparable size. Therefore, the power counting has to be modified to $m \sim a^2$, that is, all $\mathcal{O}(a^2)$ terms are promoted to be of leading order. This scenario is often called the regime of *large cutoff effects* [59]. As a consequence, the effective Lagrangian $\mathcal{L}_{\mathrm{MA}}$ in Eq. (2.60) is no longer valid at next-to-leading order, and one should in principle construct higher-order terms that could possibly serve to cancel appearing divergencies in a loop calculation. The computation of the scalar correlator in Chapter 3, however, does not yield such divergent terms. It is thus sufficient for the current purposes to work with $\mathcal{L}_{\mathrm{MA}}$.

Carrying out the expansion in the meson fields reveals the following changes in the squared meson masses for mesons made of sea-sea, sea-valence/valence-sea, or valence-valence quarks (*valence* does also include the ghosts) [31]:

$$
\begin{aligned}
M_{\mathrm{sea}}^2 &\to M_{\mathrm{sea}}^2 + \hat{a}^2 \Delta_{\mathrm{sea}} \\
M_{\mathrm{mix}}^2 &\to M_{\mathrm{mix}}^2 + \hat{a}^2 \Delta_{\mathrm{mix}} + \hat{a}^2 \Delta_{\mathrm{mix}}' \\
M_{\mathrm{val}}^2 &\to M_{\mathrm{val}}^2
\end{aligned}
\tag{2.66}
$$

The shift parameters Δ_{sea}, Δ_{mix}, and Δ_{mix}' are given by

$$\Delta_{\mathrm{sea}} = \frac{16}{f^2}(N_S W_6' + W_8') \,, \qquad \Delta_{\mathrm{mix}} = \frac{2}{f^2} W_M \,, \qquad \Delta_{\mathrm{mix}}' = \frac{4}{f^2}(2N_S W_6' + W_8') \,. \tag{2.67}$$

As expected, the masses of mesons made entirely out of valence (and/or ghost) quarks are not affected by discretization effects up to order-a^2. The squared sea-sea meson masses,

---

[9] Note that the mix-term in Ref. [28] reads $-\hat{a}^2 W_M \operatorname{str}(\tau_3 \Sigma \tau_3 \Sigma^\dagger)$, with $\tau_3 = (P_S, -P_V)$ and $P_V = \operatorname{diag}(0, \mathbb{1}_{2N_V \times 2N_V})$ being the projector on the valence sector. Since $\operatorname{str}(\tau_3 \Sigma \tau_3 \Sigma^\dagger) = 4\operatorname{str}(P_S \Sigma P_S \Sigma^\dagger) + const.$, the low-energy constant W_M differs by a factor of 4.

however, are shifted by $\hat{a}^2 \Delta_{\text{sea}}$. The mixed meson masses are the first quantities in which the new low-energy constant W_M enters, but they also receive another contribution Δ'_{mix} stemming from the sea quark. The shifts Eq. (2.66) are also implied in the neutral sector, in particular also for $M^2_{\pi_0}$ and M^2_η.

In contrast to the GSM regime, the tree-level masses of the three different meson types are no longer trivially related,

$$M^2_{iv} \neq \frac{M^2_{ii} + M^2_{vv}}{2} \,. \tag{2.68}$$

Here, i denotes a sea and v a valence quark.

Up next is the determination of the propagators. The charged ones are simply the same as in Eq. (2.25), one only has to substitute the corresponding masses for the masses in Eq. (2.66).

The neutral propagators on the other hand are not that easily computable. In Ref. [37], the valence-valence propagator was calculated for degenerate sea quarks and degenerate valence quarks. In the following, the generalization to any quark type and to the non-degenerate case will be given. For this purpose, it is adequate to adopt the authors' notation. Note, however, that they focus at first on Wilson-like mixed actions and then specify their result to the Wilson–GW and GW–GW cases. This means that the valence quarks are not necessarily chiral quarks, and the tree-level meson masses in Eq. (2.66) take a slightly different form. For further details, the reader is referred to the comments between Eqs. (13) and (14) in Ref. [37].

The operator at $\mathcal{O}(a^2)$ in the Lagrangian that is relevant for the neutral propagator is a generalization of the W'_7 term in Eqs. (2.57) and (2.62),

$$\delta\mathcal{L}_{W'_7}[a^2] = -\hat{a}^2 \frac{f^2}{16}\Big[\gamma_{SS}[\text{str}(P_S\Sigma^\dagger - \Sigma P_S)]^2 + \gamma_{VV}[\text{str}(P_V\Sigma^\dagger - \Sigma P_V)]^2$$
$$+ 2\gamma_{SV}\,\text{str}(P_S\Sigma^\dagger - \Sigma P_S)\,\text{str}(P_V\Sigma^\dagger - \Sigma P_V)\Big]\,. \tag{2.69}$$

P_S and P_V are the projectors on the sea and the valence sector, respectively. Note that in Ref. [37], f is defined with an additional factor $\sqrt{2}$.

Using the same Wilson action in both the sea and the valence sector implies $\gamma_{SS} = \gamma_{SV} = \gamma_{VV}$, and taking the valence quarks to be of GW-type results in $\gamma_{SV} = \gamma_{VV} = 0$ due to the exact chiral symmetry. In these two scenarios, $\delta\mathcal{L}_{W'_7}$ reduces to the corresponding W'_7 term in Eqs. (2.57) and (2.62), with $\gamma_{SS} = \frac{16}{f^2}W'_7$.

Before proceeding, it is useful to split the super-singlet Φ_0 into its sea and its valence/ghost part [37], $\Phi_0 = \Phi_0^S + \Phi_0^V$. These are given by

$$\Phi_0^S \equiv \frac{1}{\sqrt{N_S}}\sum_{a=1}^{N_S}\Phi_{aa}\,, \qquad \Phi_0^V \equiv \frac{1}{\sqrt{N_S}}\sum_{a=N_S+1}^{N_S+2N_V}\epsilon_a\Phi_{aa}\,. \tag{2.70}$$

As in Eq. (2.29), the effective Lagrangian must be expanded up to quadratic order in the meson fields for obtaining the neutral propagator. For the singlet part, one then finds

$$\mathcal{L}_{\Phi_0} = \mu^2_{SS}\,(\Phi_0^S)^2 + 2\mu^2_{SV}\,\Phi_0^S\Phi_0^V + \mu^2_{VV}\,(\Phi_0^V)^2\,, \tag{2.71}$$

where

$$\mu_{SS}^2 = \frac{m_0^2}{N_S} + \hat{a}^2\gamma_{SS}\,, \qquad \mu_{SV}^2 = \frac{m_0^2}{N_S} + \hat{a}^2\gamma_{SV}\,, \qquad \mu_{VV}^2 = \frac{m_0^2}{N_S} + \hat{a}^2\gamma_{VV}\,. \qquad (2.72)$$

Note that in contrast to Ref. [37], the mass term of the super-singlet is defined with an additional factor $1/N_S$.

The neutral propagator including lattice effects up to $\mathcal{O}(a^2)$ is deduced from

$$G_N^{-1} = G_0^{-1} + H \qquad (2.73)$$

with the connected propagators

$$(G_0^{-1})_{ab} = (p^2 + M_a^2)\epsilon_a\delta_{ab}\,, \qquad (2.74)$$

and the non-diagonal contribution

$$H_{ab} = \delta_{aS}\delta_{bS}\mu_{SS}^2 + (\delta_{aS}\delta_{bV} + \delta_{aV}\delta_{bS})\,\epsilon_a\epsilon_b\mu_{SV}^2 + \delta_{aV}\delta_{bV}\epsilon_a\epsilon_b\mu_{VV}^2\,. \qquad (2.75)$$

The Kronecker deltas have indices S and V, which stand for a sea quark, and a valence/ghost quark, respectively. Written in matrix form to visualize the structure of G_N^{-1}, Equation (2.73) reads

$$G_N^{-1} = \begin{pmatrix} (G_0^{-1})_{SS} & & \\ & (G_0^{-1})_{VV} & \\ & & -(G_0^{-1})_{VV} \end{pmatrix} + \begin{pmatrix} +\mu_{SS}^2 & +\mu_{SV}^2 & -\mu_{SV}^2 \\ +\mu_{SV}^2 & +\mu_{VV}^2 & -\mu_{VV}^2 \\ -\mu_{SV}^2 & -\mu_{VV}^2 & +\mu_{VV}^2 \end{pmatrix}. \qquad (2.76)$$

Here, the μ^2's are meant to be multiplying the matrix of ones with appropriate dimensions. The matrices containing the inverse connected sea and connected valence/ghost propagators are given by

$$(G_0^{-1})_{SS} = \begin{pmatrix} p^2 + M_u^2 & & \\ & p^2 + M_d^2 & \\ & & p^2 + M_s^2 \end{pmatrix} \quad \text{and} \quad (G_0^{-1})_{VV} = \begin{pmatrix} p^2 + M_x^2 & \\ & p^2 + M_y^2 \end{pmatrix}. \qquad (2.77)$$

Inspired by the neutral propagator in the continuum, Eq. (2.36), and the symmetry of G_N^{-1}, one can expect its inverse to be given by

$$G_{ab}^N(p^2) = \frac{\epsilon_a\delta_{ab}}{p^2 + M_a^2} - \frac{K_{ab}(p^2)}{(p^2 + M_a^2)\,(p^2 + M_b^2)}\,, \qquad (2.78)$$

where the K_{ab} need to be fixed by the condition $(G_N)_{ab}(G_N^{-1})_{bc} = \mathbb{1}_{ac}$. When solving this system of equations, one makes use of $K_{ab} = K_{ba}$ and of the symmetry between the sea-valence and the sea-ghost sector, $K_{i,v} = K_{i,v+N_V}$, where i denotes a sea index and v a valence index. One finds

$$K_{ab}(p^2) = \frac{\mathcal{W}_{ab}P(u,d,s) + N_S\mathcal{V}_{ab}P(\pi_0,\eta)}{P(u,d,s) + N_S\mu_{SS}^2 P(\pi_0,\eta)}\,, \qquad (2.79)$$

in which

$$
\begin{aligned}
P(u,d,s) &= (p^2 + M_u^2)(p^2 + M_d^2)(p^2 + M_s^2)\,, \\
P(\pi_0, \eta) &= (p^2 + M_{\pi_0}^2)(p^2 + M_\eta^2)\,, \\
\mathcal{W}_{ab} &= \delta_{aS}\delta_{bS}\mu_{SS}^2 + (\delta_{aS}\delta_{bV} + \delta_{aV}\delta_{bS})\,\mu_{SV}^2 + \delta_{aV}\delta_{bV}\mu_{VV}^2\,, \\
\mathcal{V}_{ab} &= \left[\mu_{SS}^2\mu_{VV}^2 - \mu_{SV}^4\right]\delta_{a\neq\mathrm{sea}}\delta_{b\neq\mathrm{sea}}\,.
\end{aligned}
\tag{2.80}
$$

Here, M_{π_0} and M_η denote the physical neutral meson masses of the pion and the eta, as defined in (2.37), now including the $\mathcal{O}(a)$ and $\mathcal{O}(a^2)$ corrections as in Eq. (2.66). Equation (2.79) is given for $N_S = 3$, but as before, the case $N_S = 2$ can be obtained by dropping the $(p^2 + M_s^2)$ and $(p^2 + M_\eta^2)$ factors in Eq. (2.80).

Interestingly, for Wilson sea quarks ($\gamma_{SS} \neq 0$), there is an $\mathcal{O}(a^2)$ contribution $\mathcal{V}_{ab}$ to the propagator that only affects the valence and the ghost sector, whether the valence quarks are chiral or not. This is due to the graded nature of the meson matrix and the equality of valence and ghost masses. For the same reason, the sea-sea and the sea-valence sector do not depend on γ_{VV}.

Finally, the super-singlet is decoupled by sending $m_0 \to \infty$:

$$
K_{ab}(p^2) = \frac{(p^2 + M_u^2)\,(p^2 + M_d^2)\,(p^2 + M_s^2)}{N_S(p^2 + M_{\pi_0}^2)(p^2 + M_\eta^2)} + \hat{a}^2\left(\gamma_{SS} + \gamma_{VV} - 2\gamma_{SV}\right)\delta_{a\neq\mathrm{sea}}\delta_{b\neq\mathrm{sea}} \quad (2.81)
$$

One immediately sees that the $\mathcal{O}(a^2)$ corrections stemming from $\delta\mathcal{L}_{W_7'}$ affect only the pure valence sector (including the ghosts). If the same Wilson action is used for both the sea and the valence quarks, that term vanishes, since $\gamma_{SS} = \gamma_{SV} = \gamma_{VV}$. This, however, does not imply that there are no $\mathcal{O}(a^2)$ corrections. The theory just reduces to standard partially quenched ChPT with the lattice corrections absorbed into the squared meson masses via a generalization of Eq. (2.66). With chiral quarks in the sea and in the valence sector, all gammas are zero.

The relevant case in the present work, however, is that of Wilson sea quarks and GW valence quarks. That is, $\gamma_{SV} = \gamma_{VV} = 0$ and $\gamma_{SS} = \frac{16}{f^2}W_7'$. The neutral propagator is thus given by

$$
\begin{aligned}
G_{ab}^N(p^2) = {}& \frac{\epsilon_a\delta_{ab}}{p^2 + M_a^2} - \frac{1}{N_S}\frac{(p^2 + M_u^2)\,(p^2 + M_d^2)\,(p^2 + M_s^2)}{(p^2 + M_a^2)\,(p^2 + M_b^2)\cdot(p^2 + M_{\pi_0}^2)\,(p^2 + M_\eta^2)} \\
& - \hat{a}^2\gamma_{SS}\frac{\delta_{a\neq\mathrm{sea}}\delta_{b\neq\mathrm{sea}}}{(p^2 + M_a^2)\,(p^2 + M_b^2)}\,.
\end{aligned}
\tag{2.82}
$$

The lack of symmetry in the sea sector, or rather the missing symmetry between the sea and the valence sector, directly influences the valence sector of the theory.

It seems like the lattice corrections coming with γ_{SS} (W_7') are independent of the number of sea flavors. This is a priori not true, since all low-energy constants do depend on N_S. A pleasant byproduct of the result in Eq. (2.82) is the fact that an actual mixed-action computation does not get a lot more complicated than a usual partially quenched one.

The only slight modification is the partial fraction decomposition of the second term. If the masses M_a and M_b are unequal, then

$$\frac{1}{(p^2 + M_a^2)(p^2 + M_b^2)} = \frac{\frac{1}{M_b^2 - M_a^2}}{p^2 + M_a^2} + \frac{\frac{1}{M_a^2 - M_b^2}}{p^2 + M_b^2}, \tag{2.83}$$

and one simply has to shift the corresponding single pole residues by $\pm \frac{N_S \hat{a}^2 \gamma_{SS}}{M_b^2 - M_a^2}$.

On the other hand, if M_a equals M_b, the double pole residue receives a shift according to $R_{\mathrm{DP}} \to R_{\mathrm{DP}} + N_S \hat{a}^2 \gamma_{SS}$.

For example, with $N_S = 2$ sea flavors, isospin symmetry $M_u = M_d$, and $M_a = M_x$, this shift reads

$$(M_u^2 - M_x^2) \to (M_u^2 - M_x^2) + 2\hat{a}^2 \gamma_{SS}. \tag{2.84}$$

The last brief comment in this chapter concerns the issue of quark mass tunings. Since the squared masses of sea-sea, mixed, and valence-valence mesons receive different shifts caused by the non-zero lattice spacing, one must decide how to tune the bare quark masses in order to get the desired meson masses. In view of the expression above, one can, e.g., tune the valence quark mass to yield $M_u = M_x$. Another possibility is to tune such that the whole double pole residue vanishes [37]. This, however, is difficult in practice since it requires a quantity sensitive to the mass of the super-singlet. In the continuum limit, these tunings are of course equivalent. In the next chapter, when the scalar correlator is discussed, the tuning of the quark masses will be addressed again.

3. The scalar correlator

This chapter is devoted to the isospin-one scalar two-point function [32, 34–36] at large time separations in partially quenched and mixed-action chiral perturbation theory. After a motivation why this is a useful quantity in lattice simulations, the leading contribution to the scalar correlator in PQChPT is derived, and the unphysical effects of the double pole are studied. Afterwards, the impact of non-zero lattice spacings and the use of mixed actions is analyzed. Chapter 4, then, will concentrate on finite volume effects, which will turn out to especially affect the double pole.

3.1. Motivation

This introduction follows mainly Ref. [35]. In lattice QCD, hadron correlators are used to compute hadron masses and energies of excited states. The concrete procedure is often referred to as *hadron spectroscopy calculations* [24]. The correlator of interest in the present work is the isospin-one scalar two-point function, which in standard unquenched QCD is given by

$$C(t) = \int \mathrm{d}^3\vec{x} \, \langle 0|\bar{d}(x)u(x)\,\bar{u}(0)d(0)|0\rangle \ . \tag{3.1}$$

Like all lattice correlators, $C(t)$ can be represented by a sum of decaying exponentials where each exponent corresponds to a specific energy level. $C(t)$ receives contributions from the propagation of the scalar a_0 meson, $C(t) \propto \mathrm{e}^{-m_{a_0}t}$, and from multi-hadron intermediate states, the most important of which is the so-called bubble contribution $B(t)$ where two pseudoscalars propagate. This is illustrated in Fig. 3.1. In $2+1$ flavor QCD, the possible intermediate states in the bubble diagram are $\pi\eta$, $K\bar{K}$, and $\pi\eta'$. For two flavors, only $\pi\eta'$ is allowed.

At large time separations and small quark masses, $B(t)$ gives a sizable contribution to the correlator and will eventually dominate its shape,

$$C(t) = A\mathrm{e}^{-m_{a_0}t} + B(t) + \dots . \tag{3.2}$$

The dots represent excited scalar meson states as well as other less important multi-hadron intermediate states, which will not be considered here.

The aim of Ref. [34, 35] was to determine the mass of the scalar a_0 meson, which appeared to be difficult due to the bubble contribution shadowing the interesting a_0-part.

Besides the extraction of m_{a_0}, the scalar correlator is interesting for another reason: It allows to gain more insight into the violation of unitarity occurring in unphysical lattice simulations, since it is a quantity which is extremely sensitive to the associated effects. Depending on the chosen quark masses and discretizations, $C(t)$ is found to be negative at large t [32–35]. This behavior can be explained in the framework of partially quenched and mixed-action ChPT, where the bubble can give rise to unphysical negative contributions to the scalar correlator, mainly due to the double pole in the disconnected
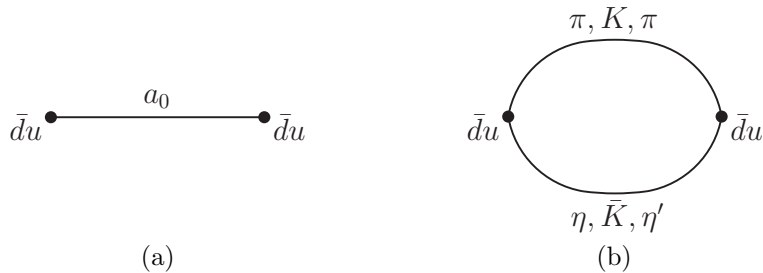
Figure 3.1.: Diagrams contributing to the scalar correlator. Figure 3.1a represents the propagation of the scalar a_0 meson, and Fig. 3.1b shows the so-called bubble diagram with the possible two-pseudoscalar intermediate states $\pi\eta$, $K\bar{K}$, and $\pi\eta'$.

propagators. At large time separations, when all heavy intermediate states have been decayed, $C(t)$ will be a tool to check whether mixed-action ChPT describes all unitarity-violating effects [38], and, if so, to quantify the size and signs of the new low-energy constants associated with them. This is one of the motivations for this thesis.

In the following, the scalar correlator is derived for Wilson sea and Ginsparg–Wilson valence quarks. Essentially, the form will be the same as in Ref. [35] where staggered sea quarks were used. The authors, however, directly computed the mixed-action correlator in a finite volume (as in Ref. [34]) and used lattice momenta instead of "standard" quantized momenta that occur in a box with periodic boundary conditions [7–9]. The final expression Eq. (24) in Ref. [34] contains five sums over all possible values of lattice momenta and is therefore quite cumbersome. As a consequence, fitting lattice data to that expression becomes very time-consuming, in particular for increasing lattice volumes. Moreover, it is not clear how the infinite volume limit is approached.

The calculation in the present work is organized in a different way. At first, the correlator is derived in the infinite volume. This will already make the unphysical effects visible. Then, the computation is carried over into a finite volume. The aim is to rewrite the sums over momenta such that the resulting expression is easy to handle in a fitting process, and, furthermore, that higher-order terms in the sums are suppressed with larger box sizes. In this way, one recovers the infinite volume result in the limit of infinitely large lattice volumes.

3.2. Partially quenched infinite volume computation

3.2.1. The computation

In partially quenched QCD, the valence-valence scalar two-point function is given by[10]

$$C_{\bar{y}x}^{\mathrm{PQQCD}}(t) = \int \mathrm{d}^3\vec{x}\, C_{\bar{y}x}^{\mathrm{PQQCD}}(x) = \int \mathrm{d}^3\vec{x}\, \langle 0|\bar{y}(x)x(x)\,\bar{x}(0)y(0)|0\rangle \;, \qquad (3.3)$$

---

[10]The space-time point x in brackets is not to be confused with the valence quark placeholders x and y.

which corresponds to

$$C_{\bar{y}x}^{\text{PQQCD}}(x) = \frac{1}{Z_{\text{PQQCD}}} \int \mathcal{D}A\,\mathcal{D}\bar{q}\,\mathcal{D}q\,\big[\bar{y}(x)x(x)\,\bar{x}(0)y(0)\big]\,\mathrm{e}^{-S_G[A] - \int \mathrm{d}^4 y\,\bar{q}\big(\slashed{D}+m\big)q} \qquad (3.4)$$

in the path integral formulation. This is the same as functional differentiating Z_{PQQCD} with respect to the corresponding entries of the mass matrix m (which is being promoted to a space-time dependent object, that is, it equals the scalar density s),

$$C_{\bar{y}x}^{\text{PQQCD}}(x) = \frac{1}{Z_{\text{PQQCD}}} \frac{\delta^2 Z_{\text{PQQCD}}}{\delta m_{xy}(0)\,\delta m_{yx}(x)}\bigg|_{m\to\text{diag}(m)} . \qquad (3.5)$$

Analogously, one considers the generating functional of PQChPT,

$$Z_{\text{PQChPT}} = \int \mathcal{D}\Sigma\,\mathrm{e}^{-\int \mathrm{d}^4 y\,[\mathcal{L}_2(y)+\mathcal{L}_4(y)+\ldots]} , \qquad (3.6)$$

and works out the same functional derivatives [34, 35]. A detailed calculation can be found in Appendix A. The expression one receives reads

$$\begin{aligned} C_{\bar{y}x}^{\text{PQChPT}}(x) = {}& \frac{B_0^2 f^4}{4}\,\langle 0|\big[\Sigma(x) + \Sigma^\dagger(x)\big]_{xy}\big[\Sigma(0) + \Sigma^\dagger(0)\big]_{yx}|0\rangle \\ & + 4B_0^2\,\delta(x)\,\langle 0|\big[2L_8\big(\Sigma_{xx}\Sigma_{yy} + \Sigma_{xx}^\dagger\Sigma_{yy}^\dagger\big)(0) + 2H_2\big]|0\rangle , \end{aligned} \qquad (3.7)$$

which has to be expanded up to quadratic oder in the meson fields $\pi(x)$. For flavor indices $x \neq y$, one finds

$$C_{\bar{y}x}^{\text{PQChPT}}(x) = B_0^2\,\langle 0|[\pi^2(x)]_{xy}[\pi^2(0)]_{yx}|0\rangle + 8B_0^2\,\delta(x)\,[2L_8 + H_2] . \qquad (3.8)$$

The two low- and high-energy constants L_8 and H_2 enter the correlator as contact terms. As explained in the first chapter, they are necessary for the renormalization of $C_{\bar{y}x}^{\text{PQChPT}}(0)$. They play no rôle at large time separations and will therefore be dropped in the following considerations.

The full PQQCD correlator includes the a_0 propagation and the $\pi\eta'$ bubble. One has no access to the $\pi\eta'$ intermediate state when the heavy eta prime meson is decoupled from the theory. At large space-time separations x, though, these heavy intermediate states have been decayed, and $C_{\bar{y}x}^{\text{PQChPT}}(x)$ matches $C_{\bar{y}x}^{\text{PQQCD}}(x)$ up to truncation errors in the chiral expansion.

According to Wick's theorem, Eq. (3.8) can be reduced to a sum of products of two-point functions, which involve only two fields. Among the non-zero contractions, the propagators with ghost quarks cancel the corresponding valence quark propagators. The correlator is then given by (see Appendix A)

$$\begin{aligned} C_{\bar{y}x}^{\text{PQChPT}}(x) = B_0^2\bigg[& \langle\pi_{xy}\pi_{yx}\rangle^{\text{con}}\big(2\,\langle\pi_{xx}\pi_{yy}\rangle^{\text{disc}} + \langle\pi_{xx}\pi_{xx}\rangle^{\text{disc}} + \langle\pi_{yy}\pi_{yy}\rangle^{\text{disc}}\big) \\ & + \sum_{i=1}^{N_S} \langle\pi_{xi}\pi_{ix}\rangle^{\text{con}}\,\langle\pi_{iy}\pi_{yi}\rangle^{\text{con}}\bigg] , \end{aligned} \qquad (3.9)$$
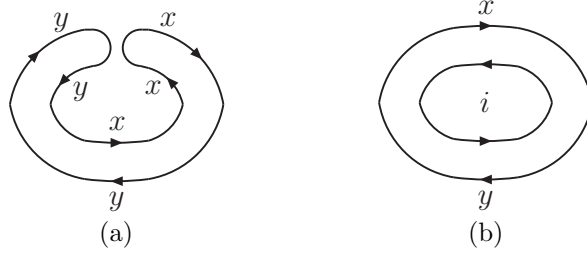
37

Figure 3.2.: Quark-flow diagrams corresponding to the bubble diagram in Fig. 3.1b. The connected-disconnected valence pion propagations are shown in Fig. 3.2a, in which the quark labels correspond to the term $\langle \pi_{xy}\pi_{yx}\rangle^{\mathrm{con}}\,\langle \pi_{xx}\pi_{yy}\rangle^{\mathrm{disc}}$ in Eq. (3.9). The other two disconnected diagrams can be obtained by changing the upper yy or xx labels to xx and/or yy, respectively. All possible iterations of sea quark loops from the disconnected propagator Eq. (2.35) are implied in this hairpin diagram. The connected mixed pion and mixed kaon propagations are visualized in Fig. 3.2b, where i stands for a sea quark u, d, or s. Note that among all connected diagrams, the valence loops have been canceled by the ghost loops as described before. This leaves only the shown diagram with a sea quark running in the loop.

where for shortness $\langle \pi_1 \pi_2 \rangle$ denotes $\langle \pi_1(x)\pi_2(0)\rangle$. These two-point functions are those of Eqs. (2.25) and (2.38),

$$\langle \pi_{ab}(x)\pi_{ba}(0)\rangle^{\mathrm{con}} = \int \frac{\mathrm{d}^4 p}{(2\pi)^4}\, G_{ab}^{\mathrm{con}}(p^2)\, \mathrm{e}^{ipx}\,, \tag{3.10}$$

$$\langle \pi_{aa}(x)\pi_{bb}(0)\rangle^{\mathrm{disc}} = \int \frac{\mathrm{d}^4 p}{(2\pi)^4}\, G_{ab}^{\mathrm{disc}}(p^2)\, \mathrm{e}^{ipx}\,, \tag{3.11}$$

with the momentum-space propagators

$$G_{ab}^{\mathrm{con}}(p^2) = \frac{\epsilon_b}{p^2 + M_{ab}^2}\,, \tag{3.12}$$

$$G_{ab}^{\mathrm{disc}}(p^2) = -\frac{1}{N_S} \frac{(p^2 + M_u^2)\,(p^2 + M_d^2)\,(p^2 + M_s^2)}{(p^2 + M_a^2)\,(p^2 + M_b^2)\cdot (p^2 + M_{\pi_0}^2)\,(p^2 + M_\eta^2)}\,. \tag{3.13}$$

The scalar correlator consists of connected and disconnected parts. For the three-flavor case, $N_S = 3$, the connected parts are mixed pion and mixed kaon intermediate states stemming from the sum over the sea index i. The other three terms give rise to disconnected contributions involving valence pions. This is illustrated in Fig. 3.2.

From now on, all calculations will be restricted to the scenario of isospin symmetry, $M_u = M_d \neq M_s$ and $M_x = M_y$. In this limit M_u equals the sea pion mass M_{π_0}, and $(M_x^2 + M_y^2)/2 \to M_x^2$ is the squared valence pion mass. The mixed pions and kaons have the masses M_{ux} and M_{sx}, respectively. The correlator will be denoted as $C_{\bar{y}x}^{\mathrm{PQChPT}} \to C_{\bar{y}x}^{2+1}$, and in the case of two sea flavors, it will be abbreviated by $C_{\bar{y}x}$. A generalization of the subsequent calculations to non-degenerate quarks involves more terms to deal with. The final expressions for $C_{\bar{y}x}^{1+1+1}$ can be found in Appendix D. The scalar correlator now simplifies to

$$C_{\bar{y}x}^{2+1}(x) = B_0^2 \left[4\,\langle \pi_{xx}\pi_{xx}\rangle^{\mathrm{con}}\,\langle \pi_{xx}\pi_{xx}\rangle^{\mathrm{disc}} + \sum_{i=u,u,s} \langle \pi_{xi}\pi_{ix}\rangle^{\mathrm{con}}\,\langle \pi_{ix}\pi_{xi}\rangle^{\mathrm{con}} \right]. \tag{3.14}$$

In the limit of equal sea and valence masses, one indeed recovers the QCD result $C_{\bar{y}x}^{2+1} \to C_{\bar{d}u}^{2+1}$ with a pion–eta and a kaon–antikaon intermediate state,

$$C_{\bar{d}u}^{2+1}(x) = B_0^2 \left[\frac{2}{3} \langle \pi\pi \rangle \langle \eta\eta \rangle + \langle K\bar{K} \rangle \langle \bar{K}K \rangle \right]. \tag{3.15}$$

Remember that the heavy eta prime meson was decoupled from the theory and therefore no $\langle \pi\pi \rangle \langle \eta'\eta' \rangle$ term appears. That is also the reason why one finds a vanishing correlator, $C_{\bar{y}x}(x) = 0$, in the case of two sea flavors, since the $\pi\eta'$ intermediate state is the only one allowed for $N_S = 2$.

Now back to the partially quenched correlator. A partial fraction decomposition yields the following expressions for the disconnected valence-valence propagator,

$$N_S = 2: \qquad G_{xx}^{\text{disc}}(p^2) = -\frac{1}{2} \left[\frac{M_u^2 - M_x^2}{(p^2 + M_x^2)^2} + \frac{1}{p^2 + M_x^2} \right], \tag{3.16}$$

$$N_S = 3: \qquad G_{xx}^{\text{disc}}(p^2) = -\frac{1}{3} \left[\frac{R_x\binom{u,s}{\eta}}{(p^2 + M_x^2)^2} + \frac{D_x^x\binom{u,s}{\eta}}{p^2 + M_x^2} + \frac{D_\eta^x\binom{u,s}{x}}{p^2 + M_\eta^2} \right], \tag{3.17}$$

with $R_x\binom{u,s}{\eta}$, $D_x^x\binom{u,s}{\eta}$, and $D_\eta^x\binom{u,s}{x}$ being the corresponding residues of the decomposition (see Eq. (2.41)). For the current purpose, it is useful to define so-called *bubble functions*. These are products of two propagators including the integration over the spatial volume, multiplied with the square of the low-energy constant B_0:

$$B_{\text{SP}}(t, M_a, M_b) \equiv B_0^2 \int d^3\vec{x} \int \frac{d^4p}{(2\pi)^4} \frac{e^{ipx}}{p^2 + M_a^2} \int \frac{d^4k}{(2\pi)^4} \frac{e^{ikx}}{k^2 + M_b^2} \tag{3.18}$$

Here, SP stands for single pole. Equivalently, the double pole (DP) contribution is being defined as

$$B_{\text{DP}}(t, M_a, M_b) \equiv B_0^2 \int d^3\vec{x} \int \frac{d^4p}{(2\pi)^4} \frac{e^{ipx}}{p^2 + M_a^2} \int \frac{d^4k}{(2\pi)^4} \frac{e^{ikx}}{(k^2 + M_b^2)^2}, \tag{3.19}$$

where in the case of isospin symmetry only $B_{\text{DP}}(t, M_a, M_a)$ is needed.

With this notation, the correlator can be written in a very convenient form. Before doing so, it is appropriate to simplify the bubble functions to expressions, which are easier to handle. Note that in comparison to Refs. [34, 35], the integrals correspond to sums over lattice momenta. The $\vec{x}$-sum projects on $\vec{p} + \vec{k} = 0$, and the authors are left with five sums, which cannot be simplified anymore. This is not the case in the present approach. In order to save writing too many subscripts, the following convention is used,

$$B_{\text{SP/DP}}(t, M_a, M_b) \to B_{\text{SP/DP}}(t, M, m), \tag{3.20}$$

where, in this notation, m must not to be confused with the quark masses.

The original expression of the bubble function Eq. (3.18) can be reduced to a single integral over a closed interval (see Appendix B),

$$B_{\text{SP}}(t, M, m) = \frac{B_0^2}{16\pi^2 |t|} \int_0^1 dc \, e^{-\sqrt{\frac{m^2 + c(M^2 - m^2)}{c(1-c)}} |t|}. \tag{3.21}$$

Although the integrand is asymmetrical for $M \neq m$, the value of the integral remains the same when interchanging M and m. This can be seen by substituting the integration variable c for $(1-c)$ and reversing the limits of integration. Setting $M = m$ yields the single pole bubble function for equal masses,

$$B_{\text{SP}}(t, m, m) = \frac{B_0^2}{16\pi^2|t|} \int_0^1 dc \; e^{-\frac{m|t|}{\sqrt{c(1-c)}}} \, . \tag{3.22}$$

The double pole bubble function can be obtained from the connected one by differentiating with respect to the mass,

$$B_{\text{DP}}(t, m, m) = -\frac{1}{2} \frac{\partial}{\partial m^2} B_{\text{SP}}(t, m, m) \, . \tag{3.23}$$

One therefore simply gets

$$B_{\text{DP}}(t, m, m) = \frac{B_0^2}{64\pi^2 m} \int_0^1 dc \; \frac{e^{-\frac{m|t|}{\sqrt{c(1-c)}}}}{\sqrt{c(1-c)}} \, . \tag{3.24}$$

Apparently, in comparison to the single pole one, the double pole bubble function is enhanced by a factor $\frac{t}{4m}$ at large t.

It is insightful to show the asymptotic behavior of the three functions using a saddle-point approximation. Up to corrections of $\mathcal{O}(t^{-5/2})$, one finds

$$B_{\text{SP}}(t, M, m) = \frac{B_0^2}{8\sqrt{2}\pi^{3/2}} \frac{\sqrt{Mm} \cdot e^{-(M+m)|t|}}{(M+m)^{3/2} |t|^{3/2}} \, ,$$

$$B_{\text{SP}}(t, m, m) = \frac{B_0^2}{32\pi^{3/2}} \frac{e^{-2m|t|}}{\sqrt{m}|t|^{3/2}} \, , \tag{3.25}$$

$$B_{\text{DP}}(t, m, m) = \frac{B_0^2}{256\pi^{3/2}} \frac{1 + 4m|t|}{m^{5/2}|t|^{3/2}} e^{-2m|t|} \, .$$

While all three bubble functions fall off exponentially and are suppressed by a factor $1/|t|^{3/2}$, the double pole bubble function has a second contribution coming with an additional factor $|t|$, which clearly dominates B_{DP} in the limit $t \to \infty$.

What are the implications for the scalar correlator? The double pole arises from valence pions in the disconnected propagator. Decreasing the valence masses while keeping the sea masses fixed therefore not only increases the partial quenching parameter $\Delta_{\text{PQ}}^2 = M_{\text{sea}}^2 - M_{\text{val}}^2$, which comes with the double pole, but it also enhances the effect of the unphysical double pole bubble contribution itself. This will be illustrated in the following subsections.

3.2.2. The scalar correlator for $N_S = 2$ sea flavors

Starting at first with two sea flavors, the scalar correlator reads

$$C_{\bar{y}x}(t) = -2\left(M_u^2 - M_x^2\right)B_{\mathrm{DP}}(t, M_x, M_x) - 2B_{\mathrm{SP}}(t, M_x, M_x) + 2B_{\mathrm{SP}}(t, M_{ux}, M_{ux}).$$
(3.26)

The first two terms are double and single pole contributions stemming from the valence pions; the factor $(M_u^2 - M_x^2)$ is the double pole residue, and the last term indicates the connected mixed pions. Due to the previously described behavior of the bubble functions, one sees that the full correlator, to which the a_0 as well as the $\pi\eta'$ intermediate state contribute with a positive sign, can get negative if the valence mass is chosen to be smaller than the sea mass. This unphysical effect of partial quenching was also observed in Refs. [34, 35].

Clearly, the correlator vanishes for equal sea and valence quark masses,

$$C_{\bar{y}x}(t) \xrightarrow{M_u = M_x} C_{\bar{d}u}(t) = 0\,,$$
(3.27)

since $M_{ux}^2 = \frac{M_u^2 + M_x^2}{2} \to M_u^2 = M_x^2$. If the same Wilson or GW action is used in the sea and in the valence sector, this result still holds. In the GW case, this is because up to order-a^2, the meson masses are not afflicted by lattice spacing artifacts. For Wilson quarks on the other hand, all squared meson masses receive the same shift caused by the non-zero lattice spacing, and thus the difference $(M_u^2 - M_x^2)$ does not depend on a.

3.2.3. The scalar correlator for $N_S = 2 + 1$ sea flavors

In this case, the partial fraction decomposition yields

$$C_{\bar{y}x}^{2+1}(t) = -\frac{4}{3}R_x\!\left(\begin{smallmatrix}u,s\\\eta\end{smallmatrix}\right) \cdot B_{\mathrm{DP}}(t, M_x, M_x) - \frac{4}{3}D_x^x\!\left(\begin{smallmatrix}u,s\\\eta\end{smallmatrix}\right) \cdot B_{\mathrm{SP}}(t, M_x, M_x)$$
(3.28)
$$- \frac{4}{3}D_\eta^x\!\left(\begin{smallmatrix}u,s\\x\end{smallmatrix}\right) \cdot B_{\mathrm{SP}}(t, M_x, M_\eta) + 2B_{\mathrm{SP}}(t, M_{ux}, M_{ux}) + B_{\mathrm{SP}}(t, M_{sx}, M_{sx})\,.$$

Again, there is a double and a single pole contribution from the valence pions, $\pi_{\mathrm{val}}\pi_{\mathrm{val}}$. The other three single pole terms originate from $\pi_{\mathrm{val}}\eta$, $\pi_{\mathrm{mix}}\pi_{\mathrm{mix}}$, and $K_{\mathrm{mix}}\bar{K}_{\mathrm{mix}}$ bubble functions. The residues are given by

$$R_x\!\left(\begin{smallmatrix}u,s\\\eta\end{smallmatrix}\right) = \frac{(M_u^2 - M_x^2)(M_s^2 - M_x^2)}{M_\eta^2 - M_x^2}\,,$$
$$D_x^x\!\left(\begin{smallmatrix}u,s\\\eta\end{smallmatrix}\right) = 1 + \frac{2}{9}\frac{(M_s^2 - M_u^2)^2}{(M_\eta^2 - M_x^2)^2}\,,$$
(3.29)
$$D_\eta^x\!\left(\begin{smallmatrix}u,s\\x\end{smallmatrix}\right) = -\frac{2}{9}\frac{(M_s^2 - M_u^2)^2}{(M_\eta^2 - M_x^2)^2}\,.$$

Independently of the choice of quark masses, the single pole residue $D_x^x\!\left(\begin{smallmatrix}u,s\\\eta\end{smallmatrix}\right)$ is always positive, while $D_\eta^x\!\left(\begin{smallmatrix}u,s\\x\end{smallmatrix}\right)$ has a negative sign. Therefore, the correlator always receives a
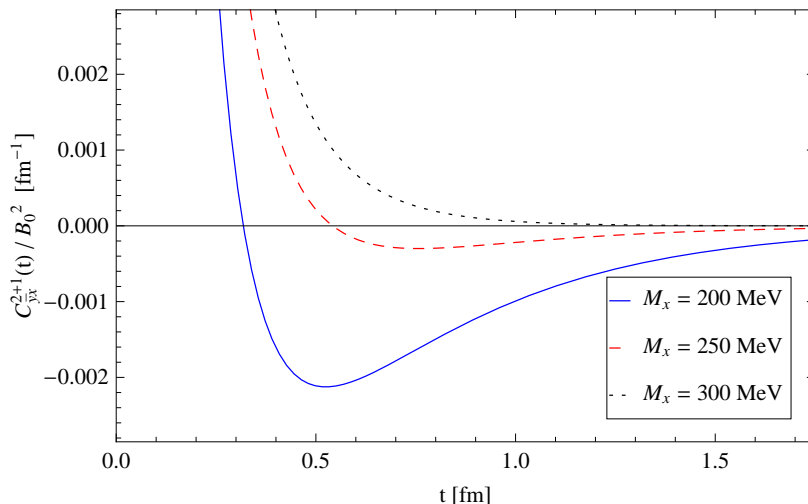
Figure 3.3.: Infinite volume partially quenched scalar correlator for $M_u = 300$ MeV, $M_s = 600$ MeV, and different values of M_x. The other occurring masses are determined by these values.

negative contribution from the $\pi_{\text{val}}\pi_{\text{val}}$ term, and a positive one from the $\pi_{\text{val}}\eta$ term. Moreover, for $M_{\text{val}} < M_{\text{sea}}$, one has $|D_x^x\binom{u,s}{\eta}| > |D_\eta^x\binom{u,s}{x}|$, plus the fact that the mass of $\pi_{\text{val}}\pi_{\text{val}}$ is much smaller compared to $\pi_{\text{val}}\eta$, which results in a less suppressed exponential decay for the $\pi_{\text{val}}\pi_{\text{val}}$ term. Both circumstances enhance the negativity of the scalar correlator and the associated violation of unitarity.

The sign of the double pole residue $R_x\binom{u,s}{\eta}$ depends on the single-flavor masses M_u, M_s, and M_x. For common choices in lattice simulations, it has a negative value and thus also adds to the unphysical nature of partial quenching.

In Fig. 3.3, the correlator is shown for $M_u = 300$ MeV, $M_s = 600$ MeV, and $M_x = (200\ldots300)$ MeV. In the limit of equal sea and valence masses ($M_x = M_u$), the double pole residue vanishes. Furthermore, $-\frac{4}{3}D_x^x\binom{u,s}{\eta} \to -2$, which means that the SP valence pion term cancels the SP mixed pion term, and one obtains the expected result

$$C_{\bar{d}u}^{2+1}(t) = \frac{2}{3}B_{\text{SP}}(t, M_{\pi_0}, M_\eta) + B_{\text{SP}}(t, M_K, M_K)\,, \qquad (3.30)$$

which is strictly positive, as can be seen in Fig. 3.3.

3.3. Consequences of using mixed actions

It is now time to incorporate the lattice spacing effects stemming from the use of Wilson quarks in the sea and Ginsparg–Wilson quarks in the valence sector. The transition is simple. As shown in the previous chapter (Section 2.2.2), the squared sea and mixed meson masses receive a shift $\hat{a}^2\Delta_{\text{sea}}$ and $\hat{a}^2\Delta_{\text{mix}} + \hat{a}^2\Delta'_{\text{mix}}$, respectively,[11] and, furthermore,

---

[11]Note that for unimproved Wilson fermions, they include a shift $\hat{a}$ and $\hat{a}/2$, respectively.

the double pole residue of the disconnected propagator must be shifted according to

$$N_S = 2: \qquad (M_u^2 - M_x^2) \to (M_u^2 - M_x^2) + 2\hat{a}^2\gamma_{SS}, \qquad (3.31)$$

$$N_S = 3: \qquad R_x\!\left(^{u,s}_\eta\right) \to R_x\!\left(^{u,s}_\eta\right) + 3\hat{a}^2\gamma_{SS}. \qquad (3.32)$$

The impact of the different discretizations on the scalar correlator is now studied, starting again with the two-flavor case:

$$C_{\bar{y}x}(t) = -2\left(M_u^2 - M_x^2 + 2\hat{a}^2\gamma_{SS}\right) \cdot B_{\mathrm{DP}}(t, M_x, M_x)$$
$$- 2B_{\mathrm{SP}}(t, M_x, M_x) + 2B_{\mathrm{SP}}(t, M_{ux}, M_{ux}) \qquad (3.33)$$

Owing to the exact chiral symmetry in the valence sector, the double and single pole valence pion bubble functions $B_{\mathrm{DP}}(t, M_x, M_x)$ and $B_{\mathrm{SP}}(t, M_x, M_x)$ are not afflicted by lattice spacing effects. The mixed pion bubble function $B_{\mathrm{SP}}(t, M_{ux}, M_{ux})$ on the other hand depends on the parameters Δ_{mix} and Δ'_{mix}. Lastly, the double pole residue has, next to γ_{SS}, a Δ_{sea}-dependence stemming from the sea pion mass M_u.

In the continuum limit, one recovers the physical vanishing correlator (at large time separations) when setting the sea meson mass equal to the valence mass. At non-zero lattice spacing, though, this is no longer the case due the different shifts in the squared meson masses. Because of these, one also has different possibilities of tuning the quark masses, which all yield the same result when taking $a \to 0$. The choice of tuning will strongly affect the shape of the scalar correlator, especially its negativity, which is a clear sign for the violation of unitarity.

The first tuning would be a matching of the sea and valence pion squared masses M_u^2 and M_x^2. Their difference thus cancels, and the correlator becomes sensitive to γ_{SS} and $\Delta_{\mathrm{mix}} + \Delta'_{\mathrm{mix}}$. The second way is to match the sea pion mass M_u to the mixed pion one M_{ux}. As a consequence, the last two terms in Eq. (3.33) cancel, and the only a^2-dependence stems from γ_{SS} and Δ_{sea}. Another possibility is to tune the whole double pole residue $(M_u^2 - M_x^2 + 2\hat{a}^2\gamma_{SS})$ to zero, which leaves the mixed pion bubble function with the parameters $\Delta_{\mathrm{mix}} + \Delta'_{\mathrm{mix}}$ as the only a^2-dependent part of the correlator. This tuning requires a quantity sensitive to γ_{SS}, that is, a quantity sensitive to the eta prime mass [37].[12]

These various tunings seem to be promising when it comes to the determination of γ_{SS}, Δ_{sea}, and $\Delta_{\mathrm{mix}} + \Delta'_{\mathrm{mix}}$ and the associated strength of unitarity violation.

In a fit of the lattice scalar correlator to Eq. (3.33), the only free parameter is γ_{SS}. The meson masses, which the bubble functions come with, can be obtained from meson spectroscopy, and the low-energy constant B_0 can be determined by the tree-level ChPT relation $M_{ab}^2 = B_0(m_a + m_b)$ between quark and squared meson masses, using for instance the pion mass $M_\pi^2 = 2B_0 m_u$.

This section is completed with the scalar correlator for $2+1$ sea flavors:

$$C_{\bar{y}x}^{2+1}(t) = -\frac{4}{3}\left[R_x\!\left(^{u,s}_\eta\right) + 3\hat{a}^2\gamma_{SS}\right] \cdot B_{\mathrm{DP}}(t, M_x, M_x) - \frac{4}{3}D_x^x\!\left(^{u,s}_\eta\right) \cdot B_{\mathrm{SP}}(t, M_x, M_x)$$

$$- \frac{4}{3}D_\eta^x\!\left(^{u,s}_x\right) \cdot B_{\mathrm{SP}}(t, M_x, M_\eta) + 2B_{\mathrm{SP}}(t, M_{ux}, M_{ux}) + B_{\mathrm{SP}}(t, M_{sx}, M_{sx}) \quad (3.34)$$

---

[12]Yet another interesting idea was suggested by the UKQCD Collaboration. They proposed to use the sign change of the scalar correlator in order to tune the sea and valence quark masses [60].

4. Finite volume corrections to the scalar correlator

Numerical calculations are necessarily performed in a finite volume. Most often, the lattice geometry is a box of size $V = L^3 \times T$ with periodic boundary conditions in the three spatial directions as well as in the time direction. Physical quantities that are obtained from such simulations will in general depend on both L and T. It is therefore imperative to study and to quantify the size of finite volume effects for the observable in question. This also means that chiral perturbation theory must be formulated in a finite volume [7–9] in order for it to yield reliable fitting formulae.

4.1. Chiral perturbation theory in a finite volume

Gasser and Leutwyler showed that in a finite volume (FV), chiral symmetry still dictates the dynamics in the low-energy regime of QCD, provided the box is large enough and the masses of the lightest pseudoscalar mesons are not too small [9]. In an isotropic box with periodic boundary conditions for the meson fields, the form of the chiral Lagrangian is exactly the same as in the infinite volume. In particular, the low-energy constants are volume-independent. The finite volume dependence enters ChPT solely through the propagators,

$$G_0^{\text{(FV)}}(x) \equiv \langle \pi(x)\,\pi^\dagger(0)\rangle_{\text{FV}} = \sum_{n\,\in\,\mathbb{Z}^4} G_0(x + n_\mu L_\mu)\,, \qquad (4.1)$$

where $G_0(x) = \langle \pi(x)\,\pi^\dagger(0)\rangle$ denotes the infinite volume propagator, and L_μ is the box extent in the μ-th direction. The propagators consist of the infinite volume contribution where all n_μ are zero, but they also receive contributions from the particles propagating multiple times around the box in each direction. Since the infinite volume propagator falls off exponentially at large distances, these additional terms are suppressed with increasing volume. The first three contributions to a propagation in time ($n_1 = n_2 = n_3 = 0$) are shown in Fig. 4.1.

Equivalently, to Eq. (4.1), integrals over four-momenta p are substituted for sums,

$$\int \frac{\mathrm{d}^4 p}{(2\pi)^4} G_{ab}^{\text{con}}(p^2)\,\mathrm{e}^{ipx} \longrightarrow \frac{1}{V}\sum_p G_{ab}^{\text{con}}(p^2)\,\mathrm{e}^{ipx} = \langle \pi_{ab}(x)\pi_{ba}(0)\rangle_{\text{FV}}^{\text{con}}\,, \qquad (4.2)$$

$$\int \frac{\mathrm{d}^4 p}{(2\pi)^4} G_{ab}^{\text{disc}}(p^2)\,\mathrm{e}^{ipx} \longrightarrow \frac{1}{V}\sum_p G_{ab}^{\text{disc}}(p^2)\,\mathrm{e}^{ipx} = \langle \pi_{aa}(x)\pi_{bb}(0)\rangle_{\text{FV}}^{\text{disc}}\,, \qquad (4.3)$$

with $V = L_0 L_1 L_2 L_3$. The now quantized momenta p_μ are integer multiples of $2\pi/L_\mu$, that is (no summation over μ),

$$p_\mu = \frac{2\pi}{L_\mu}n_\mu\,, \qquad \text{with } n_\mu \in \mathbb{Z}\,. \qquad (4.4)$$
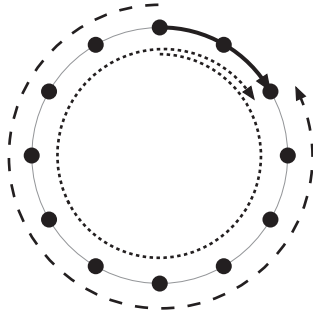
44

Figure 4.1.: One-dimensional lattice with periodic boundary conditions (ring of lattice points). The first three contributions ($n_0 = 0$, -1, and 1) to the finite volume propagator from a lattice point t to $t+2$ are shown with a thick solid, a dashed, and a dotted line, respectively.

In the present work, the box lengths are chosen to be $L_0 = T$ and $L_1 = L_2 = L_3 = L$. A generalization to arbitrary L_μ will be evident. Typically for lattice simulations, the extent in time direction is equal to or larger than the spatial extent, $T \geq L$, and it is therefore sufficient to focus on L in the following considerations.

The expansion parameters of ChPT are the momenta p and the light meson masses M_{GB}, which both have to be much smaller than the typical hadronic scale $\Lambda_{\mathrm{had}} \sim 1$ GeV

$$p \ll \Lambda_{\mathrm{had}} , \qquad M_{\mathrm{GB}} \ll \Lambda_{\mathrm{had}} . \tag{4.5}$$

Since $p_i = \frac{2\pi}{L} n_i$, the box length L must fulfill the condition

$$L \gg \frac{2\pi}{\Lambda_{\mathrm{had}}} \sim 1 \text{ fm} \tag{4.6}$$

in order to have any non-zero momenta allowing for the expansion in p. The masses M_{GB}, however, are not constrained by such a relation. If the Compton wavelengths of the light mesons are larger than the box size, $M_{\mathrm{GB}}L \ll 1$, one enters the so-called ϵ-regime [8, 9]. The propagators develop a zero-mode, $1/(M_{\mathrm{GB}}^2 V)$, which diverges in the chiral limit and cannot be treated perturbatively. On the other hand, with Compton wavelengths much smaller than the box size, $M_{\mathrm{GB}}L \gg 1$, the standard p-expansion can be adopted, in which the power-counting is as follows [7]:

$$p^2 \sim M_{\mathrm{GB}}^2 \sim m_q , \qquad p \sim \frac{1}{L} \sim \frac{1}{T} \tag{4.7}$$

In this thesis, all finite volume calculations will be restricted to the p-regime.

How observables like meson masses and decay constants are affected by the finite volume has been studied extensively, and the corrections are found to be exponentially suppressed by powers of $\exp(-M_{\mathrm{GB}}L)$, [7, 61–64].

Before tackling the FV computation of the scalar correlator, some basic strategies used in finite volume calculations are illustrated at the example of the charged meson masses [7, 61, 63].

4.2. Finite volume corrections to meson masses

In order to get familiar with finite volume calculations in ChPT, the relatively simple example of the charged meson masses is considered, following mainly Ref. [61]. For simplicity, the lattice spacing is taken to be zero. The physical masses of the charged mesons $\pi_{ab}(x)$ are defined as the pole of the full propagator

$$G_{ab}^{\text{full}}(p^2) \equiv \int \mathrm{d}^4 x\, \mathrm{e}^{-ipx}\, \langle \Omega | \pi_{ab}(x) \pi_{ba}(0) | \Omega \rangle = \frac{\epsilon_b}{p^2 + M_{ab}^2 + \Sigma_{ab}(p^2)}\,, \qquad a \neq b\,, \quad (4.8)$$

in which the self-energy $\Sigma_{ab}(p^2)$ is the negative sum of all one-particle irreducible diagrams. At one-loop order, all contributions to the self-energy are tadpole diagrams
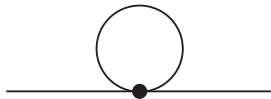
whose vertices arise from the kinetic term $\frac{f^2}{4}\mathrm{str}(\partial_\mu \Sigma\, \partial_\mu \Sigma^\dagger)$ and from the mass term $-\frac{f^2}{4}\mathrm{str}(\chi \Sigma^\dagger + \Sigma \chi)$ in the partially quenched Lagrangian. These diagrams give rise to the scalar integrals [65]

$$\mathcal{I}_i = \int \frac{\mathrm{d}^4 p}{(2\pi)^4} \frac{1}{(p^2 + M^2)^i}\,, \qquad i = 1, 2, \quad (4.9)$$

where $\mathcal{I}_2$ can be obtained from $\mathcal{I}_1$ by differentiation with respect to M^2. For the sake of simplicity, the finite volume corrections (FVCs) due to the spatial volume are taken to be much bigger than the corrections stemming from the box extent in time direction, that is, $T \to \infty$. For $i = 1$, the finite volume equivalent to Eq. (4.9) reads

$$\mathcal{I}_1^{(\text{FV})} = \frac{1}{L^3} \sum_{\vec{p}} \int \frac{\mathrm{d}p_0}{2\pi} \frac{1}{p_0^2 + \vec{p}^2 + M^2}\,. \quad (4.10)$$

The integrals and sums in Eqs. (4.9) and (4.10) are divergent and must be regulated appropriately. After doing so, one can define the dimensionless FVC

$$\delta_1 \equiv \frac{16\pi^2}{M^2}\left(\mathcal{I}_1^{(\text{FV})} - \mathcal{I}_1\right)\,. \quad (4.11)$$

The expressions $\mathcal{I}_1$ and $\mathcal{I}_1^{(\text{FV})}$ are related to the infinite volume and the finite volume propagators $G_0(x)$ and $G_0^{(\text{FV})}(x)$, respectively: The former can be written in terms of the modified Bessel function of the second kind [66], K_1,

$$G_0(x) = \int \frac{\mathrm{d}^4 p}{(2\pi)^4} \frac{\mathrm{e}^{ipx}}{p^2 + M^2} = \frac{M}{4\pi^2 |x|} K_1(M|x|)\,. \quad (4.12)$$

As discussed in the beginning, the FV propagator is given by

$$G_0^{(\text{FV})}(x) = \frac{1}{L^3} \sum_{\vec{p}} \int \frac{\mathrm{d}p_0}{2\pi} \frac{\mathrm{e}^{ipx}}{p_0^2 + \vec{p}^2 + M^2} = G_0(x) + \sum_{\vec{n} \neq 0} G_0(x + L\vec{n})\,. \quad (4.13)$$

Subtracting these two expressions and setting $x = 0$ finally yields

$$\delta_1(ML) = \frac{4}{ML} \sum_{\vec{n} \neq 0} \frac{K_1(|\vec{n}|ML)}{|\vec{n}|} \tag{4.14}$$

$$= \sqrt{\frac{\pi}{2}} \frac{24}{(ML)^{3/2}} \, \mathrm{e}^{-ML} + \mathcal{O}\left(\mathrm{e}^{-\sqrt{2}ML}\right). \tag{4.15}$$

One immediately sees the exponential suppression for large ML. In fact, for values $ML \gtrsim 3$, the sum in Eq. (4.14) converges very quickly. Note that the shown expansion is not possible in the ϵ-regime [8, 9]. If $ML < 1$, the sum does not converge, and one has to treat the zero-mode of the propagator exactly.

One can now write down the one-loop expressions for the finite volume meson masses simply by shifting the chiral logarithms [61] arising from the integration in Eq. (4.9),

$$\ln\left(\frac{M^2}{\mu^2}\right) \rightarrow \ln\left(\frac{M^2}{\mu^2}\right) + \delta_1(ML). \tag{4.16}$$

This shift applies, for instance, to the valence-valence pion mass for degenerate sea and degenerate valence quark masses, as it was discussed in Section 2.1.2, Eq. (2.44). A simpler example is the pion mass in unquenched ChPT, which was first calculated in Ref. [8],

$$M_\pi^{(\mathrm{FV})} = M_\pi \left[1 + \frac{M_\pi^2}{2N_S(4\pi f)^2} \delta_1(M_\pi L) \right]. \tag{4.17}$$

Here, M_π denotes the infinite volume pion mass. For typical values of masses and volumes, the finite volume corrections are small, e.g., if $L \approx 2$ fm and $M_\pi \approx 300$ MeV ($\Rightarrow M_\pi L \approx 3$), they are of $\mathcal{O}(1\%)$. This stands in contrast to the rather large FVCs to the scalar correlator, which will be discussed in the next section.

Generalizations of the outlined procedure but also different approaches to calculating FVCs to meson masses and decay constants were pursued in the literature [67, 68, 63]. The pion mass was even analyzed to two-loop order in standard ChPT [64]. In general, the finite volume corrections are found to be small if $M_\pi L > 5$.

4.3. A fitting formula for large volumes

The mixed-action computation of the scalar correlator is now extended to account for the finite volume. Since the only effect occurs in the propagators, one can use the infinite volume correlator of Eqs. (3.33) and (3.34) as the starting point and analyze the changes of the bubble functions when restricting them to a finite volume.

Two formulae will be derived, which are applicable for either large or small volumes. The first calculation will make the exponential suppression with factors of "meson mass times box extent" explicit and will therefore be fit for large volumes. The second calculation, on the other hand, is similar in spirit to Ref. [34], in which an asymptotic form for the bubble contributions at large times t and for $T \rightarrow \infty$ is given. The aim here, however, is to compute an exact fitting formula usable for small volumes.

The first steps of rewriting the single pole bubble function are the same as in the infinite volume case (see Appendix B). One has to deal with

$$B_{\rm SP}^{\rm (FV)}(T, L, t, M, m) = B_0^2 \int {\rm d}^3\vec{x}\, \frac{1}{TL^3} \sum_p B_{\rm SP}^{\rm (FV)}(T, L, p, M, m)\, {\rm e}^{ipx}\,. \tag{4.18}$$

The function

$$B_{\rm SP}^{\rm (FV)}(T, L, p, M, m) = \frac{1}{TL^3} \sum_k \frac{1}{(k+p)^2 + M^2} \frac{1}{k^2 + m^2} \tag{4.19}$$

is the corresponding finite volume momentum-space representation of the bubble function Eq. (3.18), and it is obtained by a convolution of the two propagators. The $\vec{x}$-integral in Eq. (4.18) is over the spatial volume L^3, and it yields a Kronecker delta $\delta_{\vec{p},\vec{0}}$ resulting in

$$B_{\rm SP}^{\rm (FV)}(T, L, t, M, m) = \frac{B_0^2}{T^2 L^3} \sum_{p_0, k} \frac{1}{(k+p_0)^2 + M^2} \frac{1}{k^2 + m^2}\, {\rm e}^{ip_0 t}\,, \tag{4.20}$$

where p_0 denotes the four-vector $(p_0, 0, 0, 0)^T$.

This equation is used in Refs. [34, 35] for a numerical evaluation of the scalar correlator. Although the authors did not employ lattice regularized chiral perturbation theory [69–71], they do not use integer multiples of $2\pi/L_\mu$ as the quantized momenta. Instead, they choose discrete lattice momenta $\hat{k}^2 = \sum_\mu \frac{4}{a^2} \sin^2(\frac{a}{2}k_\mu)$ and $\hat{p}_0^2 = \frac{4}{a^2} \sin^2(\frac{a}{2}p_0)$ in the propagators, and let the finite sums run over $k_\mu = \frac{2\pi}{L_\mu} n_\mu$ and $p_0 = \frac{2\pi}{L_0} n_0$ with $n_\mu \in \{-L_\mu/(2a), \dots L_\mu/(2a) - 1\}$ and $L_\mu/a \in \mathbb{N}$.

In the present work, the lattice spacing effects were incorporated by matching the Symanzik's effective theory to an effective continuum chiral Lagrangian [5, 6, 10]. The SET describes the underlying lattice theory at momenta much smaller than the lattice cutoff π/a, which, for typical lattice spacings of order 0.1 fm, is about 6 GeV. This is certainly much larger than the scale of chiral symmetry breaking, $\Lambda_{\rm had} \sim 1$ GeV, and it should therefore be sufficient to use the continuum Lagrangian with the quantized momenta $p_\mu = 2\pi/L_\mu n_\mu$ in order to study finite volume effects [72, 63], as illustrated in Fig. 4.2.

One can now start to rewrite Eq. (4.20). The two denominators are combined by introducing a Feynman parameter c and completing the square:

$$B_{\rm SP}^{\rm (FV)}(T, L, t, M, m) = \frac{B_0^2}{T^2 L^3} \sum_{p_0, k_0, \vec{k}} \int_0^1 {\rm d}c\, \frac{{\rm e}^{ip_0 t}}{\left[\vec{k}^2 + c(1-c)p_0^2 + (k_0 + cp_0)^2 + \alpha^2\right]^2} \tag{4.21}$$

The masses are contained in $\alpha^2 = m^2 + c(M^2 - m^2)$. In contrast to the infinite volume case, where the denominator can be written as $[k^2 + \kappa^2]$ by shifting the integration variable $k_0 \to k_0 + cp_0 \equiv k_0$, this procedure would here lead to a c-dependent summation and is therefore not appropriate. One can, however, use the expression [68]

$$\frac{1}{(u^2)^s} = \frac{1}{\Gamma(s)} \int_0^\infty {\rm d}\tau\, \tau^{s-1} {\rm e}^{-\tau u^2}\,, \quad s \geq 1\,, \tag{4.22}$$
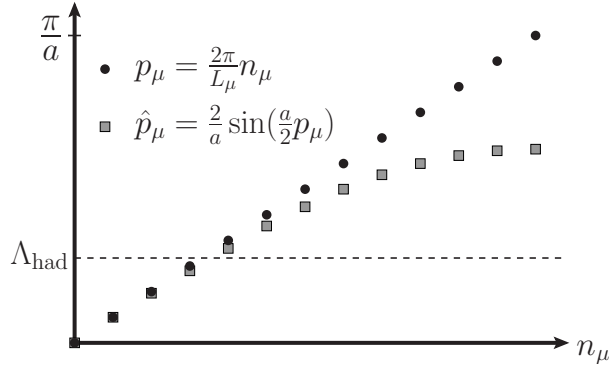
48

Figure 4.2.: Finite volume quantized momenta p_μ and discrete lattice momenta $\hat{p}_\mu$. ChPT is insensitive to momenta larger than Λ_{had}. Since the lattice cutoff π/a is much larger than Λ_{had} for typical lattice spacings, there is no difference in using p_μ or $\hat{p}_\mu$ in a calculation [72, 63].

to bring the finite volume bubble function into the following form:

$$
B_{\mathrm{SP}}^{(\mathrm{FV})}(T, L, t, M, m) = \frac{B_0^2}{T^2 L^3} \sum_{p_0, k_0, \vec{k}} \int_0^1 \mathrm{d}c \int_0^\infty \mathrm{d}\tau\, \tau\, \mathrm{e}^{-\tau \alpha^2} \mathrm{e}^{-\tau \vec{k}^2} \mathrm{e}^{-\tau c(1-c)p_0^2} \mathrm{e}^{-\tau(k_0 + c p_0)^2} \mathrm{e}^{i p_0 t}
$$

$$(4.23)$$

In the next step, the three sums over p_0, k_0, and $\vec{k}$ are taken care of. At the moment, the exponentials show a growing behavior with increasing box volume, e. g., $\exp\left(-\mathrm{const.}\,(2\pi)^2/L^2\right)$. The aim is to rewrite them into exponentially falling terms. This is achieved with the help of the Poisson summation formula (PSF) [73], which is derived in Appendix C. This convenient formula relates the values of a continuous $\mathcal{T}$-periodic function f to the values of its Fourier transform $\tilde{f}$,

$$
\sum_{n=-\infty}^{\infty} f(n\mathcal{T}) = \frac{1}{\mathcal{T}} \sum_{k=-\infty}^{\infty} \tilde{f}\left(\frac{2\pi k}{\mathcal{T}}\right).
$$

$$(4.24)$$

Although the PSF exists in many other alternative forms, the above expression is the one needed for the current purposes. With this powerful tool at hand, one can handle the occurring sums in the bubble function. They all are elliptic theta functions [74, 68, 75]

$$
\vartheta(\sigma, \omega) \equiv \sum_{n=-\infty}^{\infty} \mathrm{e}^{-\sigma(n+\omega)^2},
$$

$$(4.25)$$

which obey the Poisson resummation formula in the following way (see Appendix C):

$$
\vartheta(\sigma, \omega) = \sqrt{\frac{\pi}{\sigma}}\, \mathrm{e}^{-\sigma\omega^2} \cdot \vartheta\left(\frac{\pi^2}{\sigma}, -i\frac{\omega\sigma}{\pi}\right)
$$

$$(4.26)$$

In all three cases, σ will be proportional to either $\frac{(2\pi)^2}{L^2}$ or $\frac{(2\pi)^2}{T^2}$, and the structure of ω will be such that the exponential $\mathrm{e}^{-\sigma\omega^2}$ cancels, which makes the exponential suppression with L or T explicit. This is demonstrated now.

49

Rewriting the $\vec{k}$-sum:

The first sum, or rather three sums, read

$$\sum_{\vec{k}} e^{-\tau \vec{k}^2} = \sum_{\vec{n}=-\infty}^{\infty} e^{-\tau\left(\frac{2\pi}{L}\vec{n}\right)^2}, \tag{4.27}$$

with $\vec{n} = (n_x, n_y, n_y) \in \mathbb{Z}^3$. These are elliptic theta functions with $\omega = 0$ and $\sigma = \tau\frac{(2\pi)^2}{L^2}$. The Poisson summation formula then allows to write them as

$$\sum_{\vec{k}} e^{-\tau \vec{k}^2} = \frac{L^3}{8\sqrt[3]{\pi\tau}} \sum_{\vec{n}=-\infty}^{\infty} e^{-\frac{L^2}{4\tau}\vec{n}^2}. \tag{4.28}$$

Rewriting the k_0-sum:

This sum is an elliptic theta function with parameters $\sigma = \tau\frac{(2\pi)^2}{T^2}$ and $\omega = \frac{Tcp_0}{2\pi}$. Applying the PSF yields

$$\sum_{k_0} e^{-\tau(k_0+cp_0)^2} = \frac{T}{2\sqrt{\pi\tau}} \sum_{n_0=-\infty}^{\infty} e^{-\frac{T^2}{4\tau}\left(n_0-i\frac{2\tau cp_0}{T}\right)^2} e^{-\tau c^2 p_0^2}. \tag{4.29}$$

By combining the two previously given findings, one obtains the intermediate result

$$B_{\text{SP}}^{(\text{FV})}(T, L, t, M, m) = \frac{B_0^2}{16\pi^2}\frac{1}{T}\sum_{p_0,n_0,\vec{n}}\int_0^1 dc \int_0^\infty d\tau\, \tau^{-1} e^{-\tau\alpha^2} e^{-\frac{1}{4\tau}\left[T^2\left(n_0-i\frac{2\tau cp_0}{T}\right)^2+L^2\vec{n}^2\right]}$$

$$\times\, e^{-\tau c(1-c)p_0^2}\, e^{-\tau c^2 p_0^2}\, e^{ip_0 t}. \tag{4.30}$$

Rewriting the p_0-sum:

Now, all p_0-dependent parts are collected and the square is completed in p_0:

$$\frac{1}{T}\sum_{p_0} e^{-\frac{T^2}{4\tau}\left(n_0-i\frac{2\tau cp_0}{T}\right)^2} e^{-\tau c(1-c)p_0^2}\, e^{-\tau c^2 p_0^2}\, e^{ip_0 t} = e^{-\frac{T^2}{4\tau}n_0^2}\frac{1}{T}\sum_{p_0} e^{-\lambda\left(p_0-i\frac{\tilde{t}}{2\lambda}\right)^2} e^{-\frac{\tilde{t}^2}{4\lambda}} \tag{4.31}$$

Here, the abbreviations $\lambda = \tau c(1-c)$ and $\tilde{t} = t + cn_0 T$ were used. Again, the sum is an elliptic theta function, this time with $\sigma = \lambda\frac{(2\pi)^2}{T^2}$ and $\omega = -i\frac{\tilde{t}T}{4\pi\lambda}$. The Poisson summation formula thus leads to

$$e^{-\frac{T^2}{4\tau}n_0^2}\frac{1}{T}\sum_{p_0} e^{-\lambda\left(p_0-i\frac{\tilde{t}}{2\lambda}\right)^2} e^{-\frac{\tilde{t}^2}{4\lambda}} = e^{-\frac{T^2}{4\tau}n_0^2}\frac{1}{2\sqrt{\pi\lambda}}\sum_{\tilde{n}_0=-\infty}^{\infty} e^{-\frac{T^2}{4\lambda}\left(\tilde{n}_0-\frac{\tilde{t}}{T}\right)^2}. \tag{4.32}$$

Plugging everything together results in

$$B_{\text{SP}}^{(\text{FV})}(T, L, t, M, m) = \frac{B_0^2}{32\pi^{5/2}}\sum_{\tilde{n}_0,n_0,\vec{n}}\int_0^1 dc \int_0^\infty d\tau\, \frac{\tau^{-\frac{3}{2}}}{\sqrt{\beta}}\, e^{-\tau\alpha^2} e^{-\frac{\gamma}{4\tau}}, \tag{4.33}$$

with the short-hand notation

$$\beta = c(1-c), \qquad \gamma = \frac{T^2}{c(1-c)}\left(\tilde{n}_0 - cn_0 - \frac{t}{T}\right)^2 + T^2 n_0^2 + L^2\vec{n}^2. \tag{4.34}$$

n	0	1	2	3	4	5	6	7	8	9	10	11	12	13	14	15	16	17
$\rho(n)$	1	6	12	8	6	24	24	0	12	30	24	24	8	24	48	0	6	48

<div align="center">Table 4.1.: Multiplicities $\rho(n)$ for $n \le 17$</div>

The τ-integration can be performed analytically (see Eq. (B.10) in Appendix B), and one receives

$$B_{\text{SP}}^{\text{(FV)}}(T, L, t, M, m) = \frac{B_0^2}{16\pi^2} \sum_{\tilde{n}_0, n_0, \vec{n}=-\infty}^{\infty} \int_0^1 dc \, \frac{1}{\sqrt{\beta\gamma}} \, e^{-\sqrt{\frac{m^2 + c(M^2 - m^2)}{c(1-c)}} \sqrt{\beta\gamma}}. \tag{4.35}$$

This expression looks familiar, and indeed, the summand with $(\tilde{n}_0, n_0, \vec{n}) = (0, 0, \vec{0})$ equals the infinite volume bubble function Eq. (3.21), since $\sqrt{\beta\gamma}$ simplifies to $|t|$. All other terms in the sum occur due to the finite volume and are corrections to the corresponding integrals of the infinite volume.

In the last step, the sum over $\vec{n}$ can be written as

$$\sum_{\vec{n}=-\infty}^{\infty} f(\vec{n}^2) = \sum_{n=0}^{\infty} \rho(n) \, f(n). \tag{4.36}$$

How often the different summands $n = \vec{n}^2 = n_x^2 + n_y^2 + n_z^2$ occur, is encoded in the multiplicities $\rho(n)$, which are given in Tab. 4.1 for $n \le 17$.

By setting $M = m$, one obtains the FV single pole bubble function for equal masses. Derivation with respect to the mass, $-\frac{1}{2}\frac{\partial}{\partial m^2}$, then yields the FV double pole bubble function. The final results for $B_{\text{SP}}^{\text{(FV)}}$ and $B_{\text{DP}}^{\text{(FV)}}$ are presented with a factor mL pulled out of the exponent:

$$B_{\text{SP}}^{\text{(FV)}}(T, L, t, M, m) = \frac{B_0^2}{16\pi^2} \sum_{\tilde{n}_0, n_0=-\infty}^{\infty} \sum_{n=0}^{\infty} \int_0^1 dc \, \frac{\rho(n)}{L\sqrt{c(1-c)\tilde{\gamma}}} \, e^{-mL\sqrt{1 + c\left(\frac{M^2}{m^2} - 1\right)}\sqrt{\tilde{\gamma}}}$$

$$B_{\text{SP}}^{\text{(FV)}}(T, L, t, m, m) = \frac{B_0^2}{16\pi^2} \sum_{\tilde{n}_0, n_0=-\infty}^{\infty} \sum_{n=0}^{\infty} \int_0^1 dc \, \frac{\rho(n)}{L\sqrt{c(1-c)\tilde{\gamma}}} \, e^{-mL\sqrt{\tilde{\gamma}}} \tag{4.37}$$

$$B_{\text{DP}}^{\text{(FV)}}(T, L, t, m, m) = \frac{B_0^2}{64\pi^2} \sum_{\tilde{n}_0, n_0=-\infty}^{\infty} \sum_{n=0}^{\infty} \int_0^1 dc \, \frac{\rho(n)}{m\sqrt{c(1-c)}} \, e^{-mL\sqrt{\tilde{\gamma}}}$$

When considering the scalar correlator without isospin symmetry, one also needs the FV double pole bubble function $B_{\text{DP}}^{\text{(FV)}}(T, L, t, M, m) = -\frac{\partial}{\partial m^2} B_{\text{SP}}^{\text{(FV)}}(T, L, t, M, m)$ for unequal masses. This can be found in Appendix D together with the whole expression for the correlator $C_{\bar{y}x}^{1+1+1}(t)$.

In Eqs. (4.37), $\tilde{\gamma}$ is the abbreviation for

$$\tilde{\gamma} = \frac{T^2}{L^2} \frac{\left(\tilde{n}_0 - cn_0 - \frac{t}{T}\right)^2}{c(1-c)} + \frac{T^2}{L^2} n_0^2 + n. \tag{4.38}$$
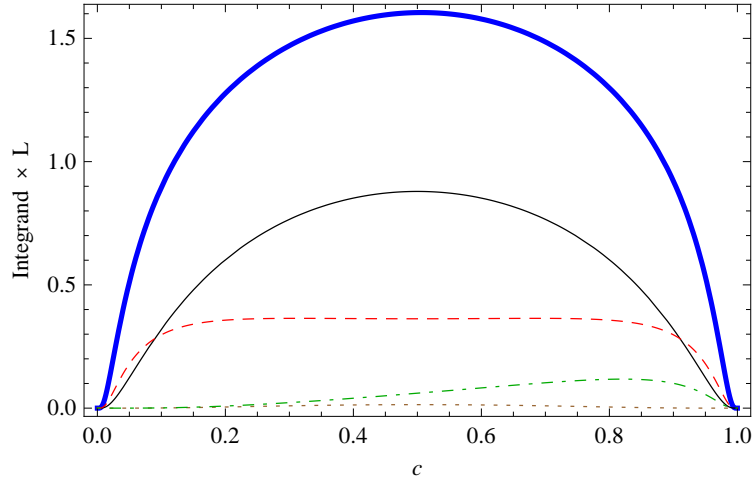
Figure 4.3.: Integrands of the four main contributions to the FV single pole bubble function with $T = 3$ fm, $L = 3$ fm, $t = T/4$, $M = m = 200$ MeV. The thin solid line is the infinite volume part $(\tilde{n}_0, n_0, n) = (0, 0, 0)$. The dotted, dashed, and dot-dashed lines correspond to $(1, 0, 0)$, $(0, 0, 1)$, and $(1, 1, 0)$, respectively. The thick solid line shows the whole finite volume integrand.

These three expressions are exact and can be used to evaluate the scalar correlator,

$N_S = 2$:

$$
\begin{aligned}
C_{\bar{y}x}(t) = &- 2\left(M_u^2 - M_x^2 + 2\hat{a}^2\gamma_{SS}\right) \cdot B_{\mathrm{DP}}^{(\mathrm{FV})}(T, L, t, M_x, M_x) \\
&- 2B_{\mathrm{SP}}^{(\mathrm{FV})}(T, L, t, M_x, M_x) + 2B_{\mathrm{SP}}^{(\mathrm{FV})}(T, L, t, M_{ux}, M_{ux}) \,,
\end{aligned}
\tag{4.39}
$$

$N_S = 2 + 1$:

$$
\begin{aligned}
C_{\bar{y}x}^{2+1}(t) = &- \frac{4}{3}\left[R_x\binom{u, s}{\eta} + 3\hat{a}^2\gamma_{SS}\right] \cdot B_{\mathrm{DP}}^{(\mathrm{FV})}(T, L, t, M_x, M_x) \\
&- \frac{4}{3}D_x^x\binom{u, s}{\eta} \cdot B_{\mathrm{SP}}^{(\mathrm{FV})}(T, L, t, M_x, M_x) - \frac{4}{3}D_\eta^x\binom{u, s}{x} \cdot B_{\mathrm{SP}}^{(\mathrm{FV})}(T, L, t, M_x, M_\eta) \\
&+ 2B_{\mathrm{SP}}^{(\mathrm{FV})}(T, L, t, M_{ux}, M_{ux}) + B_{\mathrm{SP}}^{(\mathrm{FV})}(T, L, t, M_{sx}, M_{sx}) \,,
\end{aligned}
\tag{4.40}
$$

in the p-regime, that is, as long as $ML \gg 1$ and $mL \gg 1$.

The integrals need to be solved numerically, which poses no problem: On the one hand, the integrations are over a closed interval $c \in [0, 1]$, and on the other hand, the integrands are smooth functions, as illustrated in Fig. 4.3.

The following analysis of the formula's practical applicability refers at first to the single pole bubble functions. Furthermore, $M \geq m$ and $T \geq L$ is assumed. The special rôle of the double pole is discussed afterwards.

Discussion:

The finite volume corrections, $B_{\text{SP/DP}}^{\text{(FV)}} - B_{\text{SP/DP}}$, are depending on the product $mL \gg 1$, the ratios $\frac{M}{m}$, $\frac{T}{L}$, and $\frac{t}{T}$, as well as an explicit factor $\frac{1}{L}$ in the case of the SP bubble functions, and, respectively, a factor $\frac{1}{m}$ in the DP bubble function.

The first observation is that the FVCs are indeed exponentially suppressed with powers of $\exp(-mL)$,

$$ -mL\sqrt{\tilde{\gamma}} \leq -\frac{mL}{\sqrt{3}} \left(\frac{T^2}{L^2} \frac{\left(\tilde{n}_0 - cn_0 - \frac{t}{T}\right)^2}{c(1-c)} + \frac{T^2}{L^2} n_0^2 + n \right) . \tag{4.41} $$

Physically, this makes sense, since mL determines how often the Compton wavelength $\lambda = 1/m$ of a particle fits into the box. For larger mL, the particles are less affected by the finite volume, and therefore the FVCs are smaller.

The sums' rate of convergence is determined mainly by the size of mL. Two cases are distinguished now: $t \ll T/2$ and $t \to T/2$. Numerical (theoretical) examples for the scenarios discussed in the next paragraphs can be found in Tab. 4.2.

Small t:

At small time separations $t \ll T/2$, the size of the different summands is dominated solely by the ratio T^2/L^2. If it were not for cn_0, only the zeroth term in the $\tilde{n}_0$-sum would yield a substantial contribution, since then, $t^2/T^2 \ll (1 - t/T)^2$ in the first summand of $\tilde{\gamma}$ and $0 \ll T^2/L^2$ in the second one. The explicit dependence on cn_0 slightly changes this behavior. Nevertheless, only the first few terms in n_0 are relevant, and also the n-sum can be truncated at relatively small n.

Large t:

The main interest is in large time separations, because then the mixed-action ChPT correlator matches the corresponding mixed-action QCD correlator. As a consequence of increasing t, a larger amount of higher-order terms in the sums is needed. If t approaches $T/2$, the FVCs reach their maximum, and they are at least of $\mathcal{O}(100\%)$. This can be seen by considering the terms $(\tilde{n}_0, n_0, n) = (0, 0, 0)$ and $(1, 0, 0)$, which are identical. As the particles "travel" through the box, they more and more experience the effects of the finite volume with its periodic boundary conditions.

At large t, the first terms in the n-sum will all yield a contribution of the same order of magnitude, since the first term in $\tilde{\gamma}$ is much bigger than small n. Generally, the larger t is, the more terms are needed (at fixed L and T).

Truncating the sums:

In order for the bubble functions to fulfill their purpose of practical fitting functions, it is now examined where the sums can be truncated to yield results to the accuracy of interest. The examples in Tab. 4.2 are exact up to 1% (3%). The convergence of the sums was tested numerically, and it was found that quantitatively good results with only a few number of numerical integrations are obtained when $mL > 3$ and $m > 200$ MeV. Otherwise, the sums converge too slowly, up to the point where many hundreds of integrations need to be performed.

mL	m [MeV]	L [fm]	T [fm]	t/T	$\tilde{n}_0$	n_0	n	FV/InfV
2.0	200	2.0	2.0	1/4	2 (2)	3 (2)	26 (18)	8.33
				1/3	3 (2)	3 (3)	21 (14)	14.12
				1/2	3 (2)	3 (3)	21 (15)	41.01
3.0	200	3.0	3.0	1/4	2 (1)	2 (2)	8 (6)	2.98
				1/3	2 (1)	3 (2)	9 (6)	4.95
				1/2	2 (2)	3 (2)	9 (6)	17.35
4.5	300	3.0	3.0	1/4	1 (1)	1 (1)	3 (2)	1.49
				1/3	1 (1)	1 (1)	5 (3)	2.15
				1/2	1 (1)	2 (1)	5 (3)	2.15
5.3	350	3.0	3.0	1/4	1 (1)	1 (1)	2 (2)	1.27
				1/3	1 (1)	1 (1)	3 (2)	1.69
				1/2	1 (1)	1 (1)	4 (2)	7.10
3.3	200	3.3	4.4	1/5	1 (1)	1 (1)	6 (5)	2.06
				1/4	1 (1)	1 (1)	8 (5)	2.69
				1/3	1 (1)	1 (1)	10 (6)	4.48
6.2	350	3.5	7.0	1/6	0 (0)	0 (0)	1 (1)	1.13
				1/5	0 (0)	0 (0)	2 (1)	1.20
				1/4	0 (0)	0 (0)	3 (2)	1.34
2.0	200	2.0	2.0	1/4	3 (2)	3 (3)	41 (23)	27.84
				1/3	3 (2)	3 (3)	48 (25)	39.30
				1/2	3 (2)	4 (3)	27 (20)	82.63
3.0	200	3.0	3.0	1/4	2 (2)	2 (2)	12 (8)	6.67
				1/3	2 (2)	2 (2)	14 (8)	10.07
				1/2	2 (2)	2 (2)	17 (9)	27.28
4.5	300	3.0	3.0	1/4	1 (1)	1 (1)	6 (3)	2.20
				1/3	1 (1)	2 (1)	6 (5)	3.24
				1/2	2 (2)	2 (2)	10 (7)	11.34
5.3	350	3.0	3.0	1/4	1 (1)	1 (1)	3 (2)	1.64
				1/3	1 (1)	1 (1)	5 (3)	2.30
				1/2	1 (1)	1 (1)	6 (3)	8.66
3.3	200	3.3	4.4	1/5	1 (1)	1 (1)	12 (6)	3.74
				1/4	1 (1)	2 (1)	10 (6)	4.77
				1/3	1 (1)	2 (2)	11 (6)	7.51
6.2	350	3.5	7.0	1/6	0 (0)	0 (0)	2 (2)	1.26
				1/5	0 (0)	0 (0)	3 (2)	1.36
				1/4	0 (0)	1 (0)	4 (2)	1.55

Table 4.2.: Numerical examples for where the $\tilde{n}_0$-, n_0-, and n-sum have to be truncated in order to reach at least 1% (3%) accuracy. Values for $B_{\mathrm{SP}}^{(\mathrm{FV})}(T, L, t, m, m)$ are presented in the upper half, and for $B_{\mathrm{DP}}^{(\mathrm{FV})}(T, L, t, m, m)$ in the lower half. The last column shows the ratio of finite volume to infinite volume bubble function.

Generally, when $mL > 5$ and $m > 300$ MeV, it is sufficient to truncate the sums at $\tilde{n}_0 = n_0 = \pm 1$ and $n \approx 5$. For smaller values of masses and box lengths, the FVCs grow tremendously, and the slow rate of convergence makes the numerical evaluation very time-consuming.

The power of the bubble functions as they are given in Eq. (4.37) is their applicability at large volumes (and large masses). From now on, $mL > 5$ is assumed.

If $T \gg L$, non-zero $\tilde{n}_0$- and n_0-terms are largely suppressed due to the factors $\frac{T^2}{L^2} \gg 1$ in $\tilde{\gamma}$, and one can truncate the sums at $\tilde{n}_0 = n_0 = 0$. In this case, $\tilde{\gamma}$ simplifies to

$$\tilde{\gamma} = \frac{1}{L^2}\frac{t^2}{c(1-c)} + n \,, \tag{4.42}$$

and the remaining n-sum needs to be evaluated up the first or second term only, depending on t and the size of m. If furthermore $m \geq 350$ MeV or $L \geq 3.5$ fm, only the first correction to the infinite volume term needs to be respected. That is, for each term in the scalar correlator $C^{2+1}_{\bar{y}x}(t)$, one has to compute two integrals numerically and receives the final finite volume result.

Note, however, that it is still necessary to keep $t < T/2$. One should also caution that the FVCs at a fixed ratio t/T diverge with a growing box extent in time direction T.

The double pole:

The FV double bubble function deserves a closer look. As in the infinite volume, it is enhanced by $\frac{t}{4m}$, but moreover, it experiences additional effects due to the final volume itself [76, 37]. When comparing the factors in front of the exponential in the integrands of the single and double pole bubble functions,

$$\begin{aligned} \text{SP:} \quad & 1/\sqrt{T^2\left(\tilde{n}_0 - cn_0 - \frac{t}{T}\right)^2 + c(1-c)\left(T^2 n_0^2 + L^2 \vec{n}^2\right)} \\ \text{DP:} \quad & 1/m\sqrt{c(1-c)} \,, \end{aligned} \tag{4.43}$$

one immediately sees that the double pole is also enhanced with T and L. This effect reduces as t approaches $T/2$, since the impact of $c(1-c)\left(T^2 n_0^2 + L^2 \vec{n}^2\right)$ becomes small compared to $T^2(\tilde{n}_0 - cn_0 - \frac{t}{T})^2$. Again, numerical examples can be found in Tab. 4.2. The ratio of double to single pole FVCs for $M = m = 300$ MeV, $T = 4.5$ fm, and $L = (2 \ldots 4.5)$ fm at three different values of t is shown in Fig. 4.4. For comparability, the ratios have been normalized to m. The enhancement with growing t and L is evident. The consequence of the "enhanced" prefactor in the integrands is a slower rate of convergence of all three sums. This sets new bounds to the practical applicability of the fitting formula. Whereas the $\tilde{n}_0$- and n_0-sums are just slightly affected, the n-sum must be truncated at much higher values. For $mL > 5$ and $L > 3.5$ fm, however, it is still sufficient to regard only the terms with $\tilde{n}_0 = n_0 = 0$, and the n-sum can be truncated at $n = 5$.
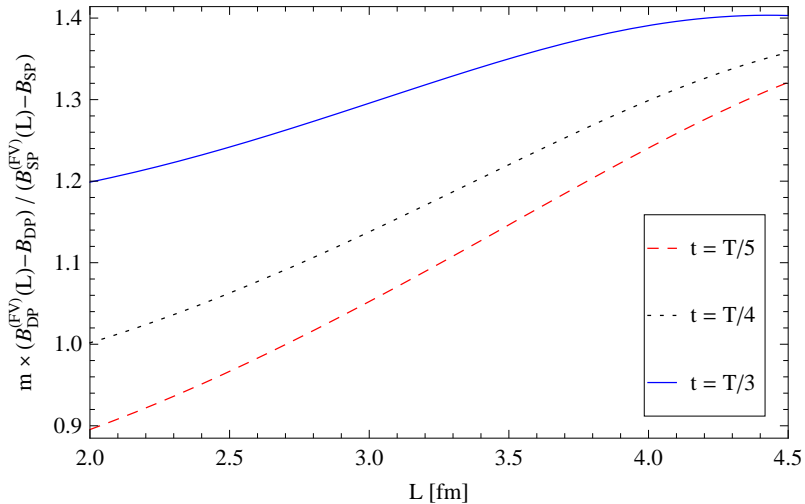
Figure 4.4.: L-dependence of the ratio of double to single pole FVCs for $M = m = 300$ MeV and $T = 4.5$ fm at three different values of t, normalized to m. The double pole is enhanced with growing t and L.

The actual size of the double and single pole terms in the scalar correlator depends on the residues of the partial fraction decomposition. The double pole enhancement is therefore more pronounced if the difference between sea and valence masses is big.

In Fig. 4.5, the dramatic effect of the double pole is exemplified. Shown are the double pole contribution, the sum of all single pole contributions, as well as the whole correlator $C_{\bar{y}x}^{2+1}(t)$ for the following set of parameters (note that $\hat{a}^2\Delta_{\text{sea}}$ is included in the sea-sea masses): $T = 3.5$ fm, $L = 3.5$ fm, $M_u = 300$ MeV, $M_s = 600$ MeV, $M_x = 250$ MeV, $\hat{a}^2\Delta_{\text{mix}} = \hat{a}^2\Delta'_{\text{mix}} = \hat{a}^2\gamma_{SS} = (160 \text{ MeV})^2$.

The other needed masses (the eta and the mixed meson masses) follow from these values: $M_\eta = 520$ MeV, $M_{ux} = 360$ MeV, $M_{sx} = 210$ MeV. The kaon mass, which does not occur explicitly in the correlator, is $M_{us} = 475$ MeV.

The actual values of $\hat{a}^2\Delta_{\text{mix}}$ and $\hat{a}^2\Delta'_{\text{mix}}$ have not yet been determined for mixed action ChPT with Wilson sea and GW valence quarks. They are inspired by the findings in Ref. [47] where staggered sea and domain-wall valence quarks were used. The authors determined the total mixed meson mass shift and found $\hat{a}^2\Delta_{\text{mix}} + \hat{a}^2\Delta'_{\text{mix}} \approx (320 \text{ MeV})^2$ for the asqtad-improved coarse MILC lattice. Then, in Ref. [31], $\hat{a}^2\Delta_{\text{mix}} \approx (160 \text{ MeV})^2$ was estimated. For this particular plot, the unknown parameter $\hat{a}^2\gamma_{SS}$ was chosen to have the same size as $\hat{a}^2\Delta_{\text{mix}}$.

The correlator's negativity is clearly dominated by the double pole (for the above choice of masses). To study the influence of $\hat{a}^2\gamma_{SS}$ on the correlator, this parameter was varied between $-(250 \text{ MeV})^2$ and $(250 \text{ MeV})^2$. Negative values suppress and positive values enhance the negativity of the double pole. The correlator was found to be positive for $\hat{a}^2\gamma_{SS} \lesssim -(190 \text{ MeV})^2$.

The parameters $\hat{a}^2\Delta_{\text{sea}}$ and $\hat{a}^2\Delta'_{\text{mix}}$, which depend on the low-energy constants W'_6 and W'_8, were also varied within a reasonable range (the meson masses should not become
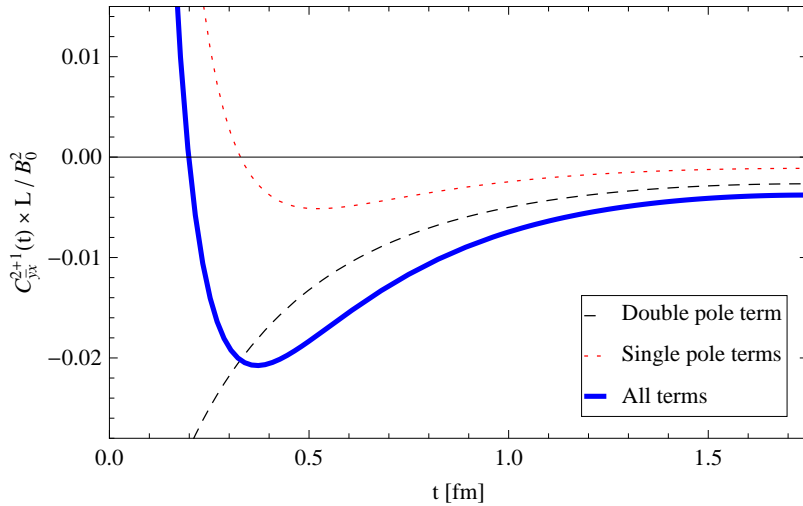
Figure 4.5.: Double pole contribution, sum of all single pole contributions, and the whole correlator for $T = 3.5$ fm, $L = 3.5$ fm, $M_u = 300$ MeV, $M_s = 600$ MeV, $M_x = 250$ MeV, and $\hat{a}^2 \Delta_{\mathrm{mix}} = \hat{a}^2 \Delta'_{\mathrm{mix}} = \hat{a}^2 \gamma_{SS} = (160 \text{ MeV})^2$.

negative). Since the shape of the correlator strongly depends on the size and signs of the other parameters, one can only make rather qualitative statements. The dependence was found to be mild for $|\hat{a}^2 \Delta_{\mathrm{sea}}|, |\hat{a}^2 \Delta'_{\mathrm{mix}}| < (160 \text{ MeV})^2$. For more extreme values, they can easily dominate the correlator's shape.

Eventually, the shift parameters $\hat{a}^2 \Delta_{\mathrm{mix}}$, $\hat{a}^2 \Delta'_{\mathrm{mix}}$, $\hat{a}^2 \Delta_{\mathrm{sea}}$, and $\hat{a}^2 \gamma_{SS}$ have to be determined by fitting lattice data.

Finite volume corrections:

Lastly, to visualize the size of the finite volume effects, the infinite volume correlator is shown in Fig. 4.6 together with the FVCs (for the masses and shift parameters given above). As can be seen in this plot and also in Tab. 4.2, the FVCs to the correlator are rather large for typical meson masses and box sizes. They are by no means a negligible contribution to the infinite volume formulae. This stands in contrast to the meson masses determined in a finite volume. The pion mass, for instance, receives a correction of $\mathcal{O}(1\%)$ if $M_\pi L > 3$ and $L > 2$ fm [63, 64]. As shown in Sec. 4.2, the only types of integrals one encounters in the calculation are the scalar integrals $\mathcal{I}_1$ and $\mathcal{I}_2$, which are "space-time independent" and thus only slightly affected when making the transition to the finite volume. The scalar two-point function, on the other hand, is a correlation function and therefore explicitly depends on the (space-)time separation. This results in much larger finite volume effects, especially for large time separations.

Summary:

The main results of this first finite volume calculation are now summarized. Starting from the momentum-space representation of the bubble functions, the Poisson summation formula allowed to rewrite the occurring sums over momenta into an expression which falls off exponentially with powers of "meson mass times box extent". In the final formulae
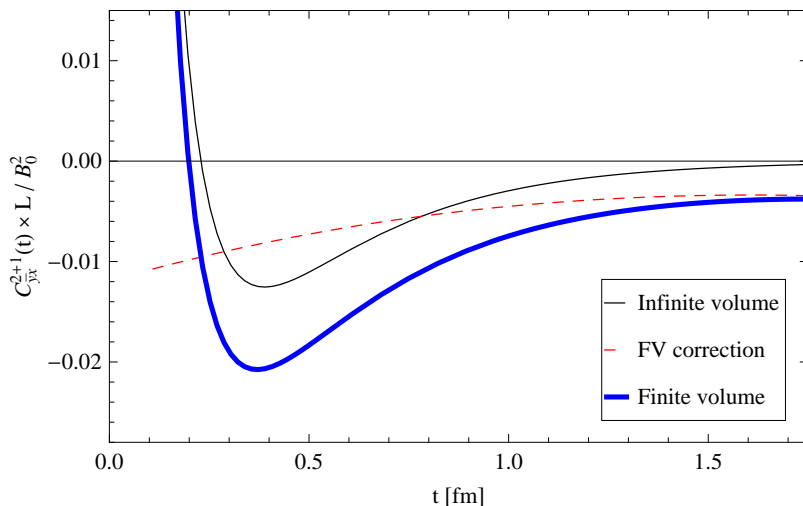
Figure 4.6.: Infinite volume correlator, finite volume corrections, and the sum of both, for $T = 3.5$ fm, $L = 3.5$ fm, $M_u = 300$ MeV, $M_s = 600$ MeV, $M_x = 250$ MeV, and $\hat{a}^2 \Delta_{\text{mix}} = \hat{a}^2 \Delta'_{\text{mix}} = \hat{a}^2 \gamma_{SS} = (160 \text{ MeV})^2$.

Eqs. (4.37) and (D.4), one is left with three sums and an integration over a closed interval, which can be performed numerically. Together with the expressions Eqs. (4.39), (4.40), and (D.2) of the scalar correlator ($C_{\bar{y}x}(t)$, $C_{\bar{y}x}^{2+1}(t)$, and $C_{\bar{y}x}^{1+1+1}(t)$), the bubble functions fulfill their purpuse as a fitting formula for data obtained from lattice simulations.

The derived form of the bubble functions is not practical for small volumes and masses due to the slow rate of convergence caused by the factor $-mL$ in the exponentials. A similar problem is present in the limit $t \to T/2$. However, for large, yet still theoretical values of masses and volumes ($ML > 5$, $mL > 5$, $L > 5$ fm, $T \geq L$, and $t \ll T/2$), they are perfectly applicable, because then the finite volume bubble functions reduce to two integrals, one of which is the infinite volume contribution and one which is the first correction term.

4.4. A fitting formula for small volumes

The aim of this second calculation is to find a fitting formula, which is applicable for small volumes (and masses). Instead of starting from momentum-space, the calculation begins with the single pole bubble function as it was first introduced in Eq. (3.18), now restricted to the finite volume,

$$
\begin{aligned}
B_{\text{SP}}^{\text{(FV)}}(T, L, t, M, m) &= B_0^2 \int \mathrm{d}^3 \vec{x} \, \frac{1}{TL^3} \sum_p \frac{\mathrm{e}^{ipx}}{p^2 + M^2} \frac{1}{TL^3} \sum_k \frac{\mathrm{e}^{ikx}}{k^2 + m^2} \\
&= \frac{B_0^2}{T^2 L^3} \sum_{p, k_0} \frac{\mathrm{e}^{i(p_0 + k_0)t}}{(p_0^2 + \vec{p}^2 + M^2)(k_0^2 + \vec{p}^2 + m^2)} \,.
\end{aligned} \tag{4.44}
$$

The finite volume double pole function is discussed afterwards. In the equation above, the $\vec{x}$-integral over the spatial volume projected on the spatial momenta $\vec{p} + \vec{k} = 0$. The $\vec{p}$-sum consists in fact of three sums: $\vec{p} = \frac{2\pi}{L}\vec{n}$ with $n_i \in \mathbb{Z}$. As before, it is more practical to evaluate the single sum

$$\sum_{\vec{p}} f(\vec{p}^2) = \sum_{n=0}^{\infty} \rho(n) f\left(n \cdot (2\pi)^2/L^2\right), \tag{4.45}$$

where the $\rho(n)$ are again the multiplicities given in Tab. 4.1. It is also convenient to define the energies $E_n(M) = \sqrt{\vec{p}^2 + M^2}$ and $E_n(m) = \sqrt{\vec{p}^2 + m^2}$. With the notation of Eq. (4.45), they read

$$E_n(M) = \sqrt{n \cdot \left(\frac{2\pi}{L}\right)^2 + M^2}, \qquad E_n(m) = \sqrt{n \cdot \left(\frac{2\pi}{L}\right)^2 + m^2}. \tag{4.46}$$

The p_0- and k_0-summations in Eq. (4.44) can be thought of as Fourier transformations of a one-dimensional momentum-space propagator with mass E_n. As before, it is possible to rewrite the sums with the help of an auxiliary integration $\frac{1}{Q} = \int_0^\infty d\tau \exp(-\tau Q)$, the Poisson summation formula (see Appendix C), and Eq. (B.10) from the Appendix B. One finds

$$\frac{1}{T} \sum_{p_0} \frac{e^{ip_0 t}}{p_0^2 + E_n(M)^2} = \sum_{\tilde{n}_0=-\infty}^{\infty} \frac{e^{-E_n(M)|t - \tilde{n}_0 T|}}{2E_n(M)}. \tag{4.47}$$

The term with $\tilde{n}_0 = 0$ equals the infinite volume propagator. All other terms occur due to the finite volume and are corrections to the corresponding Fourier integral.

Since $|t| \leq T$, the sum over $\tilde{n}_0$ can be split up, and the resulting geometric series $\sum_{n=1}^{\infty} q^n = \frac{q}{1-q}$ with $q = e^{-E_n(M)\tilde{n}_0 T}$ yields

$$\sum_{\tilde{n}_0=-\infty}^{\infty} \frac{e^{-E_n(M)|t - \tilde{n}_0 T|}}{2E_n(M)} = \frac{1}{2E_n(M)} \frac{e^{-E_n(M)t} + e^{-E_n(M)[T-t]}}{1 - e^{-E_n(M)T}}. \tag{4.48}$$

When plugging everything together, the finite volume single pole bubble function turns into

$$B_{\mathrm{SP}}^{(\mathrm{FV})}(T, L, t, M, m)$$
$$= \frac{B_0^2}{4L^3} \sum_{n=0}^{\infty} \rho(n) \left[\frac{e^{-E_n(M)t} + e^{-E_n(M)[T-t]}}{E_n(M)\left(1 - e^{-E_n(M)T}\right)}\right] \left[\frac{e^{-E_n(m)t} + e^{-E_n(m)[T-t]}}{E_n(m)\left(1 - e^{-E_n(m)T}\right)}\right]. \tag{4.49}$$

Each of the two fractions corresponds to one of the intermediate states in the bubble diagram. The periodic boundary conditions imposed on the meson fields render a propagation in time t equal to a propagation in $T - t$. This is exactly what the two nominators state. As in the fitting formula derived before, one sees that the finite volume corrections reach their maximum at $t/2$.

The above formula is exact; no approximations were made. Nevertheless, it is insightful to discuss some special theoretical cases. In the limit $T \to \infty$, the exponentials involving T tend to zero, which results in

$$B_{\text{SP}}^{\text{(FV)}}(T, L, t, M, m) \xrightarrow[T \to \infty]{t \ll T/2} \frac{B_0^2}{4L^3} \sum_{n=0}^{\infty} \rho(n) \frac{\text{e}^{-E_n(M)t}}{E_n(M)} \frac{\text{e}^{-E_n(m)t}}{E_n(m)} \, . \tag{4.50}$$

Taking also t to be large, suppresses all non-zero momentum terms in the sum and reduces the expression to the asymptotic formula given in Ref. [34],

$$B_{\text{SP}}^{\text{(FV)}}(T, L, t, M, m) \xrightarrow{\text{large } t} \frac{B_0^2}{4L^3} \frac{\text{e}^{-(M+m)t}}{Mm} \, . \tag{4.51}$$

At first glance, the bubble function seems to be suppressed by a factor L^3. One might therefore argue (as in Ref. [34]) that the influence of the bubble contributions on the correlator becomes less important for larger spatial volumes. This, however, is not true (at fixed t), since for increasing L, the difference between the energies E_{n+1} and E_n is getting smaller and so does the exponential suppression, that is, higher-order terms in the sum will be of the same order of magnitude as the zero-momentum term.

Eventually, for $L \to \infty$, the sum turns into the infinite volume single pole bubble integral, and all "summands" need to be respected. This stands in contrast to the first fitting formula Eq. (4.37), in which the sum contains one single term corresponding to the infinite volume bubble function. In this second formula, it is less clear how the infinite volume limit is approached. Loosely speaking, it works exactly the other way round. Larger L require more terms to be respected; smaller L require less, and finally, for small enough L, the zero-momentum approximation becomes exact to the precision of interest.

This second formula is perfectly applicable for fitting lattice data obtained in small volumes and with small masses. The condition, though, is still to be in the p-regime where $ML \gg 1$ and $mL \gg 1$. The formula has also the advantage that large t require less higher-order momentum terms of the sum to be respected due to the increasing exponential suppression. Furthermore, the formula involves only one summation and no integration. This makes it preferable to the first fitting formula.

Its limitations are at large spatial box extents L, at large masses M and m, and at time separations $t \ll T/2$, for then, the convergence of the sum slows down. However, it turns out that this does not happen in practice for common values of masses and volumes.

The following consideration refers to rather theoretical numerical examples:

Generally, the convergence is quick if t approaches $T/2$. Not more than 20 summands need to be respected, even at masses much larger than 500 MeV and volumes $L > 6$ fm. The other scenario is $t \ll T/2$. If the box is larger in the time than in the spatial directions, and $ML, mL > 10$, one needs about 30 terms. Bad convergence is given only for $T < L$. Then up to 100 summands must be taken into account, but still, only if the products ML and mL are much larger than 10.

Why does the sum converge this quickly? Only momenta $\frac{2\pi}{L}n$ smaller than $\Lambda_{\text{had}} \sim$ 1 GeV yield significant contributions to the bubble functions. If, e.g., $L = 4.5$ fm, then

$\frac{2\pi}{L}n = 275$ MeV, which means that only summands up to $n \approx 4$ are relevant. One therefore sees that it is more convenient to use the second derived expression Eq. (4.49) for the bubble function in an actual fitting process.

Lastly, for this purpose, the FV double pole bubble function for equal masses is needed. Setting $M = m$ in Eq. (4.49) yields

$$B_{\text{SP}}^{\text{(FV)}}(T, L, t, m, m) = \frac{B_0^2}{4L^3} \sum_{n=0}^{\infty} \rho(n) \left[\frac{\text{e}^{-E_n(m)t} + \text{e}^{-E_n(m)[T-t]}}{E_n(m)\left(1 - \text{e}^{-E_n(m)T}\right)} \right]^2 , \qquad (4.52)$$

and taking the derivative with respect to the mass, $-\frac{1}{2}\frac{\partial}{\partial m^2}$, results in the following equation:

$$B_{\text{DP}}^{\text{(FV)}}(T, L, t, m, m) = \frac{B_0^2}{8L^3} \sum_{n=0}^{\infty} \rho(n) \left[\frac{\left(\text{e}^{-Et} + \text{e}^{-E[T-t]}\right)\left(t\text{e}^{-Et} + [T-t]\text{e}^{-E[T-t]}\right)}{E^3\left(1 - \text{e}^{-ET}\right)^2} \right.$$

$$\left. + \frac{\left(1 - \text{e}^{-ET} + ET\text{e}^{-ET}\right)\left(\text{e}^{-Et} + \text{e}^{-E[T-t]}\right)^2}{E^4\left(1 - \text{e}^{-ET}\right)^3} \right] \quad (4.53)$$

Here, for brevity, $E \equiv E_n(m)$. The special features of the FV double pole bubble function, as they were discussed before, are apparent also in this form. They are, however, more obvious in the limits of $T \to \infty$ and large t, in which the above expression simplifies to

$$B_{\text{DP}}^{\text{(FV)}}(T, L, t, m, m) \xrightarrow{T \to \infty} \frac{B_0^2}{8L^3} \sum_{n=0}^{\infty} \rho(n) \frac{1 + tE_n(m)}{[E_n(m)]^4} \text{e}^{-2E_n(m)t} \qquad (4.54)$$

$$\xrightarrow{\text{large } t} \frac{B_0^2}{8L^3} \frac{1 + tm}{m^4} \text{e}^{-2mt} . \qquad (4.55)$$

Similarly to the infinite volume case, there is a contribution proportional to t. The additional factor $E_n(m)$ implies a finite volume enhancement for increasing L. The differences between two energies E_{n+1} and E_n become smaller, and hence more higher-momentum terms in the sum are required. Equation (4.55) equals the asymptotic form given in Ref. [34].

Summary:
The findings of the second finite volume calculation are now summarized. Starting point was the position-space representation of the bubble function. The Poisson summation formula allowed to rewrite two of the three occurring sums, which could then be solved by performing the geometric series. The result was one single summation over terms which are suppressed for small spatial volumes and masses, and for large time separations. The obtained fitting formulae for the scalar correlator Eqs. (4.39), (4.40), and (D.2) ($C_{\bar{y}x}(t)$, $C_{\bar{y}x}^{2+1}(t)$, and $C_{\bar{y}x}^{1+1+1}(t)$) together with the expressions Eqs. (4.49), (4.52), (4.53), and (D.5) for the bubble functions are perfectly applicable for common lattice parameters. A slow convergence of the sum is given only for extreme values of L, M, and m.

Summary and conclusions

Mixed-action lattice QCD simulations are suffering from a lack of unitarity at non-zero lattice spacing, even if the sea and valence renormalized quark masses are tuned to be equal. Although this unphysical effect is expected to vanish in the continuum limit, it is desirable to account for it when extrapolating lattice data to the physical quark masses and to the continuum as well as to the infinite volume. Chiral perturbation theory provides the framework to perform such extrapolations.

In this diploma thesis, an introduction to ChPT was given. The effective theory was then extended to partially quenched and mixed-action ChPT with Wilson sea and Ginsparg–Wilson valence quarks. It was shown that unitarity-violating effects manifest themselves in double poles in the flavor-neutral propagators and in new low-energy constants associated with new operators which arise due to the lack of symmetry between the sea and the valence sector.

The main object of interest in the present work was the isospin-one scalar two-point function for 2 and $2 + 1$ sea flavors. This quantity is known to be very sensitive to unitarity-violating effects. Since the final expression of the scalar correlator contains only one free parameter, γ_{SS}, it is a useful tool to verify if mixed-action ChPT describes all sources of unitarity-violation observed in lattice data. By fitting such data, one will gain information about the size and signs of the associated low-energy constants (or rather the combinations of low-energy constants Δ_{sea}, $\Delta_{\mathrm{mix}} + \Delta'_{\mathrm{mix}}$, and γ_{SS}).

The scalar correlator was at first analyzed in partially quenched ChPT, focusing on the so-called bubble diagram with two pseudoscalar intermediate states. The effect of the double pole was made visible: For valence quark masses smaller than the sea masses, the correlator becomes negative – a clear sign for the violation of unitarity. Mixed-action expressions were derived afterwards, and different quark mass tunings were discussed.

The main part of this work focused on the impact of finite volume effects on the correlator. For this purpose, ChPT was formulated in a finite volume with periodic boundary conditions. The working assumption for the following calculations was that one is in the p-regime of ChPT where the product of "meson mass times box extent" is much larger than one ($ML \gg 1$, $mL \gg 1$). The calculation was then split into two separate parts.

The first part was inspired by the expressions Eq. (8) and Eq. (16) in Refs. [34] and [35], respectively. These are finite volume momentum-space representations of the bubble contribution, in which the five present sums run over all possible combinations of lattice momenta.

The aim of the present work was to find simpler expressions which are more convenient to use in a fitting process and which show how the infinite volume limit is being approached. It was argued that, as long as the lattice cutoff π/a is much larger than the scale of chiral symmetry breaking Λ_{had}, it is sufficient to work with standard quantized momenta occurring in a box with periodic boundary conditions. As a consequence, the now infinite sums over these momenta could be rewritten using the Poisson summation formula.

The final expression contains three sums and an integration over a closed interval, which

can be performed numerically. For higher-order terms in the sums, the integrand is suppressed with increasing powers of $\exp(-mL)$. The rewriting thus made the infinite volume limit transparent: As the volume increases, these terms become irrelevant, and the sums reduce to a single summand which is exactly the infinite volume contribution. It was shown that, with growing box size, the double pole contribution is finite volume enhanced in comparison to the single pole contributions. The generally large size of the finite volume corrections to the correlator was explained.

The practical applicability of the fitting formula was studied, and numerical examples of where to truncate the sums in order to reach a result of satisfying accuracy were given. It was found that the sums' rate of convergence is very slow for small volumes and meson masses, as well as for large time separations $t \to T/2$. However, at large volumes and masses, $ML > 5$, $mL > 5$, $m > 300\,\mathrm{MeV}$ ($M \geq m$), only the first ~ 30 terms are needed. The strength of the fitting formula turned out to be at larger, yet still theoretical values of volumes and masses ($ML > 5$, $mL > 5$, $L > 5$ fm, $T \geq L$, and $t \ll T/2$), for then, the sums reduce to two terms: the infinite volume contribution and the first correction term.

In an actual lattice simulation, these values are still out of reach. Therefore, in a second calculation, a formula applicable for smaller volumes and masses was derived. Starting point was the position-space representation of the bubble contribution. Again, the Poisson summation formula allowed to rewrite two of the three occurring sums. These could then be solved by performing the geometric series. In the final result, one is left with a single sum over terms which are suppressed for small spatial volumes and small masses, as well as for large time separations. The sum converges rather quickly, and for standard masses and box sizes, only the first $\mathcal{O}(10)$ terms are needed. Even for extreme values of L, M, and m, not more than 100 terms are relevant.

Owing to the fast convergence of the sum and due to the fact that no integration appears, the second derived formula is superior to the first one, and it should be used for fitting lattice data. In comparison to the first formula, it is not clear, though, how the infinite volume limit is being approached. For increasing L, more and more summands need to taken into account, and finally, the sum turns into the infinite volume expression.

Lastly, the important formulae necessary for fitting the lattice correlator are listed:

The scalar correlator with isospin symmetry for 2 and $2 + 1$ sea flavors is given in Eqs. (4.39) and (4.40), respectively. A generalization to non-degenerate quark masses can be found in Eq. (D.2). The appearing bubble functions are those of Eqs. (4.37) and (D.4), relevant for the first fitting formula, and Eqs. (4.49), (4.53), and (D.5) for the second formula.

A. The bubble contribution

Consider the scalar two-point function for arbitrary (sea and/or valence) flavors a and b in partially quenched ChPT:

$$C^{ab}_{\text{PQChPT}}(x) = \langle 0|\bar{b}(x)a(x)\,\bar{a}(0)b(0)|0\rangle$$
$$= \frac{1}{Z_{\text{PQChPT}}} \frac{\delta^2 Z_{\text{PQChPT}}}{\delta m_{ab}(0)\,\delta m_{ba}(x)}\bigg|_{m\to\text{diag}(m)} \quad\text{(A.1)}$$

Here,

$$Z_{\text{PQChPT}} = \int \mathcal{D}\Sigma\, e^{-\int d^4y\,[\mathcal{L}_2(y)+\mathcal{L}_4(y)+\dots]} \quad\text{(A.2)}$$

denotes the partition function of PQChPT with the mass matrix m being promoted to a space-time dependent object (The sources l_μ and r_μ as well as the scalar density p are set to zero.). The functional derivatives are now worked out. For sea or valence flavor indices $a \neq b$, one finds

$$C^{ab}_{\text{PQChPT}}(x) = \frac{1}{Z_{\text{PQChPT}}} \int \mathcal{D}\Sigma\, \mathcal{B}(x)\, e^{-\int d^4y\,[\mathcal{L}_2(y)+\mathcal{L}_4(y)]}\bigg|_{m\to\text{diag}(m)} \quad\text{(A.3)}$$

with

$$\mathcal{B}(x) = + \frac{\partial\mathcal{L}_2}{\partial m_{ba}}(x)\frac{\partial\mathcal{L}_2}{\partial m_{ab}}(0) + \frac{\partial\mathcal{L}_2}{\partial m_{ba}}(x)\frac{\partial\mathcal{L}_4}{\partial m_{ab}}(0)$$
$$+ \frac{\partial\mathcal{L}_4}{\partial m_{ba}}(x)\frac{\partial\mathcal{L}_2}{\partial m_{ab}}(0) - \delta(x)\frac{\partial^2\mathcal{L}_4}{\partial m_{ab}\,\partial m_{ba}}(0)\,. \quad\text{(A.4)}$$

The term $\frac{\partial\mathcal{L}_4}{\partial m_{ba}}(x)\frac{\partial\mathcal{L}_4}{\partial m_{ab}}(0)$, which in principle would be also present, does not contribute, since it corresponds to the next-higher order in the chiral expansion. In the expression above, $\mathcal{L}_2$ and $\mathcal{L}_4$ must be expanded up to quadratic and zeroth order in meson fields $\Phi(x) = \frac{1}{\sqrt{2}}\pi(x)$, respectively. The LO Lagrangian $\mathcal{L}_2$ results in the following contribution:

$$\frac{\partial\mathcal{L}_2}{\partial m_{ab}}(x) = \frac{B_0 f^2}{2}\left[\Sigma(x) + \Sigma^\dagger(x)\right]_{ba}$$
$$= B_0 f^2\left[\mathbb{1} - \frac{1}{f^2}\pi^2(x)\right]_{ba} + \mathcal{O}(\pi^4)$$
$$= -B_0\left[\pi^2(x)\right]_{ba} + \mathcal{O}(\pi^4) \quad\text{(A.5)}$$

The mass dependence of the NLO Lagrangian $\mathcal{L}_4$, see Eq. (2.22), comes from the six terms containing $L_4, \dots, L_8$ and H_2. The first two, $\mathcal{L}_{L_4}$ and $\mathcal{L}_{L_5}$, include derivatives of the meson fields and are therefore of $\mathcal{O}(\pi^2)$. So are $\mathcal{L}_{L_6}$ and $\mathcal{L}_{L_7}$ due to their structure, which is similar to the LO Lagrangian Eq. (A.5). When setting the mass matrix m to

its physical value diag(m), one finds that $\mathcal{L}_{L_8}$ and $\mathcal{L}_{H_2}$ contribute only to the last term of Eq. (A.4):

$$-\delta(x)\frac{\partial^2 \mathcal{L}_4}{\partial m_{ab}\, \partial m_{ba}}(0) = 4B_0^2\, \delta(x)\left[2L_8\left(\Sigma_{aa}\Sigma_{bb} + \Sigma_{aa}^\dagger \Sigma_{bb}^\dagger\right)(0) + 2H_2\right]$$

$$= 8B_0^2\, \delta(x)\left[2L_8 + H_2\right] + \mathcal{O}(\pi^2) \tag{A.6}$$

The second and third term in Eq. (A.4) vanish completely to the order of interest. Finally,

$$C_{\text{PQChPT}}^{ab}(x) = B_0^2 \langle 0|[\pi^2(x)]_{ab}[\pi^2(0)]_{ba}|0\rangle + 8B_0^2\, \delta(x)\left[2L_8 + H_2\right]. \tag{A.7}$$

The low- and high-energy constants L_8 and H_2 enter the correlator only as contact terms. They play no rôle at large time separations and will therefore be dropped in the following considerations.

According to Wick's theorem, Eq. (A.7) can be reduced to a sum of products of two-point functions, which involve only two fields. Among the non-zero

$$C_{\text{PQChPT}}^{ab}(x) = B_0^2 \sum_{k,l=1}^{N_S+2N_V} \langle 0|\pi_{ak}(x)\pi_{kb}(x)\pi_{bl}(0)\pi_{la}(0)|0\rangle$$

$$= B_0^2 \sum_{k,l=1}^{N_S+2N_V}\Big[+ \langle \pi_{ak}(x)\pi_{kb}(x)\rangle \langle \pi_{bl}(0)\pi_{la}(0)\rangle$$
$$+ \langle \pi_{ak}(x)\pi_{bl}(0)\rangle \langle \pi_{kb}(x)\pi_{la}(0)\rangle$$
$$+ \langle \pi_{ak}(x)\pi_{la}(0)\rangle \langle \pi_{kb}(x)\pi_{bl}(0)\rangle \Big]$$

$$= B_0^2\Big[2\langle \pi_{ab}\pi_{ba}\rangle \langle \pi_{aa}\pi_{bb}\rangle + \sum_{l=1}^{N_S+2N_V} \langle \pi_{al}\pi_{la}\rangle \langle \pi_{lb}\pi_{bl}\rangle \Big]$$

$$= B_0^2\Big[2\langle \pi_{ab}\pi_{ba}\rangle \langle \pi_{aa}\pi_{bb}\rangle + \sum_{i=1}^{N_S} \langle \pi_{ai}\pi_{ia}\rangle^{\text{con}} \langle \pi_{ib}\pi_{bi}\rangle^{\text{con}}$$
$$+ \langle \pi_{ab}\pi_{ba}\rangle \langle \pi_{aa}\pi_{aa}\rangle^{\text{disc}} + \langle \pi_{ab}\pi_{ba}\rangle \langle \pi_{bb}\pi_{bb}\rangle^{\text{disc}} \Big] \tag{A.8}$$

Here, $\langle \pi_1\pi_2\rangle \equiv \langle \pi_1(x)\pi_2(0)\rangle$. Wick's theorem yields the expression in the second line. Then, most propagators are zero, which simplifies the expression to line three. There, in the sum over l, propagators with ghost quarks cancel the corresponding valence quark propagators, see Eq. (2.25), resulting in the final result.

B. Rewriting the bubble function

The rewriting of the bubble function starts with

$$B_{\mathrm{SP}}(t, M, m) = B_0^2 \int \mathrm{d}^3\vec{x} \int \frac{\mathrm{d}^4 p}{(2\pi)^4} B_{\mathrm{SP}}(p, M, m)\, \mathrm{e}^{ipx}\,, \tag{B.1}$$

where

$$B_{\mathrm{SP}}(p, M, m) = \int \frac{\mathrm{d}^4 k}{(2\pi)^4} \frac{1}{(k+p)^2 + M^2} \frac{1}{k^2 + m^2} \tag{B.2}$$

is the corresponding momentum-space representation of the bubble function Eq. (3.18). It is obtained by a convolution of the two propagators. Since the $\vec{x}$-integration projects on $\vec{p} = 0$, that is, $p = (p_0, p_1, p_2, p_3)^T \rightarrow (p_0, 0, 0, 0)^T \equiv p_0$, the integral simplifies to

$$B_{\mathrm{SP}}(t, M, m) = B_0^2 \int \frac{\mathrm{d}p_0}{2\pi} B_{\mathrm{SP}}(p_0, M, m)\, \mathrm{e}^{ip_0 x}\,. \tag{B.3}$$

At first, the two denominators in Eq. (B.2) are combined by introducing a Feynman parameter c, completing the square and shifting the integration variable k,

$$B_{\mathrm{SP}}(\kappa(p_0, M, m, c)) = \int_0^1 \mathrm{d}c \int \frac{\mathrm{d}^4 k}{(2\pi)^4} \frac{1}{[k^2 + \kappa^2]^2}\,, \tag{B.4}$$

with

$$\kappa^2 \equiv c(1-c)p_0^2 + m^2 + c\left(M^2 - m^2\right)\,. \tag{B.5}$$

It is convenient to make use of the following expression:

$$\frac{1}{(u^2)^s} = \frac{1}{\Gamma(s)} \int_0^\infty \mathrm{d}\tau\, \tau^{s-1} \mathrm{e}^{-\tau u^2}\,, \quad s \geq 1 \tag{B.6}$$

With $u^2 = k^2 + \kappa^2$, the momentum k appears in form of a standard Gaussian integral, $\int \mathrm{d}^4 k\, \mathrm{e}^{-\tau k^2} = \frac{\pi^2}{\tau^2}$, resulting in

$$B_{\mathrm{SP}}(\kappa(p_0, M, m, c)) = \frac{1}{16\pi^2 \Gamma(s)} \int_0^1 \mathrm{d}c \int_0^\infty \mathrm{d}\tau\, \tau^{s-3} \mathrm{e}^{-\tau \kappa^2}\,, \quad s = 2\,. \tag{B.7}$$

Now, $B_{\mathrm{SP}}(\kappa)$ must be Fourier-transformed back into position-space. The integration over the p_0-dependent part in κ, see Eq. (B.5), is easily done (the short-hand notation $\lambda = \tau c(1-c)$ is being used),

$$\int_{-\infty}^\infty \frac{\mathrm{d}p_0}{2\pi} \mathrm{e}^{-\lambda p_0^2} \mathrm{e}^{ip_0 t} = \int_{-\infty}^\infty \frac{\mathrm{d}p_0}{2\pi} \mathrm{e}^{-\lambda\left(p_0 - \frac{it}{2\lambda}\right)^2} \mathrm{e}^{-\frac{t^2}{4\lambda}} = \frac{\mathrm{e}^{-\frac{t^2}{4\lambda}}}{2\sqrt{\pi\lambda}}\,. \tag{B.8}$$

Being left with the integration over the Feynman parameter c and the auxiliary parameter τ, the single pole bubble function reads

$$B_{\mathrm{SP}}(t, M, m) = \frac{B_0^2}{32\pi^{5/2}\Gamma(s)} \int\limits_0^1 \mathrm{d}c \int\limits_0^\infty \mathrm{d}\tau \frac{\tau^{s-\frac{7}{2}}}{\sqrt{c(1-c)}} \, \mathrm{e}^{-\tau\left[m^2+c(M^2-m^2)\right]-\frac{t^2}{4\tau\,c(1-c)}} \,. \qquad (B.9)$$

The last step is the τ-integration, which can also be performed analytically. It is of the form

$$\int\limits_0^\infty \mathrm{d}\tau \frac{\tau^{s-\frac{7}{2}}}{\sqrt{\beta}} \, \mathrm{e}^{-\tau\alpha^2-\frac{\gamma}{4\tau}} = \frac{1}{\sqrt{\beta}} \cdot 2^{\frac{7}{2}-s} \alpha^{\frac{5}{2}-s} \gamma^{\frac{s}{2}-\frac{5}{4}} \cdot K_{\frac{5}{2}-s}\left(\alpha\sqrt{\gamma}\right) \,, \qquad (B.10)$$

where K is the modified Bessel function of the second kind, and $\alpha^2 = m^2 + c(M^2 - m^2)$, $\beta = c(1-c)$, and $\gamma = \frac{t^2}{c(1-c)}$.

For the present case, $s = 2$, the Bessel function is essentially an exponential function, $K_{1/2}(x) = \sqrt{\frac{\pi}{2x}}\mathrm{e}^{-x}$, and it follows the final result

$$B_{\mathrm{SP}}(t, M, m) = \frac{B_0^2}{16\pi^2|t|} \int\limits_0^1 \mathrm{d}c \, \mathrm{e}^{-\sqrt{\frac{m^2+c(M^2-m^2)}{c(1-c)}}|t|} \,. \qquad (B.11)$$

C. Poisson summation formula

Let the Fourier transform (F.T.) of a function f be defined as

$$f(x) = \int\limits_{-\infty}^{\infty} \frac{\mathrm{d}k}{2\pi} \tilde{f}(k)\, \mathrm{e}^{ikx}\,, \qquad \tilde{f}(k) = \int\limits_{-\infty}^{\infty} \mathrm{d}x\, f(x)\, \mathrm{e}^{-ikx}\,, \tag{C.1}$$

and consider the continuous integrable function

$$h(x) \equiv \sum_{n=-\infty}^{\infty} f(x + n\mathcal{T}) \tag{C.2}$$

with $\mathcal{T}$ being the period of h. The function $h(x)$ can be expanded in a pointwise convergent Fourier series

$$h(x) = \sum_{k=-\infty}^{\infty} h_k \cdot \mathrm{e}^{2\pi i \frac{k}{\mathcal{T}} x}\,, \tag{C.3}$$

in which its Fourier coefficients are given by

$$h_k = \frac{1}{\mathcal{T}} \int\limits_{0}^{\mathcal{T}} \mathrm{d}x\, h(x)\, \mathrm{e}^{-2\pi i \frac{k}{\mathcal{T}} x}$$

$$= \frac{1}{\mathcal{T}} \int\limits_{0}^{\mathcal{T}} \mathrm{d}x \sum_{n=-\infty}^{\infty} f(x + n\mathcal{T})\, \mathrm{e}^{-2\pi i \frac{k}{\mathcal{T}} x}\,. \tag{C.4}$$

Lebesgue's dominated convergence theorem [77, 78] justifies the commutation of integration and summation. Additionally, the integration variable is shifted to $x' = x + n\mathcal{T}$:

$$= \frac{1}{\mathcal{T}} \sum_{n=-\infty}^{\infty} \int\limits_{n\mathcal{T}}^{\mathcal{T}(n+1)} \mathrm{d}x\, f(x')\, \mathrm{e}^{-2\pi i \frac{k}{\mathcal{T}}(x' - n\mathcal{T})}$$

$$= \frac{1}{\mathcal{T}} \int\limits_{-\infty}^{\infty} \mathrm{d}x\, f(x')\, \mathrm{e}^{-2\pi i \frac{k}{\mathcal{T}} x'}$$

$$h_k = \frac{1}{\mathcal{T}} \cdot \tilde{f}\left(\frac{2\pi k}{\mathcal{T}}\right) \tag{C.5}$$

This combined with Eqs. (C.2) and (C.3) yields the Poisson summation formula

$$\sum_{n=-\infty}^{\infty} f(x + n\mathcal{T}) = \frac{1}{\mathcal{T}} \sum_{k=-\infty}^{\infty} \tilde{f}\left(\frac{2\pi k}{\mathcal{T}}\right) \mathrm{e}^{2\pi i \frac{k}{\mathcal{T}} x}\,, \tag{C.6}$$

with the special case, $x = 0$,

$$\sum_{n=-\infty}^{\infty} f(n\mathcal{T}) = \frac{1}{\mathcal{T}} \sum_{k=-\infty}^{\infty} \tilde{f}\left(\frac{2\pi k}{\mathcal{T}}\right)\,. \tag{C.7}$$

The following detailed example is showing the rewriting of the elliptic theta function $\vartheta(\sigma, \omega) \equiv \sum\limits_{n=-\infty}^{\infty} \mathrm{e}^{-\sigma(n+\omega)^2}$, which is made extensive use of in the main text, Chapter 4. For doing so, one needs

$$f(x) = \mathrm{e}^{-\beta(x+y)^2} \quad \xrightarrow{\text{F. T.}} \quad \tilde{f}(t) = \sqrt{\frac{\pi}{\beta}}\,\mathrm{e}^{-\frac{t^2}{4\beta}+iyt}\,. \tag{C.8}$$

Now,

$$f(\sigma n) = \mathrm{e}^{-\sigma(n+\omega)^2} = \mathrm{e}^{-\frac{(\sigma n + \sigma \omega)^2}{\sigma}}\,, \quad \beta = \frac{1}{\sigma}\,, \quad x = \sigma n\,, \quad y = \sigma \omega \tag{C.9}$$

$$\Rightarrow \quad \vartheta(\sigma, \omega) \equiv \sum_{n=-\infty}^{\infty} \mathrm{e}^{-\sigma(n+\omega)^2}$$

$$= \frac{1}{\sigma} \sum_{k=-\infty}^{\infty} \sqrt{\pi\sigma}\,\mathrm{e}^{-\frac{\sigma}{4}\left(\frac{2\pi k}{\sigma}\right)^2 + i\sigma\omega\frac{2\pi k}{\sigma}}$$

$$= \sqrt{\frac{\pi}{\sigma}} \sum_{k=-\infty}^{\infty} \mathrm{e}^{-\frac{\pi^2}{\sigma}k^2 + i2\pi k\omega}$$

$$= \sqrt{\frac{\pi}{\sigma}} \sum_{k=-\infty}^{\infty} \mathrm{e}^{-\frac{\pi^2}{\sigma}\left(k - i\frac{\omega\sigma}{\pi}\right)^2}\mathrm{e}^{-\sigma\omega^2}$$

$$\vartheta(\sigma, \omega) = \sqrt{\frac{\pi}{\sigma}}\,\mathrm{e}^{-\sigma\omega^2} \cdot \vartheta\left(\frac{\pi^2}{\sigma}, -i\frac{\omega\sigma}{\pi}\right)\,. \tag{C.10}$$

D. The finite volume scalar correlator without isospin symmetry

For $N_S = 3$ sea flavors, the finite volume scalar correlator for non-degenerate quark masses reads

$$C_{\bar{y}x}^{1+1+1}(x) = B_0^2 \bigg[\langle \pi_{xy}\pi_{yx} \rangle_{\text{FV}}^{\text{con}} \left(2 \langle \pi_{xx}\pi_{yy} \rangle_{\text{FV}}^{\text{disc}} + \langle \pi_{xx}\pi_{xx} \rangle_{\text{FV}}^{\text{disc}} + \langle \pi_{yy}\pi_{yy} \rangle_{\text{FV}}^{\text{disc}} \right)$$

$$+ \sum_{i=u,d,s} \langle \pi_{xi}\pi_{ix} \rangle_{\text{FV}}^{\text{con}} \langle \pi_{iy}\pi_{yi} \rangle_{\text{FV}}^{\text{con}} \bigg]. \tag{D.1}$$

When carrying out the partial fraction decomposition of the disconnected propagators and summing over the spatial volume L^3, one receives

$$C_{\bar{y}x}^{1+1+1}(t) = -\frac{2}{N_S} \sum_{v=x,y,\pi_0,\eta} R_v\big(\begin{smallmatrix} u,d,s \\ x,y,\pi_0,\eta \end{smallmatrix}\big) \cdot B_{\text{SP}}^{(\text{FV})}(T,L,t,M_{xy},M_v)$$

$$- \frac{2\hat{a}^2\gamma_{SS}}{M_y^2 - M_x^2} \Big[B_{\text{SP}}^{(\text{FV})}(T,L,t,M_{xy},M_x) - B_{\text{SP}}^{(\text{FV})}(T,L,t,M_{xy},M_y) \Big]$$

$$- \frac{1}{N_S} \sum_{w=x,y} \bigg[\Big[R_w\big(\begin{smallmatrix} u,d,s \\ \pi_0,\eta \end{smallmatrix}\big) + N_S \hat{a}^2 \gamma_{SS} \Big] \cdot B_{\text{DP}}^{(\text{FV})}(T,L,t,M_{xy},M_w)$$

$$+ \sum_{v=w,\pi_0,\eta} D_v^w\big(\begin{smallmatrix} u,d,s \\ x,y,\pi_0,\eta \end{smallmatrix}\big) \cdot B_{\text{SP}}^{(\text{FV})}(T,L,t,M_{xy},M_v) \bigg]$$

$$+ \sum_{i=u,d,s} B_{\text{SP}}^{(\text{FV})}(T,L,t,M_{ix},M_{ix}). \tag{D.2}$$

From this lengthy expression, the scalar correlator for two sea flavors, $C_{\bar{y}x}^{1+1}(t)$, can be deduced by dropping s and η in all residues and sums.
The finite volume single pole bubble function $B_{\text{SP}}^{(\text{FV})}$ is given in Eqs. (4.37) and (4.49). The residues R and D are denoted as [53]

$$R_v\big(\begin{smallmatrix} u,d,s \\ x,y,\pi_0,\eta \end{smallmatrix}\big) \equiv \frac{\prod\limits_{i=u,d,s} (M_i^2 - M_v^2)}{\prod\limits_{\substack{j=x,y,\pi_0,\eta \\ j \neq v}} (M_j^2 - M_v^2)} \quad \text{and} \quad D_v^w\big(\begin{smallmatrix} u,d,s \\ x,y,\pi_0,\eta \end{smallmatrix}\big) \equiv -\frac{\partial}{\partial M_w^2} R_v\big(\begin{smallmatrix} u,d,s \\ x,y,\pi_0,\eta \end{smallmatrix}\big), \tag{D.3}$$

where the upper and lower neutral meson states in the parenthesis of R_v correspond to the product indices i and j, respectively. The factor with $j = v$ is excluded from the product in the denominator. The residue $R_w\big(\begin{smallmatrix} u,d,s \\ \pi_0,\eta \end{smallmatrix}\big)$ is obtained from $R_v\big(\begin{smallmatrix} u,d,s \\ x,y,\pi_0,\eta \end{smallmatrix}\big)$ by dropping the x- and y- terms in the product over j.
In order to evaluate the correlator, one also needs the finite volume double pole bubble function for unequal masses, $B_{\text{DP}}^{(\text{FV})}(T,L,t,M,m) = -\frac{\partial}{\partial m^2} B_{\text{SP}}^{(\text{FV})}(T,L,t,M,m)$, which

was not considered in the main text. It is shown in the two different forms necessary for either of the two finite volume calculations in Section 4.3 and 4.4.

From Eq. (4.37), one obtains the following expression:

$$B_{\text{DP}}^{(\text{FV})}(T, L, t, M, m) = \frac{B_0^2}{32\pi^2} \sum_{\tilde{n}_0, n_0 = -\infty}^{\infty} \sum_{n=0}^{\infty} \int_0^1 dc \frac{\rho(n)\sqrt{1-c}}{\sqrt{cm^2 + c^2(M^2 - m^2)}} \, e^{-mL\sqrt{1+c\left(\frac{M^2}{m^2}-1\right)}\sqrt{\tilde{\gamma}}}$$

(D.4)

$\tilde{\gamma}$ is given in Eq. (4.38). For the second calculation, one considers Eq. (4.49) and finds

$$B_{\text{DP}}^{(\text{FV})}(T, L, t, M, m) = \frac{B_0^2}{8L^3} \sum_{n=0}^{\infty} \rho(n) \left[\frac{e^{-E_n(M)t} + e^{-E_n(M)[T-t]}}{E_n(M)\left(1 - e^{-E_n(M)T}\right)} \right]$$

$$\times \left[\frac{\left(t e^{-\tilde{E}t} + [T-t]e^{-\tilde{E}[T-t]}\right)}{\tilde{E}^2(1 - e^{-\tilde{E}T})} + \frac{\left(1 + [\tilde{E}T - 1]e^{-\tilde{E}T}\right)\left(e^{-\tilde{E}t} + e^{-\tilde{E}[T-t]}\right)}{\tilde{E}^3(1 - e^{-\tilde{E}T})^2} \right],$$

(D.5)

where, for brevity, $\tilde{E} \equiv E_n(m)$.

Bibliography

[1] J. Gasser and H. Leutwyler, "Chiral Perturbation Theory to One Loop," *Ann. Phys.* **158** (1984) 142.

[2] J. Gasser and H. Leutwyler, "Chiral Perturbation Theory: Expansions in the Mass of the Strange Quark," *Nucl. Phys.* **B250** (1985) 465.

[3] K. Symanzik, "Continuum Limit and Improved Action in Lattice Theories. 1. Principles and ϕ^4 Theory," *Nucl. Phys.* **B226** (1983) 187.

[4] B. Sheikholeslami and R. Wohlert, "Improved Continuum Limit Lattice Action for QCD with Wilson Fermions," *Nucl. Phys.* **B259** (1985) 572.

[5] S. R. Sharpe and R. L. Singleton, Jr, "Spontaneous flavor and parity breaking with Wilson fermions," *Phys. Rev.* **D58** (1998) 074501, `arXiv:hep-lat/9804028`.

[6] W.-J. Lee and S. R. Sharpe, "Partial Flavor Symmetry Restoration for Chiral Staggered Fermions," *Phys. Rev.* **D60** (1999) 114503, `arXiv:hep-lat/9905023`.

[7] J. Gasser and H. Leutwyler, "Light Quarks at Low Temperatures," *Phys. Lett.* **B184** (1987) 83.

[8] J. Gasser and H. Leutwyler, "Thermodynamics of Chiral Symmetry," *Phys. Lett.* **B188** (1987) 477.

[9] J. Gasser and H. Leutwyler, "Spontaneously Broken Symmetries: Effective Lagrangians at Finite Volume," *Nucl. Phys.* **B307** (1988) 763.

[10] O. Bär, "Chiral perturbation theory at non-zero lattice spacing," *Nucl. Phys. Proc. Suppl.* **140** (2005) 106–119, `arXiv:hep-lat/0409123`.

[11] S. R. Sharpe, "Applications of chiral perturbation theory to lattice QCD," `arXiv:hep-lat/0607016`.

[12] M. F. L. Golterman, "Applications of chiral perturbation theory to lattice QCD," `arXiv:0912.4042 [hep-lat]`.

[13] D. B. Kaplan, "A Method for simulating chiral fermions on the lattice," *Phys. Lett.* **B288** (1992) 342–347, `arXiv:hep-lat/9206013`.

[14] R. Narayanan and H. Neuberger, "Chiral determinant as an overlap of two vacua," *Nucl. Phys.* **B412** (1994) 574–606, `arXiv:hep-lat/9307006`.

[15] Y. Shamir, "Chiral fermions from lattice boundaries," *Nucl. Phys.* **B406** (1993) 90–106, `arXiv:hep-lat/9303005`.

[16] H. Neuberger, "Exactly massless quarks on the lattice," *Phys. Lett.* **B417** (1998) 141–144, `arXiv:hep-lat/9707022`.

[17] P. H. Ginsparg and K. G. Wilson, "A Remnant of Chiral Symmetry on the Lattice," *Phys. Rev.* **D25** (1982) 2649.

[18] M. Lüscher, "Exact chiral symmetry on the lattice and the Ginsparg–Wilson relation," *Phys. Lett.* **B428** (1998) 342–345, `arXiv:hep-lat/9802011`.

[19] A. D. Kennedy, "Algorithms for lattice QCD with dynamical fermions," *Nucl. Phys. Proc. Suppl.* **140** (2005) 190–203, `arXiv:hep-lat/0409167`.

[20] K. G. Wilson, "Confinement of quarks," *Phys. Rev.* **D10** (1974) 2445–2459.

[21] **Alpha** Collaboration, R. Frezzotti, P. A. Grassi, S. Sint, and P. Weisz, "Lattice QCD with a chirally twisted mass term," *JHEP* **08** (2001) 058, `arXiv:hep-lat/0101001`.

[22] C. Aubin *et al.*, "Light hadrons with improved staggered quarks: Approaching the continuum limit," *Phys. Rev.* **D70** (2004) 094505, `arXiv:hep-lat/0402030`.

[23] O. Bär, G. Rupak, and N. Shoresh, "Simulations with different lattice Dirac operators for valence and sea quarks," *Phys. Rev.* **D67** (2003) 114505, `arXiv:hep-lat/0210050`.

[24] C. Gattringer and C. B. Lang, "Quantum chromodynamics on the lattice," *Lect. Notes Phys.* **788** (2010) 1–211.

[25] C. W. Bernard and M. F. L. Golterman, "Partially quenched QCD and staggered fermions," *Nucl. Phys. Proc. Suppl.* **34** (1994) 331–333, `arXiv:hep-lat/9311070`.

[26] C. W. Bernard and M. F. L. Golterman, "Partially quenched gauge theories and an application to staggered fermions," *Phys. Rev.* **D49** (1994) 486–494, `arXiv:hep-lat/9306005`.

[27] S. R. Sharpe and N. Shoresh, "Partially quenched chiral perturbation theory without Φ_0," *Phys. Rev.* **D64** (2001) 114510, `arXiv:hep-lat/0108003`.

[28] O. Bär, G. Rupak, and N. Shoresh, "Chiral perturbation theory at $\mathcal{O}(a^2)$ for lattice QCD," *Phys. Rev.* **D70** (2004) 034508, `arXiv:hep-lat/0306021`.

[29] O. Bär, C. W. Bernard, G. Rupak, and N. Shoresh, "Chiral perturbation theory for staggered sea quarks and Ginsparg-Wilson valence quarks," *Phys. Rev.* **D72** (2005) 054502, `arXiv:hep-lat/0503009`.

[30] J.-W. Chen, D. O'Connell, and A. Walker-Loud, "Universality of Mixed Action Extrapolation Formulae," *JHEP* **04** (2009) 090, `arXiv:0706.0035 [hep-lat]`.

[31] J.-W. Chen, M. F. L. Golterman, D. O'Connell, and A. Walker-Loud, "Mixed Action Effective Field Theory: an Addendum," *Phys. Rev.* **D79** (2009) 117502, `arXiv:0905.2566 [hep-lat]`.

[32] W. A. Bardeen, A. Duncan, E. Eichten, N. Isgur, and H. Thacker, "Chiral loops and ghost states in the quenched scalar propagator," *Phys. Rev.* **D65** (2001) 014509, `arXiv:hep-lat/0106008`.

[33] **RBC** Collaboration, S. Prelovsek and K. Orginos, "Quenched scalar meson correlator with domain wall fermions," *Nucl. Phys. Proc. Suppl.* **119** (2003) 822–824, `arXiv:hep-lat/0209132`.

[34] S. Prelovsek, C. Dawson, T. Izubuchi, K. Orginos, and A. Soni, "Scalar meson in dynamical and partially quenched two-flavor QCD: Lattice results and chiral loops," *Phys. Rev.* **D70** (2004) 094503, `arXiv:hep-lat/0407037`.

[35] S. Prelovsek, "Effects of staggered fermions and mixed actions on the scalar correlator," *Phys. Rev.* **D73** (2006) 014506, `arXiv:hep-lat/0510080`.

[36] C. W. Bernard, C. E. DeTar, Z. Fu, and S. Prelovsek, "Scalar Meson Spectroscopy with Lattice Staggered Fermions," *Phys. Rev.* **D76** (2007) 094504, `arXiv:0707.2402 [hep-lat]`.

[37] M. F. L. Golterman, T. Izubuchi, and Y. Shamir, "The role of the double pole in lattice QCD with mixed actions," *Phys. Rev.* **D71** (2005) 114508, `arXiv:hep-lat/0504013`.

[38] C. Aubin, J. Laiho, and R. S. Van de Water, "Discretization effects and the scalar meson correlator in mixed-action lattice simulations," *Phys. Rev.* **D77** (2008) 114501, `arXiv:0803.0129 [hep-lat]`.

[39] A. Walker-Loud, "Topics in effective field theory for lattice QCD," `arXiv:hep-lat/0608010`.

[40] F. Bernardoni, N. Garron, P. Hernandez, S. Necco, and C. Pena, "Mixed action computations on fine dynamical lattices," `arXiv:0911.3756 [hep-lat]`.

[41] M. E. Peskin and D. V. Schroeder, *An Introduction to quantum field theory.* Westview Press, 1995.

[42] A. Pich, "Chiral perturbation theory," *Rept. Prog. Phys.* **58** (1995) 563–610, `arXiv:hep-ph/9502366`.

[43] S. Scherer, "Introduction to chiral perturbation theory," *Adv. Nucl. Phys.* **27** (2003) 277, `arXiv:hep-ph/0210398`.

[44] G. Ecker, "Quantum chromodynamics," `arXiv:hep-ph/0604165`.

[45] S. Weinberg, "Phenomenological Lagrangians," *Physica* **A96** (1979) 327.

[46] H. Leutwyler, "On the foundations of chiral perturbation theory," *Ann. Phys.* **235** (1994) 165–203, `arXiv:hep-ph/9311274`.

[47] K. Orginos and A. Walker-Loud, "Mixed meson masses with domain-wall valence and staggered sea fermions," *Phys. Rev.* **D77** (2008) 094505, `arXiv:0705.0572 [hep-lat]`.

[48] C. Aubin, J. Laiho, and R. S. Van de Water, "Light pseudoscalar meson masses and decay constants from mixed action lattice QCD," *PoS* **LATTICE2008** (2008) 105, `arXiv:0810.4328 [hep-lat]`.

[49] C. Aubin, J. Laiho, and R. S. Van de Water, "The neutral kaon mixing parameter B_K from unquenched mixed-action lattice QCD," `arXiv:0905.3947 [hep-lat]`.

[50] A. Morel, "Chiral Logarithms in Quenched QCD," *J. Phys. (France)* **48** (1987) 1111–1119.

[51] C. W. Bernard and M. F. L. Golterman, "Chiral perturbation theory for the quenched approximation of QCD," *Phys. Rev.* **D46** (1992) 853–857, `arXiv:hep-lat/9204007`.

[52] S. R. Sharpe and N. Shoresh, "Physical results from unphysical simulations," *Phys. Rev.* **D62** (2000) 094503, `arXiv:hep-lat/0006017`.

[53] C. Aubin and C. W. Bernard, "Pseudoscalar decay constants in staggered chiral perturbation theory," *Phys. Rev.* **D68** (2003) 074011, `arXiv:hep-lat/0306026`.

[54] S. R. Sharpe, "Enhanced chiral logarithms in partially quenched QCD," *Phys. Rev.* **D56** (1997) 7052–7058, `arXiv:hep-lat/9707018`.

[55] S. R. Beane and M. J. Savage, "Nucleon nucleon interactions on the lattice," *Phys. Lett.* **B535** (2002) 177–180, `arXiv:hep-lat/0202013`.

[56] G. Rupak and N. Shoresh, "Chiral perturbation theory for the Wilson lattice action," *Phys. Rev.* **D66** (2002) 054503, `arXiv:hep-lat/0201019`.

[57] S. R. Sharpe and J. M. S. Wu, "The phase diagram of twisted mass lattice QCD," *Phys. Rev.* **D70** (2004) 094029, `arXiv:hep-lat/0407025`.

[58] S. R. Sharpe and J. M. S. Wu, "Twisted mass chiral perturbation theory at next-to-leading order," *Phys. Rev.* **D71** (2005) 074501, `arXiv:hep-lat/0411021`.

[59] S. Aoki, O. Bär, and B. Biedermann, "Pion scattering in Wilson ChPT," *Phys. Rev.* **D78** (2008) 114501, `arXiv:0806.4863 [hep-lat]`.

[60] **UKQCD** Collaboration, K. C. Bowler, B. Joo, R. D. Kenway, C. M. Maynard, and R. J. Tweedie, "Lattice QCD with mixed actions," *JHEP* **08** (2005) 003, arXiv:hep-lat/0411005.

[61] **MILC** Collaboration, C. W. Bernard, "Chiral Logs in the Presence of Staggered Flavor Symmetry Breaking," *Phys. Rev.* **D65** (2002) 054031, arXiv:hep-lat/0111051.

[62] D. Arndt and C. J. D. Lin, "Heavy meson chiral perturbation theory in finite volume," *Phys. Rev.* **D70** (2004) 014503, arXiv:hep-lat/0403012.

[63] G. Colangelo, S. Dürr, and C. Haefeli, "Finite volume effects for meson masses and decay constants," *Nucl. Phys.* **B721** (2005) 136–174, arXiv:hep-lat/0503014.

[64] G. Colangelo and C. Haefeli, "Finite volume effects for the pion mass at two loops," *Nucl. Phys.* **B744** (2006) 14–33, arXiv:hep-lat/0602017.

[65] G. 't Hooft and M. J. G. Veltman, "Scalar One Loop Integrals," *Nucl. Phys.* **B153** (1979) 365–401.

[66] S. Weinberg, *The Quantum theory of fields. Vol. 1: Foundations.* Cambridge University Press, 1995.

[67] M. Lüscher, "Volume Dependence of the Energy Spectrum in Massive Quantum Field Theories. 1. Stable Particle States," *Commun. Math. Phys.* **104** (1986) 177.

[68] D. Bećirević and G. Villadoro, "Impact of the finite volume effects on the chiral behavior of $f(K)$ and $B(K)$," *Phys. Rev.* **D69** (2004) 054010, arXiv:hep-lat/0311028.

[69] R. Lewis and P.-P. A. Ouimet, "Lattice regularization for chiral perturbation theory," *Phys. Rev.* **D64** (2001) 034005, arXiv:hep-ph/0010043.

[70] B. Borasoy, R. Lewis, and P.-P. A. Ouimet, "Lattice regularized chiral perturbation theory," *Nucl. Phys. Proc. Suppl.* **128** (2004) 141–147, arXiv:hep-lat/0310054.

[71] B. Borasoy and R. Lewis, "Volume dependences from lattice chiral perturbation theory," *Phys. Rev.* **D71** (2005) 014033, arXiv:hep-lat/0410042.

[72] S. R. Sharpe, "Quenched chiral logarithms," *Phys. Rev.* **D46** (1992) 3146–3168, arXiv:hep-lat/9205020.

[73] M. J. Lighthill, *Introduction to Fourier analysis and generalised functions.* Cambridge University Press, 1958.

[74] E. Elizalde, "Multidimensional extension of the generalized Chowla–Selberg formula," *Commun. Math. Phys.* **198** (1998) 83–95, arXiv:hep-th/9707257.

[75] C. T. Sachrajda and G. Villadoro, "Twisted boundary conditions in lattice simulations," *Phys. Lett.* **B609** (2005) 73–85, `arXiv:hep-lat/0411033`.

[76] C. W. Bernard and M. F. L. Golterman, "Finite volume two pion energies and scattering in the quenched approximation," *Phys. Rev.* **D53** (1996) 476–484, `arXiv:hep-lat/9507004`.

[77] E. J. McShane, *Unified integration.* Academic Press, 1983.

[78] C. Goffman and G. Pedrick, *First course in functional analysis.* American Mathematical Society, 1983.

Acknowledgements

Selbstständigkeitserklärung

Hiermit erkläre ich, die vorliegende Arbeit selbstständig und nur unter Verwendung der angegebenen Literatur und Hilfsmittel verfasst zu haben.

Andreas Furchner

Berlin, den 23. Februar 2010